Niels Köster, BSc.

A regularized Shape Optimization Approach for the Bernoulli Free Boundary Problem with the Boundary Element Method

MASTERARBEIT

zur Erlangung des akademischen Grades

Diplom-Ingenieur

Masterstudium Technomathematik

eingereicht an der

Technischen Universität Graz

Betreuer

Prof. Dr. O. Steinbach

Institut für Angewandte Mathematik

Graz, Juni 2018

Kurzfassung

Diese Arbeit beschäftigt sich mit der Formoptimierung. Diese versucht, ein Gebiet zu finden, welches ein gegebenes Kostenfunktional über einer Menge zugelassener Gebiete minimiert. Um dieses Gebiet zu finden, wird die Geschwindigkeitsmethode benutzt, welche sukzessive Verformungen an einem Anfangsgebiet vornimmt. Falls das Anfangsgebiet polygonal berandet ist oder ein Lipschitzgebiet ist, ist diese Verformung nicht unbedingt stabil. Deswegen führt diese Arbeit eine Variation der Geschwindigkeitsmethode ein, die auch für polygonal berandete Geometrien und Lipschizgebiete stabil ist. Die beiden Verformungen werden auf das freie Randwertprobleme von Bernoulli angewendet und miteinander verglichen. Dafür werden mit der Randelementmethode numerische Annäherungen des Gebietes berechnet, welches das Kostenfunktional minimiert.

Abstract

Shape optimization is used to minimize a cost functional over a set of admissible geometries. An example where this can be used is the design of structures. But the standard speed method, which are used to solve the shape optimization problem, often have problems, when they are applied to geometries with polygonal boundaries and Lipschitz domains. Therefore, in this work a modification of the speed method is introduced, which works for geometries with polygonal boundaries and Lipschitz domains. This modification of the speed method, furthermore, is applied to the Bernoulli free boundary problem and an approximation of the optimal geometry is calculated with the boundary element method.

Vorwort

Zuerst geht mein Dank an Univ.-Prof. Dr. Olaf Steinbach dafür, dass er den Workshop organisierte, der diese Arbeit inspirierte. Außerdem möchte ich ihm dafür danken, dass er mich mit viel Geduld betreut hat. Vielen Dank auch an Marco Zank, Markus Holzmann, Lars Köster, Tobias Hochscherf und Marlene Rachholz für das intensive Korrekturlesen. Ich möchte auch meiner Mutter danken, die mich immer unterstützt hat. Sie ist es, die mir ermöglicht hat, diesen Bildungsweg einzuschlagen.

Contents

Introduction

Shape optimization is important for the design and construction of structures, for example in the aircraft industry, for electromagnetic devices, in fluid mechanics and in image processing. For examples of this see [5, Examples 2.1 - 2.4].

Shape optimization is used to find a domain in a set M of admissible domains which minimizes a cost functional subject to a constraint. In general the constraint takes the form of a partial differential equation, and the cost functional is an integral over the domain or boundary of the domain, which depends on the solution of the partial differential equation, and its first order derivatives.
An iterative method of solving a shape optimization problem is the speed method, see [9]. The speed method calculates a direction v, such that the cost functional decreases if the domain is deformed in the direction v. But as shown in Chapter 4 the standard speed method does has problems with domains with polygonal boundaries.
In this work a modification of the speed method is introduced, which regularizes v by applying a boundary integral operator. This modification is particularly suitable for less regular domains, including polygonal domains. Additionally, in Chapter 3.3 Remark 8 a mixed boundary value problem is introduced, which can be used to get the same regularization.

The model shape optimization problem, on which the modification of the speed method is applied, is inspired by the optimization of high-voltage electrical devices, where prevention of electrical breakdown is the optimization parameter by limiting the electrical field strength on critical components.
The electrical field strength is determined by the electrostatic field equation, which reduces to the Laplace equation. The electrical field strength on the surface is maximized over all the shapes, where the electrical problem is solvable.

This electrical problem is modeled with the Bernoulli free boundary problem, where a domain $\Omega \in M$ has to be found, where the following overdetermined boundary value

problem is fulfilled:

$$\begin{aligned} -\Delta\hat{u} &= 0 \quad \text{in } \Omega := \Omega_O \setminus \overline{\Omega_I}, \\ \hat{u} &= 1 \quad \text{on } \Gamma_I := \partial\Omega_I, \\ \hat{u} &= 0 \quad \text{on } \Gamma_O := \partial\Omega_O, \\ \frac{\partial\hat{u}}{\partial n} &= \lambda \quad \text{on } \Gamma_I. \end{aligned} \tag{0.1}$$

The domain Ω has to be in the set of admissible domains M, that means all Ω are annulus domains with inner boundary Γ_I and outer boundary Γ_O. Since the boundary value problem (0.1) is overdetermined, the inner boundary Γ_I is a free parameter.

The shape optimization problem to (0.1) is given as a cost functional

$$J(\Omega) = \int_\Omega |\nabla u|^2 \, dx + \lambda^2 \int_\Omega dx \quad \text{for } \Omega \in M$$

subject to the constraint

$$\begin{aligned} -\Delta u &= 0 \quad \text{in } \Omega, \\ u &= 1 \quad \text{on } \Gamma_I, \\ u &= 0 \quad \text{on } \Gamma_O. \end{aligned}$$

In this shape optimization problem a domain $\tilde{\Omega} \in M$ has to be found which minimizes the cost functional

$$J(\tilde{\Omega}) = \min_{\Omega \in M} J(\Omega).$$

The partial differential equation is solved using the boundary element method, because the cost functional $J(\Omega)$ can be represented on the boundary $\partial\Omega$, and depends only on the normal derivative of u. An additional advantage of the boundary element method is that only the boundary $\partial\Omega$ has to be discretized, which simplifies the moving of the mesh in every step of the shape optimization algorithm.

In Chapter 4 the shape optimization problem with the cost functional $J(\Omega)$ is solved numerically. All domains, which are considered in Chapter 4, are domains with polygonal boundaries. The examples contrast the standard speed method with the modified speed method.
Additionally, the original problem of finding a domain in M with minimal stress on Γ_O is solved by finding he minimal $\lambda > 0$ such that there exist a solution of shape optimization problem. This is solved for Ω_O being a L-shape in Section 4.5.

The presentation of the shape optimization and the speed method in this work are based on "Introduction to Shape Optimization" by J. Sokolowski and J. Zolesio [9] and

"Methods of Shape Optimization in Free Boundary Problems" by Jerico B. Bacani [1] is used specifically for the shape optimization of the Bernoulli free boundary problem. The chapter on the boundary element method and the Sobolev spaces are based on "Numerical Approximation Methods for Elliptic Boundary Value Problems" by O. Steinbach [10] and "Strongly Elliptic Systems and Boundary Integral Equations" by W. McLean [6].

1 Shape Optimization

In this chapter some basic definitions and concepts of shape optimization are introduced:

- The **cost functional** $J(\Omega)$.
- The **set of admissible domains** M.
- The **constraint** and the **material solution**.
- The **Fréchet derivative** of $J(\Omega)$.
- The iterative solution method: The **speed method**.

This chapter is based on the work [9, Chapter 2.1-2.33]. A good starting point certainly is a simple example that visualizes the various different concepts.

Example 1. *To introduce a shape optimization method this example considers a model problem in* $\mathbb{R}$*, where an interval*

$$I \in M_I = \{(0, 1+s) \mid 0 \leq s \leq b\} \tag{1.1}$$

has to be found for a given $b > 0$*. This interval has to minimize the* ***cost functional***

$$J(I) = \int_0^{1+s} \left(\tilde{u}(s,y) - \frac{y}{4}\right)^2 \, dy. \tag{1.2}$$

Every interval I^s *in the* ***set of admissible intervals*** M_I *has an ordinary differential equation of the second order as a* ***constraint***

$$\begin{aligned} -\frac{d^2\tilde{u}(s,y)}{dy^2} + \tilde{u}(s,y) = 0 \quad &\text{for } y \in I^s, \\ \tilde{u}(s,0) = 0, \\ \tilde{u}(s,1+s) = 1. \end{aligned} \tag{1.3}$$

The solution of (1.3) is called the ***material solution*** *and for this example it is represented as*

$$\tilde{u}(s,y) = \frac{\sinh(y)}{\sinh(1+s)} \quad \text{for } y \in \overline{I^s}.$$

Therefore the cost functional can be represented as a function $j(s)$*, see Figure 1.1 for a plot of this function for* $s \in (0,3)$*.*

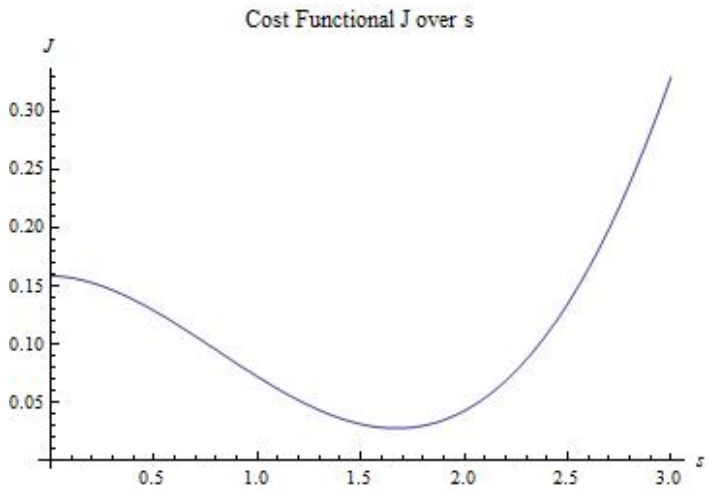

Figure 1.1: Plot of the cost functional $J(I^s) = j(s)$ for $s \in (0, 3)$.

The interval $\tilde{I}$ *which minimizes* $J(I^s)$ *in* M_I *is calculated by considering the first derivative* $\frac{dj}{ds}(s)$ *of* $j(s)$ *with respect to* s*, which for* $s > 0$ *has the stationary point* $s_1 \approx 1.67221$*. The second derivative of* $j(s)$ *is* $\frac{d^2 j(s_1)}{ds^2} \approx 0.253653 > 0$*. Therefore, the interval* $\tilde{I} = I^{s_1}$ *is the minimizing interval of* J*, where*

$$J(\tilde{I}) = \min_{I \in M_I} J(I).$$

In this example all important aspects were introduced, which are considered in the following section.

- There is a **cost functional** J in (1.2) which is minimized over a **set of admissible domains** M_I in (1.1).
- The **constraint** in (1.3) is a differential equation.
- Te set of domains M_I is represented as a transformation of an initial domain $(0, 1)$. This is a transformation in the normal direction.
- A derivative over a set of domains in the direction $+1$ is introduced, called the **Fréchet derivative** of J, i.e. $\frac{dj}{ds}(s)$. Its stationary points are used to find the minimizing interval.
- Example 1 calculates the general derivative of J over M_I, but in general this is not possible and an iterative method is necessary. One of these methods is the **speed method**, see [9, Chapter 2.9].

1.1 Cost Functionals

A shape optimization problem is a minimization problem over a set of domains. In this section the cost functional of this minimization problem and the set of admis-

sible domains M over which the cost functional is minimized are introduced. The cost functional generally takes the form of an integral over a domain or its boundary dependent on a solution u of a partial differential equation. Example 1 is a example for a shape optimization problem where a interval I has to be found such that the physical property $\tilde{u}$ in (1.3) is as close as possible to the linear function $\frac{y}{4}$ for $y \in I$.

Definition 1 (Cost Functional, [9, Chapter 2.5])**.** *Let $d = 2, 3$ and $\Omega \subset \mathbb{R}^d$ be a Lipschitz domain and $u \in H^1(\Omega)$. Then a cost functional of a shape optimization problem is defined as*

$$J(\Omega) = \int_\Omega j_1(x, u(x), \nabla u(x))\, dx + \int_\Gamma j_0(x, u(x), \nabla u(x))\, ds_x,$$

where $j_0 : (x, p, q) \to j_0(x, p, q)$ with $j_0 : \Gamma \times \mathbb{R} \times \mathbb{R}^d \to \mathbb{R}$ and $j_1 : (x, p, q) \to j_1(x, p, q)$ with $j_1 : \Omega \times \mathbb{R} \times \mathbb{R}^d \to \mathbb{R}$ are continuous.
If the function $j_0 = 0$, the cost functional $J(\Omega)$ is called distributed, and if the function $j_1 = 0$, then $J(\Omega)$ is called a boundary cost functional.

A Lipschitz domain is a domain with a Lipschitz continuous boundary, see Definition 12. For the definition of the Sobolev space $H^1(\Omega)$ see (6.6) in the appendix. This work considers only distributed cost functionals, but most of the concepts also work for boundary cost functionals.

Example 2. *Examples of cost functionals are*

$$J_1(\Omega) = meas(\Omega) = \int_\Omega dx,$$
$$J_2(\Omega) = meas(\Gamma) = \int_\Gamma ds_x,$$
$$J_3(\Omega) = \int_\Omega (u(x) - w(x))^2\, dx.$$

The cost functional in (1.2) *used in the Example 1 is J_3 with $w(x) = \frac{1}{4}x$.*

Definition 2 (Admissible Domains)**.** *The set M is called a set of admissible domains Ω for the cost functional J if the following is true:*

- *Each $\Omega \in M$ is a domain in $\mathbb{R}^d$, that means $\emptyset \neq \Omega \subset \mathbb{R}^d$ and Ω is open and connected.*
- *For $\Omega \in M$ the cost functional $J(\Omega)$ is well defined and $J(\Omega) \in \mathbb{R}$.*
- *All domains $\Omega \in M$ are bounded and there exists a bounded domain U_M with $\Omega \subset U_M$ for all $\Omega \in M$.*

The existence of a solution to a shape optimization problem can be considered with:

Theorem 1 (Weierstraß Theorem, [8, Theorem 4.16])**.** *Let K be a compact set and let $f : K \to \mathbb{R}$ be a continuous function. Then f is bounded and there exist $p, q \in K$ such that $f(p) = \sup_{x \in K} f(x)$ and $f(q) = \inf_{x \in K} f(x)$.*

Applying Theorem 1 to a cost functional J as given in Definition 1 and to a set of admissible domains Ω as introduced in Definition 2 results in the conditions:

- M has to be compact,
- and $M \ni \Omega \to J(\Omega)$ has to be continuous.

If the cost functional J depends on a solution u of a partial differential equation, then $M \ni \Omega \to u$ has to be continuous for J to be continuous. Often this means that all Ω have to be at least Lipschitz domain, otherwise there exists no solution of the partial differential equation which is regular enough. Therefore, a transformation of domains such that Lipschitz domains can only be transformed into Lipschitz domains is considered in Section 1.2.
For an example of a cost functional which depends on the solution of a differential equation see (1.2).
But the existence of the optimum for shape optimization problems is not the focus of this work. In the following it is assumed that the cost functional $J(\Omega)$ and the set of admissible domains M are chosen such that J has a minimum in M.

1.2 Transformation of Domains

This section is based on [9, Chapter 2.7-2.15] and [1, Chapter 2].
Usually a topology on a set of domains M is introduced with the characteristic function $\chi_\Omega \in L^\infty(\mathbb{R}^d)$ for $\Omega \in M$, see Definition 14 for the definition of L^p spaces. This means that the distance between domains $\Omega_1, \Omega_2 \in M$ is

$$d(\Omega_1, \Omega_2) = \|\chi_{\Omega_1} - \chi_{\Omega_2}\|_{L^\infty(\mathbb{R}^d)}. \tag{1.4}$$

For a series of Lipschitz domains $\{\Omega_i\}_{i=1}^\infty$, which is convergent in terms of d, it can not be guaranteed that $\Omega = \lim_{i \to \infty} \Omega_i$ is also a Lipschitz domain. Therefore, if the distance d is used it does not preserve the regularity of the boundary, see [9, Section 2.7]. This is a problem, because the domains $\Omega \in M$ have to be C^k-domains $k \geq 1$ or Lipschitz, for the definition of C^k-domains see Definition 13 in the appendix, to ensure the existence of a solution in $H^1(\Omega)$ of a partial differential equation. A topology, therefore, is defined which preserves the regularity of the domain, when a domain is transformed during the shape optimization process. So, transformations $\psi : \Omega_1 \to \Omega_2$ are considered which preserve the regularity of the domain if the $L^\infty(\Omega_1)$-norm of $\psi(x) - x$ is small enough. This motivates the following definition of domains Ω^s close to a domain Ω.

Definition 3. *Let $\Omega \in M$, for a set of admissible domains M as in Definition 2. Then $\Omega^s \in M$ is defined by*

$$\Omega^s = \{y(s) = \varphi(s,x) \text{ for } x \in \Omega\} \subset \mathbb{R}^d$$

for $s \in [0,\varepsilon)$ with $\varepsilon > 0$ and with the deformation function $\varphi(s,\cdot) : U_M \to \mathbb{R}^d$, which has the following properties:

1. *The initial domain is deformed onto itself: $\varphi(0,x) = x$ for $x \in \Omega$.*
2. *For all $s \in [0,\varepsilon)$ The deformation is continuously differentiable in U_M , i.e. $\varphi(s,\cdot) \in C^1(U_M;\mathbb{R}^d)$.*
3. *for all $s \in [0,\varepsilon)$ the deformation $\varphi(s,\cdot)$ is bijective and the inverse of the deformation is also continuously differentiable, i.e. $\varphi^{-1}(s,\cdot) \in C^1(U_M;\mathbb{R}^d)$.*
4. *For all $s \in [0,\varepsilon)$ and for $x \in U_M$ the determinant of the Jacobi matrix of the deformation φ is positive, i.e. $\det D_x\varphi(s,x) > 0$. The Jacobi matrix is defined as*

$$D_x\varphi(s,x) = \left(\frac{\partial\varphi_i(s,x)}{\partial x_j}\right)_{i,j=1}^{d}.$$

Here $C^k(U_M)$ is the set of continuous differentiable function in U_M, see (6.2) in the appendix, and $C^k(U_M,\mathbb{R}^d)$ is the set of continuous differentiable vector valued functions, see (6.3) in the appendix.

Definition 4. *The a deformation $\varphi : \mathbb{R}_+ \times U_M \to \mathbb{R}^d$ is defined to be in $C^1([0,\varepsilon);\mathbb{R}^d)\times C^1(U_M;\mathbb{R}^d)$ if $\varphi(\cdot,x) \in C^1([0,\varepsilon);\mathbb{R}^d)$ for all $x \in U_M$ and $\varphi(s,\cdot) \in C^1(U_M;\mathbb{R}^d)$ for $s \in [0,\varepsilon)$*

A deformation φ as given in Definition 3, therefore, fulfills $\varphi \in C^1([0,\varepsilon);\mathbb{R}^d) \times C^1(U_M;\mathbb{R}^d)$. With such a deformation φ a distance between $\Omega \in M$ and $\Omega^s \in M$ is defined by

$$d_r(\Omega,\Omega^s) = \|\varphi(s,\cdot) - I_\Omega\|_{L^\infty(U_M)}, \tag{1.5}$$

where $I_\Omega = \varphi(0,x) = x$ for $x \in \Omega$. The speed method, which is introduced in Section 1.6, only calculates the speed of the deformation on the boundary $\Gamma = \partial\Omega$, where the speed of the deformation φ is given by the derivative of $\varphi(s,x)$ with respect to s:

Definition 5. *For a given $\varphi \in C^1([0,\varepsilon);\mathbb{R}^d) \times C^1(U_M;\mathbb{R}^d)$ the speed vector is defined as*

$$v(s,x) := \frac{d}{ds}\varphi(s,x).$$

The speed method gives only the speed vector $v(0,\cdot)$, hence a deformation φ_v must be calculated depending on the given speed vector v.

Lemma 2 ([9, Chapter 2.9, Chapter 2.10])**.** *Let $\varepsilon > 0$ be small enough and let the speed vector $v \in C^0([0,\varepsilon);\mathbb{R}^d) \times C^1(U_M;\mathbb{R}^d)$ fulfill*

$$(v(s,x), n(x)) = 0 \quad \text{for allmost all } x \in \partial U_M$$

for the normal vector n. (If n is not defined on a singular point $\tilde{x}$ of the boundary ∂U_M then let $v(s,\tilde{x}) = 0$.) Then there exists a deformation φ with all properties as stated in Definition 3.

Next it is shown that a deformation φ as introduced in Definition 3 transforms Lipschitz domains into Lipschitz domains. The requirements in the following theorem on φ are actually strong enough to transform C^1-domains into C^1-domains.

Theorem 3. *Let $\Omega \subset \mathbb{R}^d$ be a Lipschitz domain and the deformed domain Ω^s be given as in Definition 4. Then Ω^s is also a Lipschitz domain.*

Proof. Given $y \in \partial\Omega^s$ then $x = \varphi^{-1}(s,y) \in \partial\Omega$. Then there exists an open subset W_j and a Lipschitz hypograph Ω_j such that $x \in W_j$ and $\Omega_j = \Omega \cap W_j$, see Definition 12 in the appendix. Since φ^{-1} is continuous $\varphi(s,W_j)$ is open and $\cup_j \varphi(s,W_j)$ is a cover of $\partial\Omega^s$. Then $\Omega_j^s = \varphi(s,\Omega_j)$ is also a Lischitz hypograph, because Ω_j is a Lipschitz hyopgraph and $\varphi(s,\cdot) \in C^1(U_M;\mathbb{R}^d)$. □

Remark 1. *Actually we need only $\varphi(s,\cdot) \in C^{0,1}(U_M)$ to prove Theorem 3, but then $D_x\varphi(s,x)$ has to be defined in a weaker form. This is not done in this work. Nevertheless it would not change much in the stated results of this work, excepting that all the results are only valid for almost all x.*

The topology of the deformation introduced in (1.5) is much stronger then the topology of the characteristic functions in (1.4), because it transforms Lipschitz domains into Lipschitz domains, see Theorem 3.

Additional Properties of the Deformation φ

Next, a few properties of the deformation φ are presented which are needed later.

Corollary 4. *Let φ be as in Definition 3 with $\varphi, \varphi^{-1} \in C^1([0,\varepsilon);\mathbb{R}^d) \times C^1(U_M;\mathbb{R}^d)$ and with the deformation $y(s) = \varphi(s,x)$ as given in Definition 3. Then the derivatives of φ and φ^{-1} at $s = 0$ for fixed $y(0) = x \in U_M$ have the following properties:*

1. *The derivative with respect to s of the inverse of φ is given by*

$$\frac{d}{ds}\left[\varphi_k^{-1}(s,y(s))\right]_{s=0} = -v_k(0,x)$$

for $k = 1,\dots,d$.

2. *The derivative with respect to s of the Jacobi matrix $D_x\varphi(s,x)$ of the deformation φ is given by*
$$\frac{d}{ds}\left[\frac{\partial\varphi_k(s,x)}{\partial x_l}\right]_{s=0} = \frac{\partial v_k(0,x)}{\partial x_l}$$
for $k,l = 1,\dots,d$.

3. *The derivative with respect to s of the inverse of the Jacobi matrix of the deformation φ, which is $D_y\varphi^{-1}(s,y) = \left(\frac{\partial\varphi_k^{-1}(s,y(s))}{\partial y_l}\right)_{l,k=1}^{d}$, is given by*
$$\frac{d}{ds}\left[\frac{\partial\varphi_k^{-1}(s,y(s))}{\partial y_l}\right]_{s=0} = -\frac{\partial v_k(0,x)}{\partial x_l}$$
for $k,l = 1,\dots,d$.

4. *For $s \in [0,\varepsilon)$ and $\varepsilon > 0$ small enough the determinant of the Jacobi matrix $D_x\varphi(s,x)$ of the deformation φ is given by*
$$\det D_x\varphi(s,x) = 1 + s\,\operatorname{div} v(0,x) + \mathcal{O}(s^2).$$

5. *The derivative with respect to s at $s = 0$ of the determinant of the Jacobi matrix of the deformation is given by*
$$\frac{d}{ds}\left[\det D_x\varphi(s,x)\right]_{s=0} = \operatorname{div} v(0,x).$$

Proof. 1. Since φ^{-1} is the inverse of φ the representation
$$x = \varphi_k^{-1}(s,\varphi_k(s,x))$$
is valid. Then the derivative is applied to both sides of the equation and it results in
$$0 = \frac{d}{ds}\left[\frac{\partial\varphi_k^{-1}(s,x)}{\partial x_l}\right]_{s=0} + \frac{d}{ds}\left[\frac{\partial\varphi_k(s,x)}{\partial x_l}\right]_{s=0},$$
since $\varphi_k(0,x) = \varphi_k^{-1}(0,x) = x_k$.

2. This is true since $\varphi \in C^1([0,\varepsilon);\mathbb{R}^d) \times C^1(U_M;\mathbb{R}^d)$ and so $\frac{\partial\varphi_l(s,x)}{\partial x_k}$ is continuously differentiable in s and continuous in x.

3. Since φ^{-1} is the inverse of φ the representation of I is
$$I = D_x\varphi(s,x)\left(D_y\varphi^{-1}(s,y(s))\right),$$
for $y(s) = \varphi(s,x)$. And if the derivative is applied to both sides it follows that
$$0 = \left(\frac{d}{ds}D_x\varphi(s,x)\right) D_y\varphi^{-1}(s,y(s)) + D_x\varphi(s,x)\left(\frac{d}{ds}D_y\varphi^{-1}(s,y(s))\right).$$

Using that $\varphi(0,x) = \varphi^{-1}(0,x) = x$ results in

$$0 = \frac{d}{ds}\left[D_x\varphi(s,x)\right]_{s=0} I + I\frac{d}{ds}\left[D_y\varphi^{-1}(s,y(s))\right]_{s=0}.$$

The stated result follows from property 2.

4. The proof of this is based on [1, Lemma 2.11]: For s small enough the deformation can be represented with a Taylor series $\varphi(x,s) = x + sv(0,x) + \mathcal{O}(s^2)$. The Jacobi matrix of the deformation $A(s) = (a_{i,j})_{i,j=1,\dots,d} = \frac{\partial\varphi_l(s,x)}{\partial x_k}$, therefore, is

$$\begin{aligned} a_{i,i} &= \frac{\partial\varphi_i(x,s)}{\partial x_i} = 1 + s\frac{\partial v_i(0,x)}{\partial x_i} + \mathcal{O}(s^2), \\ a_{i,j} &= \frac{\partial\varphi_j(x,s)}{\partial x_i} = s\frac{\partial v_j(0,x)}{\partial x_i} + \mathcal{O}(s^2) \quad \text{for } i \neq j. \end{aligned}$$

The determinant can be expressed with the Leibnitz formula

$$\det A(s) = \sum_{\sigma\in S_d} \operatorname{sign}(\sigma) \prod_{i=1}^{d} a_{i,\sigma(i)},$$

where S_d covers all permutations of $\{1,\dots,d\}$.
The sets are defined as

- I includes only the identity permutation,
- $F_d = \{\sigma \in S_d \mid \exists k \leq d \text{ such that } \sigma(k) = k\}$ as all permutations where at least on $k \leq d$ exists such that the permutation is

$$\sigma = \{\sigma(1),\dots,\sigma(k-1), k, \sigma(k+1),\dots,\sigma(d)\}.$$

Then S_d can be split into $S_d = I \cup (F_d \setminus I) \cup (S_d \setminus F_d)$. Consequently the determinant can be split into three parts as well,

$$\begin{aligned} \det A &= \prod_{i=1}^{d} a_{i,i} + \sum_{\sigma\in(F_d\setminus I)} \operatorname{sign}(\sigma) \prod_{i=1}^{d} a_{i,\sigma(i)} + \sum_{\sigma\in(S_d\setminus F_d)} \operatorname{sign}(\sigma) \prod_{i=1}^{d} a_{i,\sigma(i)} \\ &=: A_1 + A_2 + A_3. \end{aligned}$$

These three parts are examined as follows:

- $\sigma = \{1,\dots,d\} = I$ results in

$$A_1 = \prod_{i=1}^{d}\left(1 + s\frac{\partial v_i(0,x)}{\partial x_i} + \mathcal{O}(s^2)\right) = 1 + s\operatorname{div} v(0,x) + \mathcal{O}(s^2).$$

- For each $\sigma \in F_d \setminus I$ at least two j_1, j_2 exist such that $\sigma(j_1) \neq j_1$, $\sigma(j_2) \neq j_2$ and $a_{j_i,\sigma(j_i)} = s\frac{\partial v_{\sigma(j_i)}(0,x)}{\partial x_{j_i}} + \mathcal{O}(s^2)$, because otherwise $\sigma = \{1, \ldots, d\}$. In this case for each $\sigma \in F_d \setminus I$ it turns out that

$$\prod_{i=1}^{d} a_{i,\sigma(i)} = \left(s^2 \frac{\partial v_{\sigma(j_1)}(0,x)}{\partial x_{j_1}} \frac{\partial v_{\sigma(j_2)}(0,x)}{\partial x_{j_2}} + \mathcal{O}(s^2) \right) \prod_{i=1, i\neq j_1, j_2}^{d} a_{i,\sigma(i)} = \mathcal{O}(s^2)$$

  and that means $A_2 = \mathcal{O}(s^2)$.
- From $\sigma \in S_d \setminus F_d$ it follows $\sigma(i) \neq i$ for $i = 1, \ldots, d$ that means

$$\prod_{i=1}^{d} a_{i,\sigma(i)} = s^d \prod_{i=1}^{d} \left(\frac{\partial v_{\sigma(i)}(0,x)}{\partial x_i} + \mathcal{O}(s^2) \right) = \mathcal{O}(s^2)$$

  and $A_3 = \mathcal{O}(s^2)$.

It follows that $\det A(s) = A_1 + A_2 + A_3 = 1 + s \operatorname{div} v(0,x) + \mathcal{O}(s^2)$.

5. From 4. it follows that

$$\det A(s) = A_1 + A_2 + A_3 = 1 + s \operatorname{div} v(0,x) + \mathcal{O}(s^2)$$

and the derivative of this determinant is

$$\frac{d}{ds} \det A(s) = \operatorname{div} v(0,x) + \mathcal{O}(s).$$

□

Eulerian and Lagrangian descriptions

The Eulerian descriptions and the Lagrangian descriptions are defined for functions living on all Ω^s with $s \in [0, \varepsilon)$ and $\varepsilon > 0$ small enough such that Lemma 2 is true. This means that any function $\tilde{f}$ defined on Ω^s has an Eulerian description $\tilde{f}$ in y and an Lagrangian description f in x which are convertible into each other with

$$\begin{aligned} \tilde{f}(s,y) &= \tilde{f}(s, \varphi(s,x)) = f(s,x), \\ f(s,x) &= f(s, \varphi^{-1}(s,y)) = \tilde{f}(s,y), \end{aligned}$$

since the deformation φ is bijective.

For a set of functions $\tilde{f}(s,\cdot) : \Omega^s \to \mathbb{R}$ for $s \in [0,\varepsilon)$ the derivative of $\tilde{f}$ in the direction $v \in C^0([0,\varepsilon); \mathbb{R}^d) \times C^1(U_M; \mathbb{R}^d)$ at $s = 0$ is

$$\left[\frac{d\tilde{f}}{ds}(s, y(s)) \right]_{s=0} = \lim_{s \to 0^+} \frac{\tilde{f}(s, y(s)) - \tilde{f}(0, y(0))}{s}$$

with $y(s) = \varphi(s,x)$ and $\varphi(s,x)$ is given by Lemma 2. For the functions $f(s,x) = \tilde{f}(s,\varphi(s,x))$ for $s \in [0,\varepsilon)$ the derivative of $\tilde{f}$ in the partial direction $v \in C^0([0,\varepsilon);\mathbb{R}^d) \times C^1(U_M;\mathbb{R}^d)$ at $s = 0$ is

$$\left[\frac{\partial \tilde{f}}{\partial s}(s,y(s))\right]_{s=0} = \lim_{s\to 0^+} \frac{f(s,x)) - f(0,x)}{s}$$

with $y(s) = \varphi(s,x)$ and $\varphi(s,x)$ is given by Lemma 2.

1.3 Material and Shape Derivatives

This section is based on [9, Chapter 2.25 - 2.33].
The derivative of the cost functional $J(\Omega)$ as given in Definition 1 is represented by derivatives of the material solution u, this is shown later in Theorem 8. These derivatives are called the material derivative $\dot{u}$ and the shape derivative u'. Both depend on the speed vector v since the domains Ω^s are given by v as stated in Lemma 2.
The domain $\Omega^s \in M$ is a transformation of an initial domain Ω as introduced in Definition 3. For $s \in [0,\varepsilon)$ the material solution $\tilde{u}(s,\cdot) \in H^1(\Omega^s)$ is defined as the weak solution of

$$\begin{aligned} -\Delta_y \tilde{u}(s,y) &= \tilde{f}(s,y) \quad \text{for } y \in \Omega^s, \\ \tilde{u}(s,y) &= \tilde{h}(s,y) \quad \text{for } y \in \Gamma^s = \partial\Omega^s \end{aligned} \tag{1.6}$$

by finding $\tilde{u}(s,\cdot) \in V_h = \{w \in H^1(\Omega^s) \mid w(y) = \tilde{h}(s,y) \text{ for } y \in \Gamma^s\}$ such that

$$\int_{\Omega^s} (\nabla \tilde{u}(s,y), \nabla v(y))\, dy = \int_{\Omega^s} \tilde{f}(s,y) v(y)\, dy \quad \forall v \in H_0^1(\Omega^s).$$

The Sobolev space $H^1(\Omega^s)$ is defined by (6.6) in the appendix and $H_0^1(\Omega^s)$ is the Sobolev space with trace zero on Γ which is defined by (6.11) in the appendix.

Definition 6 (Material derivative, [9, Chapter 2.25])**.** *Let $v \in C^0([0,\varepsilon);\mathbb{R}^d) \times C^1(U_M;\mathbb{R}^d)$ and let a function $\tilde{f}(s,\cdot) \in L^2(\Omega^s)$ for all $s \in [0,\varepsilon)$, where the domains Ω^s with points $y(s) = \varphi(s,x)$ and $x = y(0) \in \Omega$. The deformation $\varphi(s,x)$ is given by Lemma 2. Then the material derivative (or the total derivative) of $f = \tilde{f}(0,\cdot)$ at $s = 0$ in the direction v is defined by*

$$\dot{f}(x;v) = \left.\frac{d}{ds}\tilde{f}(s,y(s))\right|_{s=0}$$

if $\dot{f}(\cdot;v) \in L^2(\Omega)$.

Definition 7 (Shape derivative, [9, Chapter 2.30]). *Let $v \in C^0([0,\varepsilon);\mathbb{R}^d)\times C^1(U_M;\mathbb{R}^d)$ and let a function $\tilde{f}(s,\cdot) \in L^2(\Omega^s)$ for all $s \in [0,\varepsilon)$, where the domains Ω^s with points $y(s) = \varphi(s,x)$ are defined by v, see Lemma 2. Set $f(s,x) = \tilde{f}(s,\varphi(s,x))$. Then the shape derivative (or partial derivative) of f at $s = 0$ in direction v is*

$$f'(x;v) = \frac{\partial}{\partial s} f(s,x)\bigg|_{s=0}$$

if $f'(\cdot;v) \in L^2(\Omega)$.

If f is regular enough the shape derivative f' in direction v can be expressed by the following:

Corollary 5. *Let $f'(\cdot,v) \in H^1(\Omega)$, $\dot{f}(\cdot,v) \in H^1(\Omega)$ and $(\nabla f(0,\cdot), v(0,\cdot)) \in H^1(\Omega)$. Then the shape derivative of f in the direction v is*

$$f'(x;v) = \dot{f}(x;v) - (\nabla f(0,x), v(0,x)) \quad \text{for } x \in \Omega.$$

For a Lipschitz domain Ω and its boundary $\Gamma = \partial\Omega$ and let $f'(\cdot,v) \in H^1(\Gamma)$, $\dot{f}(\cdot,v) \in H^1(\Gamma)$ and $(\nabla_\Gamma f(0,\cdot), v(0,\cdot)) \in H^1(\Gamma)$. Then the shape derivative of f in the direction v is

$$f'(\tilde{x};v) = \dot{f}(\tilde{x};v) - (\nabla_\Gamma f(0,\tilde{x}), v(0,\tilde{x})) \quad \text{for } \tilde{x} \in \Gamma.$$

For $\tilde{x} \in \Gamma$ the surface gradient of f is defined by

$$\nabla_\Gamma f(\tilde{x}) = \lim_{\Omega \ni x \to \tilde{x} \in \Gamma} \left(\nabla f(x) - (n(\tilde{x}), \nabla f(x)) n(\tilde{x})\right).$$

Proof. This is proven by considering the material derivative $\dot{f} \in H^1(\Omega)$:

$$\begin{aligned}\dot{f}(x;v) &= \frac{d}{ds}\tilde{f}(s,\varphi(s,x))\bigg|_{s=0} = \frac{\partial}{\partial s}\tilde{f}(s,\varphi(s,x))\bigg|_{s=0} + \left(\nabla_y \tilde{f}(s,y), \frac{d}{ds}\varphi(s,x)\right)\bigg|_{s=0} \\ &= f'(x;v) + (\nabla_x f(0,x), v(0,x)).\end{aligned}$$

The same can be done on the boundary Γ. From this follows the statement of the corollary. □

Remark 2. *If the result of Lemma 5 is applied to a solution of boundary value problem as in (1.6) the requirement $(\nabla f(0,\cdot), v(0,\cdot)) \in H^1(\Omega)$ is fulfilled if $u(0,\cdot) \in H^2(\Omega)$ and $v_i \in C^1(U_M)$ for $i = 1,\dots,d$. If Ω is a $C^{l,1}$-domain with $l \geq 1$ the Theorem in [4, Theorem 2.5.1.1] states that the solution of (1.6) is $u \in H^{l+1}(\Omega)$, hence if Ω is a $C^{1,1}$-domain then the requirements of Lemma 5 are fulfilled.*

Then the material derivative $\dot{u}(\cdot;v) \in H^1(\Omega)$ is

$$\dot{u}(x;v) = \frac{d}{ds}\tilde{u}(s,y(s))\bigg|_{s=0} \quad \text{for } x \in \Omega$$

and the shape derivative $u' \in H^1(\Omega)$ is

$$u'(x;v) = \dot{u}(x;v) - (\nabla u(0,x), v(0,x)) \quad \text{for } x \in \Omega. \tag{1.7}$$

In Section 1.5 the shape derivative u' is explicitly calculated for the general Dirichlet boundary value problem (1.6). Generally for Lipschitz domains Ω the term is $(\nabla u(0,\cdot), v(0,\cdot)) \notin H^1(\Omega)$. Therefore, in Section 2.2 $u'(\cdot; v) \in H^{1/2}(\Omega)$ is calculated for the Bernoulli free boundary problem.

Next, a representation of

$$\frac{d}{ds}\left[(D_x\varphi(s,x))^{-\top}\nabla_x u(s,x)\right]_{s=0}$$

is given, with the shape derivative u', which is needed in the following section.

Corollary 6. *For φ as given in Definition 3 and $u'(\cdot, v) \in H^1(\Omega)$, $\dot{u}(\cdot, v) \in H^1(\Omega)$ and $u(0,\cdot) \in H^2(\Omega)$ there holds*

$$\frac{d}{ds}\left[(D_x\varphi(s,x))^{-\top}\nabla_x u(s,x)\right]_{s=0} = \nabla u'(x;v) + H_u(x)v(0,x) \quad \text{for } x \in \Omega,$$

where $H_u(x)$ is the Hessian matrix of u given by $H_u(x) = \left(\frac{\partial^2 u(0,x)}{\partial x_j \partial x_i}\right)_{i,j=1}^{d}$.

Proof. This is proven by differentiating in parts

$$\begin{aligned} D &:= \frac{d}{ds}\left[(D_x\varphi(s,x))^{-\top}\nabla_x u(s,x)\right]_{s=0} \\ &= \frac{d}{ds}\left[\nabla_x u(s,x)\right]_{s=0} + \frac{d}{ds}\left[(D_x\varphi(s,x))^{-\top}\right]_{s=0}\nabla_x u(0,x) \end{aligned} \tag{1.8}$$

with $D_x\varphi(0,x)^{-\top} = I$. Next, the derivatives with respect to s and x are interchanged:

$$\frac{d}{ds}\left(\nabla_x u(s,x)\right)\Big|_{s=0} = \nabla_x \frac{d}{ds}\tilde{u}(s,y(s))\Big|_{s=0} = \nabla_x \dot{u}(x;v),$$

which results in the gradient of the material derivative $\dot{u}$ of $\tilde{u}$. Using the expression of the shape derivative u' as given in Corollary 5 the material derivative is represented as

$$\nabla_x \dot{u}(x;v) = \nabla_x u'(x;v) + (D_x v(0,x))^{\top}\nabla u(0,x) + H_u(x)v(0,x).$$

For the second term in (1.8) it is used that $\frac{d}{ds}\left((D_x\varphi(s,x))^{-1}\right) = -D_x v(0,x)$, see Corollary 4. Hence, the second term is

$$\frac{d}{ds}\left[(D_x\varphi(s,x))^{-\top}\right]_{s=0}\nabla_x u(0,x) = -(D_x v(0,x))^{\top}\nabla_x u(0,x).$$

Finally it follows that

$$\begin{aligned} D &= \nabla_x u'(x;v) + (D_x v(0,x))^{\top}\nabla u(0,x) + H_u(x)v(0,x) - (D_x v(0,x))^{\top}\nabla_x u(0,x) \\ &= \nabla_x u'(x;v) + H_u(x)v(0,x). \end{aligned}$$

□

1.4 Fréchet Derivative of Shape Functionals

This section is based on [9, Chapter 3.3].
The derivative of the cost functional $J(\Omega^s)$ with respect to s is introduced. This is the same as the derivative in the direction of the speed vector v, because Ω^s is given by v, see Lemma 2. The cost functional considered is of the form

$$J(\Omega) = \int_\Omega F_1(u(x), \nabla u(x))\, dx, \tag{1.9}$$

where $F_1(p, q) : \mathbb{R} \times \mathbb{R}^d \to \mathbb{R}$ is a given function. As example, the cost functional of the Bernoulli free boundary problem in Chapter 2 is as in (1.9) with

$$F_1(u(x), \nabla u(x)) = (\nabla u(x), \nabla u(x)).$$

Definition 8. *For $v \in C^0([0, \varepsilon); \mathbb{R}^d) \times C^1(U_M; \mathbb{R}^d)$ the Fréchet derivative of the cost functional $J(\Omega)$ at $\Omega = \Omega^0$ in the direction of v is defined as the limit*

$$dJ(\Omega; v) := \lim_{s \to 0^+} \frac{J(\Omega^s) - J(\Omega)}{s}, \tag{1.10}$$

where Ω^s is defined by v, see Lemma 2.
The functional $J(\Omega)$ is called differentiable if the limit in (1.10) exists for all directions $v \in C^0([0, \varepsilon); \mathbb{R}^d) \times C^1(U_M; \mathbb{R}^d)$ and if the mapping $dJ(\Omega; v)$ is continuous and linear for $v \in C^0([0, \varepsilon); \mathbb{R}^d) \times C^1(U_M; \mathbb{R}^d)$.

Theorem 7 (The Hadamard formula, [9, Theorem 2.27])**.** *Let J be a cost functional which is differentiable for any C^k-domain $\Omega \subset U_M$ for $k \geq 0$. Then there exists a scalar distribution*

$$g = g(\Gamma) \in D^{-k}(\Gamma),$$

where $D^{-k}(\Gamma) = \big(D^k(\Gamma)\big)'$ is the dual space of $D^k(\Gamma) = C^k(\Gamma)$ such that

$$dJ(\Omega; v) = \langle g, (v, n) \rangle_{D^{-k}(\Gamma) \times D^k(\Gamma)}.$$

The Hadamard formula shows that if g is smooth enough, the Fréchet derivative of $J(\Omega)$ can be represented as an integral of the form:

$$dJ(\Omega; v) = \int_{\partial\Omega} g(x)(n(x), v(0, x))\, ds_x, \tag{1.11}$$

with a function g which depends on u.

Optimality Conditions

If the Hadamard formula given in (1.11) is valid and g is regular enough then the Fréchet derivative of the cost functional J at $\Omega = \Omega^0$ as introduced in Definition 8 is given by

$$\frac{d}{ds}\left[J(\Omega^s)\right]_{s=0} = dJ(\Omega; v)$$

and the Fréchet derivative of the cost functional J at $s = t > 0$ is

$$\frac{d}{ds}\left[J(\Omega^s)\right]_{s=t} = dJ(\Omega^t; v(t,\cdot)). \tag{1.12}$$

Hence the second derivative is defined as

$$\frac{d^2}{ds^2} J(\Omega^s)\bigg|_{s=0} = \lim_{s\to 0^+} \frac{dJ(\Omega^s; v(s,\cdot)) - dJ(\Omega; v)}{s}. \tag{1.13}$$

Let $\tilde{\Omega} \in M$ be the domain which has the minimal value of J, i.e.

$$J(\tilde{\Omega}) \leq J(\Omega) \quad \forall \Omega \in M,$$

then for all speed vectors $v(0,\cdot) \in C^1(U_M; \mathbb{R}^d)$ which fulfill the condition

$$(v(0,x), n(x)) = 0 \quad \text{for } x \in \partial U_M$$

the following necessary optimality conditions hold

$$\begin{aligned} dJ(\Omega_0; v) &= 0, \\ \frac{d^2}{ds^2} J(\Omega^s)\bigg|_{s=0} &\geq 0, \end{aligned} \tag{1.14}$$

where $\Omega^s = \varphi(s, \tilde{\Omega})$ are all deformations close to $\tilde{\Omega}$ as introduced in Definition 3 and $n(x)$ is the normal vector of ∂U_M. If U_M is a Lipschitz domain the normal vector is defined by (6.4). For more information on optimality conditions of shape optimization problems see [9, Section 3.3].

Representation of $dJ(\Omega; v)$ by the Shape Derivative u'

The Fréchet derivative $dJ(\Omega; v)$ of the cost functional J is expressed using u' and the derivatives of $F_1 : \mathbb{R} \times \mathbb{R}^d \to \mathbb{R}$ in p and q, which are given by

$$\begin{aligned} \partial_u F_1(u(x), \nabla u(x)) &:= \frac{\partial}{\partial p} F_1(p,q)\bigg|_{(p,q)=(u(x),\nabla u(x))}, \\ \operatorname{grad}_{\nabla u} F_1(u(x), \nabla u(x)) &:= \operatorname{grad}_q F_1(p,q)\big|_{(p,q)=(u(x),\nabla u(x))}, \end{aligned}$$

if the shape derivative u' is given.

Theorem 8. *Let $u' \in H^1(\Omega)$, $u \in H^2(\Omega)$ and let the cost functional J be given as in (1.9) with $F_1(p,q)$ continuous differentiable in p and q. Then the Fréchet derivative in the direction of $v \in C^0([0,\varepsilon);\mathbb{R}^d) \times C^1(U_M;\mathbb{R}^d)$ is*

$$\begin{aligned} dJ(\Omega;v) = &\int_\Omega \left(\partial_u F_1(u(x),\nabla u(x))\right) u'(x)\, dx \\ &+ \int_\Omega \left(\operatorname{grad}_{\nabla u} F_1(u(x),\nabla u(x)), \nabla u'(x)\right) dx \\ &+ \int_\Omega \operatorname{div}\left[F_1(u(x),\nabla u(x)) v(0,x)\right]\, dx. \end{aligned}$$

Proof. The deformation φ is inserted into the Definition 8 of $dJ(\Omega;v)$ and it results in

$$\begin{aligned} dJ(\Omega;v) &= \lim_{s\to 0} \frac{1}{s}\left(\int_{\Omega^s} F_1(\tilde{u}(s,y),\nabla_y \tilde{u}(s,y))\, dy - \int_\Omega F_1(u(x),\nabla u(x))\, dx\right) \\ &= \int_\Omega \lim_{s\to 0} \frac{1}{s}\left(F_1(u(s,x), D_x\varphi(s,x)^{-\top}\nabla_x u(s,x)) \det D_x\varphi(s,x) - F_1(u(x),\nabla u(x))\right)\, dx. \end{aligned}$$

Since F_1 is differentiable and $\det D_x\varphi(0,x) = 1$ the limit is equal to the derivative for $s = 0$. The Fréchet derivative $dJ(\Omega;v)$, therefore, is calculated with the product rule:

$$\begin{aligned} dJ(\Omega;v) &= \int_\Omega \frac{d}{ds}\left[F_1(u(s,x), D_x\varphi(s,x)^{-\top}\nabla_x u(s,x)) \det D_x\varphi(s,x)\right]_{s=0}\, dx \\ &= \int_\Omega \frac{d}{ds}\left[F_1(u(s,x), D_x\varphi(s,x)^{-\top}\nabla_x u(s,x))\right]_{s=0}\, dx \\ &+ \int_\Omega F_1(u(0,x),\nabla_x u(0,x)) \frac{d}{ds}\left[\det D_x\varphi(s,x)\right]_{s=0}\, dx \\ &=: B_1 + B_2. \end{aligned} \tag{1.15}$$

The Fréchet derivative is split in two parts B_1 and B_2. First, B_2 is calculated using Corollary 4 for the derivative of $\det D_x\varphi(s,x)$. This results in

$$\begin{aligned} B_2 &= \int_\Omega F_1(u(0,x),\nabla_x u(0,x)) \operatorname{div}(v(0,x))\, dx \\ &= \int_\Omega \operatorname{div}(F_1(u(0,x),\nabla_x u(0,x)) v(0,x))\, dx \\ &- \int_\Omega \left(\operatorname{grad}_x F_1(u(0,x),\nabla_x u(0,x)), v(0,x)\right) dx. \end{aligned} \tag{1.16}$$

The gradient $\operatorname{grad}_x(F_1(u(0,x),\nabla_x u(0,x))$ can be expressed as

$$\operatorname{grad}_x F_1(u,\nabla u) = \left(\partial_u F_1(u,\nabla u)\right)\nabla u + \left(\operatorname{grad}_{\nabla u} F_1(u,\nabla u)\right) H_u, \tag{1.17}$$

where $H_u(x)$ is the Hessian matrix of u. Then the term B_2 is expressed as

$$B_2 = \int_\Omega \left[\operatorname{div}(F_1(u, \nabla u)v) - \partial_u F_1(u, \nabla u)(\nabla u, v) - (\operatorname{grad}_{\nabla u} F_1(u, \nabla u), H_u v)\right] dx,$$

using (1.16) and (1.17). Next, B_1 as defined in (1.15) is calculated by using the chain rule:

$$\begin{aligned} B_1 = &\int_\Omega \partial_u F_1(u(0,x), \nabla u(0,x))\dot{u}(x;v)\, dx \\ &+ \int_\Omega \left(\operatorname{grad}_{\nabla u} F_1(u(0,x), \nabla u(0,x)), \frac{d}{ds}\left[D_x\varphi(s,x)^{-\top}\nabla_x u(s,x)\right]_{s=0}\right) dx. \end{aligned} \tag{1.18}$$

Using Corollary 6 for $\frac{d}{ds}\left[D_x\varphi(s,x)^{-\top}\nabla_x u(s,x)\right]_{s=0}$ in (1.18), B_1 is expressed as

$$B_1 = \int_\Omega \partial_u F_1(u, \nabla u)\dot{u} + (\operatorname{grad}_{\nabla u} F_1(u, \nabla u), \nabla u') + (\operatorname{grad}_{\nabla u} F_1(u, \nabla u), H_u v)\, dx.$$

Inserting B_1 and B_2 into the expression for the Fréchet derivative in (1.15) gives an expression of dJ by

$$\begin{aligned} dJ(\Omega; v) &= \int_\Omega \partial_u F_1(u, \nabla u)\dot{u} + (\operatorname{grad}_{\nabla u} F_1(u, \nabla u), \nabla u')\, dx \\ &\quad + \int_\Omega \operatorname{div}(F_1(u, \nabla u)v) - \partial_u F_1(u, \nabla u)(\nabla u, v)\, dx \\ &= \int_\Omega \partial_u F_1(u, \nabla u)u' + (\operatorname{grad}_{\nabla u} F_1(u, \nabla u), \nabla u') + \operatorname{div}(F_1(u, \nabla u)v)\, dx. \end{aligned}$$

In the last step Corollary 5 is used, which states

$$u'(x;v) = \dot{u}(x;v) - (\nabla u(0,x), v(0,x))$$

and the assertion is proved. □

Remark 3. *If the cost functional J in* (1.9) *depends additionally on x with*

$$J(\Omega) = \int_\Omega F_1(x, u(x), \nabla u(x))\, dx$$

then the Fréchet derivative of J is

$$\begin{aligned} dJ(\Omega; v) = &\int_\Omega (\partial_u F_1(x, u(x), \nabla u(x)))\, u'(x)\, dx \\ &+ \int_\Omega (\operatorname{grad}_{\nabla u} F_1(u(x), \nabla u(x)), \nabla u'(x))\, dx \\ &+ \int_\Omega \operatorname{div}\left[F_1(u(x), \nabla u(x))v(0,x)\right] dx \\ &+ \int_\Omega (\partial_x F_1(x, u(x), \nabla u(x)), v(0,x))\, dx \end{aligned}$$

with

$$\partial_x F_1(x, u(x), \nabla u(x)) := \frac{\partial}{\partial y} F_1(y, p, q)\Big|_{(y,p,q)=(x,u(x),\nabla u(x))}.$$

For an example for this kind of cost functionals see Example 1.

1.5 Shape Derivative for the Laplace Dirichlet Boundary Value Problem

In this section concepts for elliptic boundary value problems are used, since the Laplacian is a linear, self-adjoint elliptic operator. See the appendix for a short review of Lipschitz domains Ω and Sobolev spaces $H^s(\Omega)$. For a more detailed introduction of Sobolev spaces see [6, Chapter 3]. And for an introduction to the variational methods used in this section to solve weak formulation of the Dirichlet boundary value problem, see [10, Chapter 3].

If the material function $\tilde{u}(s,\cdot) : \Omega^s \to \mathbb{R}$ is the solution of a Dirichlet boundary value problem, the shape derivative u' is also a solution of a Dirichlet boundary value problem. In this section the Dirichlet boundary value problem is calculated which has the solution $u'(\cdot; v)$.
First, the material solution $\tilde{u}(s,\cdot)$ of the boundary value problem in (1.6) is considered for all domains Ω^s for $s \in [0, \epsilon)$, which are deformations of Ω by Definition 3. Thus, if the functions $\tilde{f}(s,\cdot) \in L^2(\Omega^s)$ and $\tilde{h}(s,\cdot) \in H^{1/2}(\Gamma^s)$ are given, the material solution $\tilde{u}(s,\cdot) \in V^s$, for

$$V^s := \{\tilde{v} \in H^1(\Omega^s) \mid \tilde{v}(y) = \tilde{h}(s,y) \quad \text{for } y \in \Gamma^s\},$$

is the solution of the weak formulation of the boundary value problem in (1.6):

$$\int_{\Omega^s} (\nabla \tilde{u}(s,y), \nabla v(y))\, dy = \int_{\Omega^s} \tilde{f}(s,y) v(y)\, dy \quad \forall v \in H_0^1(\Omega^s). \tag{1.19}$$

This problem is uniquely solvable, see [6, Theorem 4.10], since for each bounded Lipschitz domain Ω^s there exists a solution $\tilde{u}(s,\cdot) \in V^s$. Thus, the Eulerian representations $u(s,x), f(s,x)$ and $h(s,x)$ are used as introduced in Section 1.2. In particular the functions in $\Omega = \Omega^0$ are

$$u(0,x) := \tilde{u}(0, \varphi(0,x)), \quad f(0,x) := \tilde{f}(0, \varphi(0,x)), \quad h(0,x) := \tilde{h}(0, \varphi(0,x)) \quad \text{for } x \in \Omega.$$

In the following it is assumed that the shape derivatives $f'(\cdot; v) \in L^2(\Omega)$, $h'(\cdot; v) \in H^{1/2}(\Gamma)$ and $u'(\cdot; v) \in L^2(\Omega)$ as in Definition 5 exist, with the speed vector v as given in Definition 5.

Weak Formulation for u' in Ω

So, to find the boundary value for u' the weak formulation in (1.19) is considered for test functions in $C_0^\infty(\Omega^s) \subset H_0^1(\Omega^s)$,

$$\int_{\Omega^s} (\nabla \tilde{u}(s,y), \nabla \psi(y))\, dy = \int_{\Omega^s} \tilde{f}(s,y)\psi(y)\, dy \quad \forall \psi \in C_0^\infty(\Omega^s). \tag{1.20}$$

For s small enough the test function $\psi \in C_0^\infty(\Omega^s)$ is also a test function in $\Omega = \Omega^0$. This is the case since $\Omega^s = \varphi(s,\Omega)$ with φ continuous and $K = \operatorname{supp}\psi$ is compact. Therefore, there exists $\hat{s} > 0$ such that $K \subset \Omega^{\hat{s}}$ and consequently $\psi \in C_0^\infty(\Omega) \cap C_0^\infty(\Omega^s)$ for all $s \leq \hat{s}$.
Hence, if from both sides of the weak formulation (1.20) the derivative at $s = 0$ is taken, it follows that

$$\int_\Omega (\nabla u'(x;v), \nabla \psi(x))\, dx = \int_\Omega f'(x;v)\psi(x)\, dx \quad \forall \psi \in C_0^\infty(\Omega),$$

using Theorem 8, $\psi(x) = \psi(y)$ and that ψ disappears on the boundary. This means that $u' \in H^1(\Omega)$ fulfills the weak formulation of

$$-\Delta u'(x;v) = f'(x;v) \quad \text{for } x \in \Omega.$$

Dirichlet Condition u' on Γ

In the next part a Dirichlet condition for $u'(x;v)$ is calculated. Note that for a function $u \in H^1(\Omega)$ the shape derivative and the trace on Γ are not commutative, see (6.10) in the appendix for the definition of the trace γ_0^{int}. In the following the transformation from the trace of a shape derivative $\gamma_0^{int}(u')$ is converted to the shape derivative of the trace $(\gamma_0^{int} u)'$.
First, the trace of a shape derivative is

$$\gamma_0^{int}(u')(x;v) = \dot{u}(x;v) - (\nabla u(0,x), v(0,x)) \quad \text{for } x \in \Gamma.$$

For $u \in H^1(\Omega)$ its trace belongs to $H^{1/2}(\Gamma)$, cf. [10, Theorem 2.21]. Secondly, the shape derivative of the trace is

$$\begin{aligned}
\left(\gamma_0^{int} u\right)'(x;v) &= \dot{u}(x;v) - (\nabla_\Gamma u(0,x), v(0,x)) \\
&= \dot{u}(x;v) - (\nabla u(0,x), v(0,x)) + (n(x), \nabla u(0,x))(v(0,x), n(x)) \\
&= \gamma_0^{int}(u')(x;v) + \frac{\partial u(0,x)}{\partial n}(v(0,x), n(x)) \quad \text{for } x \in \Gamma.
\end{aligned} \tag{1.21}$$

With this the weak formulation of the Dirichlet condition in (1.19) is

$$\int_{\Gamma^s} \gamma_0^{int} \tilde{u}(s,y)\psi(y)\, ds_y = \int_{\Gamma^s} \tilde{h}(s,y)\psi(y)\, ds_y \quad \forall \psi \in C_0^\infty(\mathbb{R}^d).$$

If the derivative at $s = 0$ on both sides is taken the weak formulation is

$$\begin{aligned}&\int_\Gamma \left(\left(\gamma_0^{int} u\right)'(x;v) + \kappa u_{|\Gamma}(0,x)(v(0,x),n(x)) \right) \psi(x)\, ds_x \\ &= \int_\Gamma \left(h'(x;v) + \kappa h(0,x)(v(0,x),n(x))\right) \psi(x)\, ds_x \quad \forall \psi \in C_0^\infty(\mathbb{R}^d),\end{aligned}$$

see [9, Section 2.33]. This results in

$$\int_\Gamma \left(\gamma_0^{int} u\right)'(x;v)\psi(x)\, ds_x = \int_\Gamma h'(x;v)\psi(x)\, ds_x \quad \forall \psi \in C_0^\infty(\mathbb{R}^d),$$

because $u(0,\cdot) \in V^0$. Thus, $u(0,x) = h(0,x)$ for $x \in \Gamma$. Note that

$$\left(\gamma_0^{int}\psi\right)'(x;v) = \frac{\partial \psi(x)}{\partial n}(v(0,x),n(x)) = 0,$$

since $\frac{\partial \psi}{\partial n} = 0$ on Γ. Hence, applying the transformation of the shape derivatives to the boundary in (1.21) is

$$\int_\Gamma \left(\gamma_0^{int}\left(u'\right)(x;v) + \frac{\partial u(0,x)}{\partial n}(v(0,x),n(x)) \right) \psi(x)\, ds_x = \int_\Gamma h'(x;v)\psi(x)\, ds_x \quad \forall \psi \in C_0^\infty(\mathbb{R}^d).$$

Boundary Value Problem for u'

It follows that $u'(\cdot;v) \in L^2(\Omega)$ is the weak solution of

$$\begin{aligned}-\Delta_x u'(x;v) &= f'(x;v) \quad \text{for } x \in \Omega, \\ u'(x;v) &= h'(x;v) - \frac{\partial u(0,x)}{\partial n}(v(0,x),n(x)) \quad \text{for } x \in \Gamma,\end{aligned} \tag{1.22}$$

where $f'(\cdot,v) \in L^2(\Omega)$ and $h'(\cdot,v) \in H^{1/2}(\Gamma)$.

Remark 4 (Solvability in $H^1(\Omega)$)**.** *For the solvability of the Dirichlet boundary value problem (1.22) in $H^1(\Omega)$ the function*

$$\Gamma \ni x \mapsto l(x;v) := \frac{\partial u(0,x)}{\partial n}(v(0,x),n(x)) \tag{1.23}$$

has to be in $H^{1/2}(\Gamma)$ as well. If Ω is a C^1-domain then $u \in H^2(\Omega)$ and $(v(0,\cdot),n) \in C(\Gamma)$ and then

$$l(\cdot;v) \in H^{1/2}(\Gamma).$$

Therefore, there exists a solution $u'(\cdot;v) \in H^1(\Omega)$ of (1.22). But if $l(\cdot;v) \in H^{t-1/2}(\Gamma)$ with $t < 1$ the solutions of (1.22) are in $H^t(\Omega)$, see Section 2.2 for an example of this for $t = 1/2$.

1.6 The Speed Method and Admissible Speed Vector Fields

In the previous sections the tools for shape optimization were introduced, which are used in this section to give deformation by the speed method. On the other hand this section gives an explicit deformation φ, which deforms a domain $\Omega \in M$ into a domain Ω^s such that

$$J(\Omega^s) \leq J(\Omega),$$

for a given cost functional as given in Definition 1, a given set of admissible domains M as introduced in Definition 2 and s small enough. From the optimality conditions in (1.14) it follows that a deformation φ with

$$\frac{d}{ds} J(\Omega^s)\bigg|_{s=0} = dJ(\Omega; v) \leq 0$$

results in $J(\Omega^s) \leq J(\Omega)$ for s small enough. This is the case since the speed vector v gives a deformation φ, see Lemma 2. For s small enough this deformation φ can be approximated by

$$\varphi(s, x) \approx \varphi_v(s, x) := x + sv(0, x). \tag{1.24}$$

If $v(0, \cdot) \in C^0([0, \varepsilon); \mathbb{R}^d) \times C^1(U_M; \mathbb{R}^d)$ and s is small enough such that all $\varphi_v(s, x) \in U_M$ then $\varphi_v \in C^1([0, \varepsilon); \mathbb{R}^d) \times C^1(U_M; \mathbb{R}^d)$ and φ_v fulfills all conditions in Definition 3. Furthermore, the Fréchet derivative is represented with the Hadamard formula (1.11) as

$$dJ(\Omega; v) = \int_\Gamma g(x)(v(0, x), n(x))ds_x$$

with a function g depending on the material solution u. Finally, Theorem 8 shows that $dJ(\Omega; v)$ is expressed with the shape derivative $u'(\cdot; v)$, which also depends on the speed vector v. An example is the Bernoulli free boundary problem, see Section 2.3.

Consequently our original problem of finding a domain Ω^s is equivalent to finding a speed vector $v(0, \cdot)$ on the boundary with

$$dJ(\Omega; v) \leq 0, \tag{1.25}$$

$$(v(0, x), n(x)) = 0 \quad \text{for } x \in U_M \tag{1.26}$$

and there exists a shape derivative $u'(\cdot, v) \in H^r(\Omega)$ for $0 \leq r \leq 1$. If the conditions (1.25) and (1.26) are fulfilled the speed vector v is called a valid descent direction. Generally the first choice is the speed vector

$$v_G(0, x) = -g(x)n(x) \quad \text{for } x \in \Gamma \tag{1.27}$$

and this guarantees that

$$dJ(\Omega; v) = -\int_\Gamma (g(x))^2 \, dx \leq 0.$$

If $g \in L^2(\Gamma)$, the integral exists and the descent direction v_G is valid. In general for Lipschitz domains Ω the function $g \notin L^2(\Gamma)$, because it holds $g \in H^{-1/2}(\Gamma)$ only, see (2.20) in Chapter 2. The Dirichlet datum of the shape derivative u', additionally, depends on

$$l(x; v) = \frac{\partial u(x)}{\partial n}(v(0, x), n(x)).$$

For a solution $u'(\cdot; v) \in H^1(\Omega)$ the regularity $l(\cdot; v) \in H^{1/2}(\Gamma)$ is needed.
This all suggests that a higher regularity of $v(0, \cdot)$ is preferable.

Lemma 9. *Let $A : H^{-1/2}(\Gamma) \to H^{1/2}(\Gamma)$ be an $H^{-1/2}(\Gamma)$-elliptic and bounded boundary integral operator and let $gn^i \in H^{-1/2}(\Gamma)$ be for $i = 1, \ldots, d$ then the speed vector $v_A = \left(v_A^1, \ldots, v_A^d\right)^\top$ with*

$$\begin{aligned} v_A^i(0, x) &= -A(gn^i)(x) \quad x \in \Gamma \quad \text{for } i = 1, \ldots, d, \\ (v_A(x), n(x)) &= 0 \qquad\qquad x \in \partial U_M \end{aligned} \tag{1.28}$$

is a valid descent direction.

Proof. The condition (1.25) is fulfilled since

$$J(\Omega; v_A) = \sum_{i=1}^d \left\langle v_A^i(0, \cdot), gn^i \right\rangle_\Gamma = -\sum_{i=1}^d \left\langle A(gn^i), gn^i \right\rangle_\Gamma \leq -c \sum_{i=1}^d \left\| gn^i \right\|^2_{H^{-1/2}(\Gamma)} \leq 0.$$

□

The Lemma 9 introduces a valid descent direction v_A which is more or at least as regular as v_G. The two valid directions

$$\begin{aligned} v_G &= -gn, \\ v_A &= -A(gn). \end{aligned}$$

are compared in Chapter 4. Nevertheless, it can be stated already:
The descent direction v_A is valid for less regular g, and since g generally depends on the material solution u, and since the regularity of u depends on the regularity of the boundary of the domain Ω, v_A is valid for less regular domains Ω. In Section 2 it is shown that for the Bernoulli free boundary problem

- v_A is valid for Lipschitz domains,
- v_G is valid for C^1-domains.

In Section 1.5 it is shown that g dependents on u, for example for the shape optimization problem considered in Chapter 2

$$g(x) = \left(\lambda^2 - \left(\frac{\partial u(x)}{\partial n} \right)^2 \right).$$

For the Bernoulli free boundary problem in Chapter 2 the regularity of the shape derivative is

- $u'(\cdot; v_A) \in H^{1/2}(\Omega)$ for Lipschitz domains,
- $u'(\cdot; v_A), u'(\cdot; v_G) \in H^1(\Omega)$ for C^1-domains.

The speed vectors v_A and v_G are not the only possible valid descent directions. But independent of the choice of the descent direction v, as long as it is valid, a domain $\Omega^s = \varphi_v(s, \Omega)$ can be found by (1.24).

2 Free Boundary Shape Optimization Problem

In Chapter 1 shape optimization problems over Lipschitz domains are discussed and in Section 1.6 a speed vector v_A is introduced, see (1.28), which is in $H^{1/2}$. The the Fréchet derivative of the cost functional is given by Theorem 8, if the shape derivative $u'(\cdot; v)$ exists.
In this chapter the discussed concepts and definitions in Chapter 1 are used and then they are applied to a model problem. In particular, in Section 2.2 the shape derivative $u'(\cdot; v)$ is shown to be in $H^{1/2}(\Omega)$ if Ω is a Lipschitz domain and v is regular enough. This stands in stark contrast to $u'(\cdot; v) \in H^1(\Omega)$ if Ω is a C^1 domain and the same regularity for v. This regularity of the shape derivative is necessary to use Theorem 8 in Section 1.4 to calculate the Fréchet derivative dJ of the shape functional J in the Bernoulli free boundary problem. But the standard descent direction

- $v_G \in H^{1/2}(\Gamma)$ if Ω is a C^1-domain,
- $v_G \in H^{-1/2}(\Gamma)$ if Ω is a Lipschitz domain.

Therefore, the regularized descent direction v_A is used as introduced in Section 1.6.

Bernoulli free boundary problem

In high voltage electrical devices the prevention of an electrical breakdown is an important concern. High electrical field strength on the boundary can damage the device. This can be modeled by using the normal flux of the electrical potential.
The electrical field strength on the boundary is minimized for a given electrical potential to reduce the stress on the boundary. Using Ohm's Law, this problem can be modeled as the Laplace equation, where a boundary has to be found such that the conormal derivative is small enough. For a domain $\Omega \subset \mathbb{R}^2$ and for linear homogeneous Dirichlet conditions the problem is called the Bernoulli free boundary problem [1, Section 1.1], but in this work the Bernoulli free boundary problem is also defined for domains Ω in $\mathbb{R}^d$ for $d = 2, 3$. It is divided into the exterior and the interior free boundary problem, depending on the location of the free boundary. This work only considers the interior free boundary problem, which is formulated in the following way: For a given bounded and connected domain $\Omega_O \subset \mathbb{R}^2$ with a fixed boundary $\Gamma_O = \partial\Omega_O$ and for a given constant $\lambda > 0$ a domain $\overline{\Omega_I} \subset \Omega_O$ with $\Gamma_I = \partial\Omega_I$ has to be found, see

Figure 2.1. Furthermore, the state function $\hat{u} : \Omega = \Omega_O \setminus \overline{\Omega}_I \to \mathbb{R}$ should satisfy

$$\begin{aligned} -\Delta \hat{u} &= 0 \quad \text{in } \Omega = \Omega_O \setminus \overline{\Omega}_I, \\ \hat{u} &= h \quad \text{on } \Gamma = \Gamma_I \cup \Gamma_O, \\ \frac{\partial \hat{u}}{\partial n} &= \lambda \quad \text{on } \Gamma_I \end{aligned} \tag{2.1}$$

with

$$h(x) := \begin{cases} 1 \text{ for } x \in \Gamma_I, \\ 0 \text{ for } x \in \Gamma_O. \end{cases} \tag{2.2}$$

This mixed boundary value problem is overdetermined, because a Neumann and a Dirichlet condition are given on the inner boundary Γ_I. This makes it possible to have the boundary Γ_I as a free parameter, when a shape optimization formulation of (2.1) is considered.

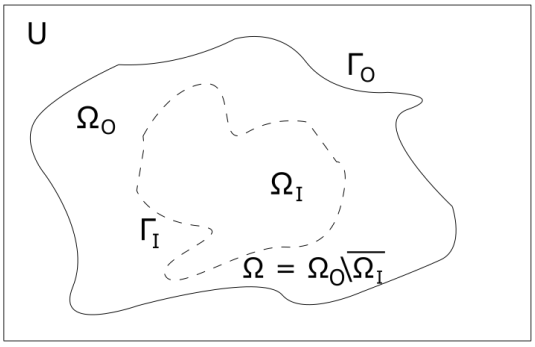

Figure 2.1: A domain Ω of the interior Bernoulli free boundary problem.

Shape Optimization Problem

As seen in Chapter 1 a shape optimization problem consists of a cost functional, see Definition 1, which depends on a function u which is the solution of a given partial differential equation and a set of admissible domains M. There are different ways of formulating the Bernoulli free boundary problem (2.1) as a shape optimization problem. For this elaboration the cost functional

$$J(\Omega) = \int_\Omega |\nabla u|^2 \, dx + \lambda^2 \int_\Omega dx \tag{2.3}$$

is minimized over M, subject to the constraint

$$\begin{aligned} -\Delta u &= 0 \quad \text{in } \Omega, \\ u &= h \quad \text{on } \Gamma. \end{aligned} \tag{2.4}$$

The solution u of (2.4) is the material solution. The boundary value problem (2.4) is as in Section 1.5 and the results from this section are applicable, i.e the shape derivative $u'(\cdot; v) \in L^2(\Omega)$ of u is the weak solution of

$$\begin{aligned} -\Delta_x u'(x; v) &= 0 \quad \text{for } x \in \Omega, \\ u'(x; v) &= h'(x; v) - \frac{\partial u(0, x)}{\partial n}(v(0, x), n(x)) \quad \text{for } x \in \Gamma. \end{aligned}$$

Admissible Domains

In this work shape optimization problems over Lipschitz domains are considered. In Section 1.6 a modification of the speed method is introduced where the speed vector v is in $H^{1/2}(\Omega)$ for Lipschitz domains Ω.
Therefore, the shape optimization problem with a cost functional J as in (2.3) is considered over all Lipschitz domains which are annulus domains, i.e. for a given fixed bounded simply connected Lipschitz domain $\Omega_O \neq \emptyset$ the set of admissible domains is

$$M = \{\Omega = \Omega_O \setminus \overline{\Omega_I} \subset \mathbb{R}^d \mid \emptyset \neq \Omega_I \,, \overline{\Omega_I} \subset \Omega_O\}. \tag{2.5}$$

This set M fulfills all conditions of Definition 2:

- All $\Omega \in M$ are bounded, because $\Omega \subset U_M = \Omega_O$ which is bounded.
- For all $\Omega \in M$ the cost functional in (2.3) is well defined. Since for each $\Omega \in M$ the boundary value problem (2.4) has a solution $u \in H^1(\Omega)$, see [6, Theorem 4.10]. This is the case, since $\Omega \in M$ is a bounded Lipschitz domains with $\Omega_I \neq \emptyset$. The solvability of (2.4) and regularity of u is discussed in more detail in Section 2.1.

The domains in M are described as a transformation of an initial domain $\Omega \in M$, as in Section 1.2. So, for $s \in [0, \epsilon)$ the transformed domain Ω^s is given by

$$\Omega^s = \{y(s) = \varphi(s, x) \text{ for } x \in \Omega\}, \tag{2.6}$$

where φ is a deformation function, see Definition 3.
The domains $\Omega^s = \Omega_O \setminus \overline{\Omega}_I^s$ have the boundary $\Gamma^s = \partial\Omega^s$, which consists of the free interior boundary $\Gamma_I^s = \partial\Omega_I^s$ and the fixed exterior boundary $\Gamma_O^s = \Gamma_O = \partial\Omega_O$, see Figure 2.1.

Additional Remarks

The solution $\hat{u}$ of the Bernoulli free boundary problem (2.1) is a solution of the minimization problem with the cost functional (2.3) subject to the constraint (2.4). But the Bernoulli free boundary problem (2.1) is not solvable for all $\lambda \geq 0$. The possible $\lambda \geq 0$, for which there exists a domain $\Omega \in M$ such that a solution of overdetemined boundary value problem in (2.1) exists, depends on the choice of the outer domain Ω_O. For example, in Section 4.1 it is shown that for a disk with radius 1 as Ω_O there exists no solution for $\lambda < e$. This results in the question which is the minimal $\lambda > 0$ such that there exists a domain $\Omega \in M$, where (2.1) is fulfilled. The question of a which is the minimal λ is considered in Section 4.5, where a possible solution for a L-shape as Ω_O is calculated. The domain $\Omega \in M$, where (2.1) is fulfilled with the minimal $\lambda \geq 0$, is the domain where the electrical field strength on the boundary is minimal.

The cost functional $J(\Omega)$ can be transferred to the boundary Γ:

$$\begin{aligned} J(\Omega) &= \int_\Omega |\nabla u(x)|^2 \, dx + \alpha \int_\Omega dx \\ &= \int_\Gamma \frac{\partial u}{\partial n}(x) u(x) \, ds_x + \alpha \int_\Omega \operatorname{div}\left(\frac{x}{d}\right) \, dx \\ &= \int_{\Gamma_I} \frac{\partial u}{\partial n}(x) \, ds_x + \int_\Gamma \frac{\alpha}{d}(x, n(x)) \, ds_x \\ &= \int_{\Gamma_I} \left(\frac{\partial u}{\partial n}(x) + \frac{\alpha}{d}(x, n(x)) \right) \, ds_x + \int_{\Gamma_O} \frac{\alpha}{d}(x, n(x)) \, ds_x. \end{aligned} \tag{2.7}$$

In our setting the cost functional $J(\Omega)$ and the descent direction v only depend on the normal derivative $\frac{\partial u}{\partial n}$ on Γ_I. Thus, the material solution u in the domain is not needed to calculate the value of $J(\Omega)$, if $\frac{\partial u}{\partial n} \in H^{-1/2}(\Gamma)$ is given.

In the following sections

- the Fréchet derivative dJ of the cost functional J,
- the shape derivative $u'(v; \cdot)$ of the material function u for the Fréchet derivative $dJ(\Omega; v)$,
- and multiple speed vector field v such that $dJ(\Omega; v) < 0$,

are calculated. This defines an iterative descent algorithm, which is used to find a local minimum of $J(\Omega)$ in M.

2.1 Material Solution and its Regularity for the Free Boundary Shape Optimization Problem

In this section the material solution in (2.4) are calculated and the regularity of the material solution is considered in different domains Ω. The material solution is the solution of a Dirichlet boundary value problem:

$$\begin{aligned} -\Delta u &= 0 \quad \text{in } \Omega, \\ u &= h \quad \text{on } \Gamma = \Gamma_I \cup \Gamma_O. \end{aligned} \tag{2.8}$$

In our case h is a constant function on Γ, therefore, h is in all $H^s(\Gamma)$ for $s \geq 0$. Thus, the regularity of h is not noted in the following regularity examination.
First, the weak formulation of the problem (2.8) is considered, where a function $u \in X = \{w \in H^1(\Omega) \mid w = h \text{ on } \Gamma\}$ has to be found which fulfills

$$a(u,v) := \int_\Omega (\nabla u, \nabla v)\, dx = 0 \quad \forall v \in H_0^1(\Omega).$$

With the Inverse Trace Theorem in [10, Theorem 2.22] an H^1-extension U of the Dirichlet datum h is defined, which is in $H^k(\Omega)$ if Ω is a $C^{k-1,1}$-domain for $1 \leq k \in \mathbb{N}$. Thus, the solution is split in $u = u_0 + \mathrm{U} \in X$ with $\mathrm{U} \in H^1(\Omega)$ being the H^1-extension of h and $u_0 \in H_0^1(\Omega)$ being the solution of

$$a(u_0, v) = -a(\mathrm{U}, v) \quad \forall v \in H_0^1(\Omega).$$

For a bounded Lipschitz domain Ω, see Definition 12, the theorem in [10, Theorem 4.6] gives $u \in H^{3/2}(\Omega)$ with

$$\|u\|_{H^{3/2}(\Omega)} \leq c_1 \|h\|_{H^1(\Gamma)}$$

and furthermore the conormal derivative $\frac{\partial u}{\partial n}$ is in $L^2(\Gamma)$ with

$$\left\| \frac{\partial u}{\partial n} \right\|_{L^2(\Gamma)} \leq c_2 \|h\|_{H^1(\Gamma)},$$

see [7, Theorem 1.1].
If Ω is a $C^{l,1}$-domain with $l \geq 1$ the theorem in [4, Theorem 2.5.1.1] states that the solution of (2.8) is $u \in H^{l+1}(\Omega)$. If Ω is a bounded $C^{l,1}$-domain and $u \in H^{l+1}(\Omega)$ then the conormal derivative is $\frac{\partial u}{\partial n} \in H^{l-1/2}(\Gamma)$, see [4, Theorem 1.5.1.2]. Therefore, the solution of (2.8) is $u \in H^{l+1}(\Omega)$ and its normal derivative is $\frac{\partial u}{\partial n} \in H^{l-1/2}(\Gamma)$, if Ω is a $C^{l,1}$-domain with $l \geq 1$.

For all the following sections of this chapter Ω is a domain in M. Consequently, Ω is a Lipschitz domain and only the regularity results proven in [10, Theorem 4.6.] are applied:

- $u \in H^{3/2}(\Omega)$,
- $\frac{\partial u}{\partial n} \in L^2(\Gamma)$.

But the results for $C^{1,1}$-domains are needed to explain why the standard speed method with v_G converges for $C^{1,1}$-domains.

2.2 Material and Shape Derivative for the Free Boundary Shape Optimization Problem

To calculate the Fréchet derivative of the cost functional $J(\Omega)$ the shape derivative of the material solution u is used, which is a derivative of the material solution over the deformation, see Section 1.3.
The constraint in (2.4) of the shape optimization problem in (2.3) is a Dirichlet boundary value problem. Therefore, the calculation done in Section 1.5 for general Dirichlet boundary value problem holds. The constraint (2.4) has for $s \in [0, \epsilon)$ the right hand side

$$f(s, y) = 0 \quad \text{for } y \text{ in } \Omega^s,$$

and the Dirichlet condition

$$h(s, y) = \begin{cases} 0 & \text{for } y \text{ on } \Gamma_O^s, \\ 1 & \text{for } y \text{ on } \Gamma_I^s. \end{cases}$$

This means $f' = 0$ and $h' = 0$ since they are constant for all $s \in [0, \epsilon)$. It follows for (1.22) that $u'(\cdot, v)$ is the solution of

$$\begin{aligned} -\Delta u'(x, v) &= 0 \quad \text{for } x \text{ in } \Omega, \\ u'(x, v) &= -\frac{\partial u(x)}{\partial n}(v(0, x), n(x)) = -l(x; v) \quad \text{for } x \text{ on } \Gamma_I, \\ u'(x, v) &= 0 \quad \text{for } x \text{ on } \Gamma_O \end{aligned} \tag{2.9}$$

with the speed vector v, see Section 1.6. In Section 2.1 it is shown that in $C^{k+1,1}$-domains for $k \geq 0$ the conormal derivative fulfills $\frac{\partial u}{\partial n} \in H^{k+1/2}(\Gamma)$ and for Lipschitz domains it holds $\frac{\partial u}{\partial n} \in L^2(\Gamma)$. That means for C^1-domains $l(\cdot; v)$ is in $H^{1/2}(\Gamma_I)$ if the speed vector field v is regular enough. Therefore, the shape derivative is $u'(\cdot; v) \in H^1(\Omega)$.
For the unique solvability of the boundary value problem (2.9) in $H^1(\Omega)$ the Dirichlet datum $l(\cdot; v) \in H^{1/2}(\Gamma_I)$ is needed, but since for Lipschitz domains Ω the conormal derivative $\frac{\partial u}{\partial n} \in L^2(\Gamma)$ this is not necessarily fulfilled.

Ultra weak Formulation of $u'(\cdot; v)$

In this section the ultra weak solution in $H^{1/2}(\Omega)$ of the Dirichlet boundary value problem in (2.9) is calculated. This is done with a ultra weak formulation but then $l(\cdot; v) \in L^2(\Gamma)$ is needed.

Lemma 10. *Let $\Omega \subset \mathbb{R}^d$ with $d = 2, 3$ be a bounded Lipschitz domain and $v \in L^2(\Gamma)$, then $l(\cdot; v) \in L^1(\Gamma)$ with*

$$\|l(\cdot; v)\|_{L^1(\Gamma)} \leq c \left(\sum_{i=1}^{d} \|v_i\|^2_{L^2(\Gamma)} \left\| \frac{\partial u}{\partial n} n_i \right\|^2_{L^2(\Gamma)} \right)^{1/2}. \tag{2.10}$$

If $\Omega \subset \mathbb{R}^2$ is a bounded Lipschitz domain and $(v, n) \in H^{1/2+\epsilon}(\Gamma)$ for $\epsilon > 0$, then it holds $l(\cdot; v) \in L^2(\Gamma)$ with

$$\|l(\cdot; v)\|_{L^2(\Gamma)} \leq c \left\| \frac{\partial u}{\partial n} \right\|_{L^2(\Gamma)} \|(v, n)\|_{H^{1+\epsilon}(\Gamma)}. \tag{2.11}$$

If $\Omega \subset \mathbb{R}^3$ is a bounded Lipschitz domain and $(v, n) \in H^{1+\epsilon}(\Gamma)$ for $\epsilon > 0$, then it holds $l(\cdot; v) \in L^2(\Gamma)$ with

$$\|l(\cdot; v)\|_{L^2(\Gamma)} \leq c \left\| \frac{\partial u}{\partial n} \right\|_{L^2(\Gamma)} \|(v, n)\|_{H^{1/2+\epsilon}(\Gamma)}. \tag{2.12}$$

Proof. In Section 2.1 the conormal derivative $\frac{\partial u}{\partial n}$ is shown to be in $\in L^2(\Gamma)$ for a Lipschitz domain Ω, this was proven in [7, Theorem 1.1]. And the estimate of the L^1-norm in (2.10) is proven with the Cauchy-Schwarz inequality:

$$\|l(\cdot; v)\|^2_{L^1(\Gamma)} = \sum_{i=1}^{d} \int_\Gamma |v_i \frac{\partial u}{\partial n} n_i| ds_x \leq c \sum_{i=1}^{d} \|v_i\|_{L^2(\Gamma)} \left\| \frac{\partial u}{\partial n} \right\|_{L^2(\Gamma)}.$$

The estimate of the L^2-norm for $\Omega \subset \mathbb{R}^2$ in (2.11) is proven with the Imbedding Theorem of Sobolev [6, Theorem 3.26]. From this theorem it follows that $(v, n) \in L^\infty(\Gamma)$ and $l(\cdot; v) \in L^2(\Gamma)$ with

$$\|l(\cdot; v)\|^2_{L^2(\Gamma)} \leq c \|(v, n)\|^2_{L^\infty(\Gamma)} \left\| \frac{\partial u}{\partial n} \right\|^2_{L^2(\Gamma)} \leq c \|(v, n)\|^2_{H^{1/2+\epsilon}(\Gamma)} \left\| \frac{\partial u}{\partial n} \right\|^2_{L^2(\Gamma)}.$$

This can be repeated for the case $\Omega \subset \mathbb{R}^3$. □

The ultra weak formulation of the Dirichlet boundary value problem in (2.9) for $u'(\cdot, v) \in H^{1/2}(\Omega)$ is

$$\langle Bu', q \rangle_\Omega := -\langle u'(\cdot; v), \Delta q \rangle_\Omega = \int_\Gamma l(x; v) \frac{\partial q(x)}{\partial n} ds_x =: F(q) \quad \forall q \in H^{3/2}(\Omega) \cap H^1_0(\Omega), \tag{2.13}$$

where the operator is defined as $B : H^{1/2}(\Omega) \to \left[H^{3/2}(\Omega) \cap H_0^1(\Omega)\right]'$. For a given $v \in H^{\frac{d-1}{2}+\epsilon}(\Gamma;\mathbb{R}^d)$ is $l(\cdot;v) \in L^2(\Gamma)$ as stated in Lemma 10. Therefore, $F : H^{3/2}(\Omega) \to \mathbb{R}$ is a linear bounded functional with

$$|F(q)| \leq c\|l(\cdot;v)\|_{L^2(\Gamma)}\|q\|_{H^{3/2}(\Omega)}, \tag{2.14}$$

where the Trace Theorem [6, Theorem 3.38] is used.

Theorem 11. *Let $\Omega \subset \mathbb{R}^d$ be a bounded Lipschitz domain for $d = 2, 3$ and $v \in H^{\frac{d-1}{2}+\epsilon}(\Gamma)$ for $\epsilon > 0$ then the ultra weak formulation in (2.13) has a solution $u'(\cdot, v) \in H^{1/2}(\Omega)$.*

Proof. The operator B is linear and bounded since

$$\begin{aligned}|\langle Bu', q\rangle_\Omega| = |\langle u'(\cdot;v), \Delta q)\rangle_\Omega| &\leq \|u'(\cdot;v)\|_{H^{1/2}(\Omega)}\|\Delta q\|_{H^{-1/2}(\Omega)} \\ &\leq c\|u'(\cdot;v)\|_{H^{1/2}(\Omega)}\|q\|_{H^{3/2}(\Omega)}.\end{aligned}$$

As shown in (2.14) F is bounded and linear. If $F \in \mathrm{Im}_{H^{1/2}(\Omega)}B$ the problem (2.13) has a solution, where the image of B is

$$\mathrm{Im}_{H^{1/2}(\Omega)}B = \{g \in \left[H^{3/2}(\Omega) \cap H_0^1(\Omega)\right]' \mid \langle g, q\rangle = 0 \quad \forall q \in \mathrm{ker}B'\},$$

see the Closed Range Theorem [10, Theorem 3.6].
The space kernel of B' is given by

$$\mathrm{ker}B' = \{q \in H^{3/2}(\Omega) \cap H_0^1(\Omega) \mid \langle Bv, q\rangle = 0 \quad \forall v \in H^{1/2}(\Omega)\} = \{0\},$$

because $q \in \mathrm{ker}B'$ is equivalent to $q \in H^{3/2}(\Omega) \cap H_0^1(\Omega)$ which is the solution of

$$-\langle \Delta q, \phi\rangle_\Omega = 0 \quad \forall \phi \in C_0^\infty(\Omega) \subset H^{1/2}(\Omega).$$

It holds $F \in \mathrm{Im}_{H^{1/2}(\Omega)}B$, because $F(q) = 0$ for all $q \in \mathrm{ker}B' = \{0\}$. □

Remark 5. *Theorem 11 only proves the solvability of the ultra weak formulation for $u'(\cdot;v) \in H^{1/2}(\Omega)$, because only the existence of a $u'(\cdot;v) \in H^{1/2}(\Omega)$ is needed. But the solution is also unique in $H^{1/2}(\Omega)$, this can be proven with the inf-sup condition [10, Theorem 3.7].*

2.3 Fréchet Derivative for the Free Boundary Shape Optimization Problem

The Fréchet derivative of the cost functional $J(\Omega)$ is defined in Section 1.4. The Hadamard formula in Theorem 7 shows that Fréchet derivative $dJ(\Omega;v)$ is linear in

the speed vector v. Additionally, in Section 1.4 it is stated that a necessary condition for $J(\Omega^s) \leq J(\Omega)$ is that the Fréchet derivative has to fulfill

$$dJ(\Omega; v) \leq 0. \tag{2.15}$$

Then a deformation of the domain Ω can be given as $\Omega^s := \varphi(s, \Omega)$. This domain Ω^s can be calculated only by the speed vector v if a $v \in C^0([0, \varepsilon); \mathbb{R}^d) \times C^1(U_M; \mathbb{R}^d)$ is chosen such that the condition (2.15) is fulfilled. This deformation is shown to exists by Lemma 2 and can be approximated by

$$\varphi_v(s, x) = x + sv(0, x).$$

Therefore, the speed vector v, which defines the deformed domain Ω^s, is calculated by finding a v such that the Fréchet derivative $dJ(\Omega; v)$ of the current domain $\Omega \in M$ is negative.

Calculation of the Fréchet Derivative

For the problem in Section 2 the cost functional is

$$J(\Omega; v) = \int_\Omega j(x, u(x), \nabla u(x))\, dx$$

with $j(x, q, \underline{p}) = \big(\underline{p}, \underline{p}\big) + \lambda^2$ with $q = u(x)$ and $\underline{p} = \nabla u(x)$, where $u := u(0, \cdot) \in H^1(\Omega)$ is material solution in 2.4. The Fréchet derivative is calculated using the derivatives of j

$$\frac{\partial j(x, q, \underline{p})}{\partial q} = 0, \quad \frac{\partial j(x, q, \underline{p})}{\partial \underline{p}} = 2\underline{p}.$$

Using these derivatives of j, Theorem 8 is applied to calculate the Fréchet derivative of $J(\Omega)$,

$$\begin{aligned} dJ(\Omega; v) &= \int_\Omega \left(\frac{\partial j(x, u(x), \nabla u(x))}{\partial q} u'(x; v) + \Big(\operatorname{grad}_{\underline{p}} j(x, u(x), \nabla u(x)), \nabla u'(x; v) \Big) \right) dx \\ &\quad + \int_\Omega \operatorname{div}(j(x, u(x), \nabla u(x)) v(0, x))\, dx \\ &= \underbrace{\int_\Omega 2(\nabla u(x), \nabla u'(x; v))\, dx}_{=:A} + \underbrace{\int_\Omega \operatorname{div}\left(\left(|\nabla u(x)|^2 + \lambda^2 \right) v(0, x) \right) dx}_{=:B}. \end{aligned} \tag{2.16}$$

Thus, the Fréchet derivative $dJ(\Omega; v)$ can be represented by two integrals which are denoted by term A and term B. For the term B in (2.16) Theorem 19 in the appendix

is used together with $(v(0,x),n(x))=0$ for x on Γ_O to conclude

$$\int_\Omega \operatorname{div}\left(\left(|\nabla u(x)|^2+\lambda^2\right)v(0,x)\right)\,dx = \int_\Gamma \left(|\nabla u(x)|^2+\lambda\right)(v(0,x),n(x))\,ds_x$$
$$= \int_{\Gamma_I}\left(|\nabla u(x)|^2+\lambda^2\right)(v(0,x),n(x))\,ds_x = \int_{\Gamma_I}\left(\frac{\partial u(x)}{\partial n}\right)^2(v(0,x),n(x))\,ds_x. \quad (2.17)$$

In the term A (2.16) the shape derivative $u'(\cdot;v)\in H^{1/2}(\Omega)$ is inserted which is a solution of the boundary value problem in (2.9). Additionally, Green's First Formula is used to conclude

$$\int_\Omega 2(\nabla u(x),\nabla u'(x;v))\,dx = 2\left(\int_\Omega -\Delta u(x)u'(x;v)\,dx + \int_\Gamma \frac{\partial u(x)}{\partial n}u'(x;v)ds_x\right).$$

The term A is well-defined by duality since $u'(\cdot;v)\in H^{1/2}(\Omega)$ and $u\in H^{3/2}(\Omega)$. The material solution $u\in H^1(\Omega)$ is a weak solution of $-\Delta u=0$ and the shape derivative $u'(\cdot;v)\in H^{1/2}(\Omega)\subset L^2(\Omega)$, then the integral

$$\int_\Omega -\Delta u u'(\cdot;v)\,dx = 0,$$

because $C_0^\infty(\Omega)$ is dense in $L^2(\Omega)$, see [6, Corollary 3.5]. Here the integral is interpreted as the duality product. Therefore, the term A has the representation on the boundary:

$$\begin{aligned} 2\int_\Omega(\nabla u(x),\nabla u'(x;v))\,dx &= 2\int_\Gamma \frac{\partial u(x)}{\partial n}u'(x;v)\,ds_x \\ &= -2\int_{\Gamma_I}\frac{\partial u(x)}{\partial n}\frac{\partial u(x)}{\partial n}(v(0,x),n(x))\,ds_x \\ &= -2\int_{\Gamma_I}\left(\frac{\partial u(x)}{\partial n}\right)^2(v(0,x),n(x))\,ds_x. \end{aligned} \quad (2.18)$$

Hadamard representation of the Fréchet derivative

Therefore, the Hadamard representation of the Fréchet derivative of the cost functional $J(\Omega)$is

$$dJ(\Omega;v) = \int_{\Gamma_I} g(x)(v(0,x),n(x))\,dx \quad (2.19)$$

with

$$g(x) = \left(\lambda^2 - \left(\frac{\partial u(x)}{\partial n}\right)^2\right) \quad \text{for } x\in\Gamma_I. \quad (2.20)$$

The function g is only defined on the interior boundary Γ_I, because the exterior boundary Γ_O is fixed and that means

$$(v(0,x),n(x))=0 \quad \text{for } x\in\Gamma_O.$$

2.4 Deformation and the Speed Vector Field for the Free Boundary Shape Optimization Problem

The deformation φ is approximated by $\varphi_v(s,x) = x + sv(0,x)$ for $x \in \overline{\Omega}$ and s sufficiently small, see (1.24). A valid speed vector field $v(0,x)$ has to fulfill

$$\int_{\Gamma_I} g(x)(v(0,x),n(x))\,ds_x = dJ(\Omega;v) \leq 0, \tag{2.21}$$

$$(v(0,x),n(x)) = 0 \quad \text{for } x \in \Gamma_O, \tag{2.22}$$

see Section 1.6. The condition (2.22) is necessary because the outer boundary Γ_O is fixed. But an easy solution for (2.22) is

$$v(0,x) = 0 \quad \text{for } x \in \Gamma_O.$$

For the free boundary problem with the cost functional J in (2.3) the function g is

$$g(x) = \left(\lambda^2 - \left(\frac{\partial u}{\partial n}(x)\right)^2\right) \quad \text{for } x \in \Gamma_I.$$

Therefore, an example for a valid speed vector field is

$$v(0,x) = v_G(x) := -g(x)n(x) \quad \text{for } x \in \Gamma_I, \tag{2.23}$$

because the descent condition in (2.21) is satisfied with

$$dJ(\Omega;v_G) = -\int_{\Gamma} g^2(x)\,ds_x \leq 0.$$

This is the standard approach, cf. [2]. For domains with C^1-boundaries this approach leads to a normal vector $n \in C(\Gamma;\mathbb{R}^d)$ so the function g is in $H^{1/2}(\Gamma)$ and so $v(0,\cdot) \in H^{1/2}(\Gamma,\mathbb{R}^d)$.
But there are some drawbacks of this approach when the domain regularity changes over the iteration or the initial domain is not C^1. An example is given in Section 4.2, where a initial piecewise C^1-boundary with corners has to be transformed into a smoother boundary. The problems in this example arise when this approach is applied to Lipschitz boundaries or even piecewise C^1-boundaries. The reason is that in general normal vector n is not in $C(\Gamma)$. And it can only be guaranteed that

$$v_G^i = gn \in H^{-1/2}(\Gamma_I) \quad \text{for } i = 1,\dots,d.$$

This work, therefore, introduces a different approach, where a speed vector field $v_A = \left(v^1,\dots;v^d\right)^\top$ with higher regularity is used. For $i = 1,\dots,d$ the speed vector has to

fulfill at least $v_A^i \in H^{1/2}(\Gamma)$ on the boundaries of Lipschitz domains to guarantee the existence of an ultra weak shape derivative $u' \in H^{1/2}(\Omega)$ in (2.13). A bounded, elliptic boundary operator $A : H^{-1/2}(\Gamma) \to H^{1/2}(\Gamma)$ is used satisfying

$$\langle Aw, w\rangle_\Gamma \geq c_1^A \|w\|^2_{H^{-1/2}(\Gamma)} \quad \forall w \in H^{-1/2}(\Gamma),$$

to achieve $v_A^i \in H^{1/2}(\Gamma)$ for $i = 1, \dots, d$. Therefore, the speed vector field $v(0,\cdot) = v_A(x) = \left(v_A^1(x), \dots, v_A^d(x)\right)^\top$ is

$$\begin{aligned} v_A^i(x) &= -A\left(gn^i\right)(x) \\ &= A\left(\left(\left(\frac{\partial u}{\partial n}\right)^2 - \lambda^2\right) n^i\right)(x) \quad \text{for } x \in \Gamma_I \end{aligned} \tag{2.24}$$

for $i = 1, \dots, d$.

Remark 6. *In Section 3.3 the Laplace single layer potential is chosen for the elliptic boundary operator A, but other choices are possible. In Remark 8 A is chosen as the the inverse of the Steklov–Poincaré Operator and this results in equivalent mixed boundary value problem for v_A.*

The weak formulation of the approach in (2.24) for a speed vector $v_A = \left(v_A^1, \dots, v_A^d\right)^\top$ with $v_A^i \in H^{1/2}(\Gamma_I)$ is

$$\int_{\Gamma_I} v_A^i(x)\psi(x)\, ds_x = \int_{\Gamma_I} A\left(\left(\left(\frac{\partial u}{\partial n}\right)^2 - \lambda^2\right) n^i\right)(x)\, \psi(x)\, ds_x \quad \forall \psi \in H^{1/2}(\Gamma_I) \tag{2.25}$$

for $i = 1, \dots, d$. This defines a valid speed vector field since A is elliptic and the descent condition in (2.21) is fulfilled with

$$\begin{aligned} dJ(\Omega; v_A) &= -\int_{\Gamma_I} \sum_{i=1}^d \left(A\left(gn^i\right)(x)\, g(x) n^i(x)\right) ds_x \\ &\leq -c_1^A \sum_{i=1}^d \left\|gn^i\right\|^2_{H^{-1/2}(\Gamma_I)} \leq 0. \end{aligned}$$

The speed vectors in (2.23) and (2.24) are not the only choices for speed vectors. All speed vectors v which fulfill the conditions (2.22) and (2.21) are possible. On the other hand, to guarantee the solvability of the problem (2.9) for the shape derivative $u' \in H^{1/2}(\Gamma)$ it is assumed that $(v, n) \in H^{1/2+\epsilon}(\Gamma)$. For the regularized approach in (2.24) it holds that

$$(v_A, n) \in H^{1/2+\epsilon}(\Gamma)$$

if $gn \in H^{-1/2+\epsilon}(\Gamma; \mathbb{R}^d)$ for a $\epsilon > 0$.
To summarize the iterative algorithm for a valid v is:

0. Choose an initial domain Ω.
1. Calculate the material solution u.
2. Calculate $g(x) = \left(\lambda^2 - \left(\frac{\partial u}{\partial n}(x)\right)^2\right)$ for $x \in \Gamma_I$.
3. Calculate the speed vector field v on Γ_I.
4. Deform the domain Ω into $\Omega^s = \{y(s) = \varphi(s, x) = x + sv(0, x),\ x \in \Omega\}$ with s small enough.
5. If $|J(\Omega^s) - J(\Omega)| \leq \delta$ stop, else go to Step 1 with the new domain $\Omega = \Omega^s$.

3 Discretization with the Boundary Element Method

In this chapter a numerical formulation of the shape optimization problem (2.3) of the Bernoulli free boundary problem is given with the boundary element method (BEM) which is also reviewed in this chapter. This shape optimization problem consists of a Dirichlet boundary value problem problem as a constraint and a boundary equation for the speed vector. Therefore, only the Dirichlet boundary value problem

$$\begin{aligned} -\Delta u &= 0 \quad \text{in } \Omega \subset \mathbb{R}^d, \\ u &= g \quad \text{on } \Gamma = \partial\Omega \end{aligned} \tag{3.1}$$

is examined. The domain $\Omega \subset \mathbb{R}^d$ is a bounded Lipschitz domain and consequently the Trace Theorem [6, Theorem 3.38] defines the Dirichlet trace $\gamma_0^{int} u \in H^{1/2}(\Gamma)$ and the conormal derivative $\gamma_1^{int} u \in H^{-1/2}(\Gamma)$ for solutions $u \in H^1(\Omega)$ of (3.1).
In this chapter the concepts used in the boundary element method are only reviewed for a more in-depth introduction see [6] and [10]. First, the fundamental solution to the Laplace operator is introduced as given in [6] and [10].

Lemma 12 (Fundamental Solution)**.** *Given the Laplace-Operator*

$$(Lu)(x) := -\Delta u(x) \quad \text{for } x \in \mathbb{R}^d \tag{3.2}$$

the fundamental solution is

$$U^*(x,y) = \begin{cases} -\frac{1}{2\pi}\log(|x-y|) & \text{for } d = 2, \\ \frac{1}{4\pi}\frac{1}{|x-y|} & \text{for } d = 3 \end{cases} \tag{3.3}$$

for $x, y \in \mathbb{R}^d$, $x \neq y$.

Secondly, the representation formula gives a solution of (3.1), see [6, Theorem 7.5] and [10, p. 90]. With the fundamental solution $U^*(x,y)$ the solution u of the Laplace equation is given by the following Lemma.

Lemma 13. *The solution of $-\Delta u = 0$ is given by the representation formula*

$$u(x) = \int_\Gamma U^*(x,y)\gamma_1^{int} u(y)\, ds_y - \int_\Gamma \left[\gamma_{1,y}^{int} U^*(x,y)\right] \gamma_0^{int} u(y)\, ds_y \quad \text{for } x \in \Omega. \tag{3.4}$$

with the fundamental solution $U^*(x,y)$ as in Lemma 12.

3.1 Boundary Integral Operators

In this section the boundary integral operators are introduced which are needed for solving the Dirichlet boundary value problem (3.1) with the boundary element method. Only the single layer potential $\tilde{V}$ and the double layer potential W are introduced, for more details see [6].

3.1.1 Single Layer Potential

Definition 9. *For a bounded domain and a function w the single layer potential is defined as*

$$\left(\tilde{V}w\right)(x) = \int_\Gamma U^*(x,y)w(y)\,ds_y \quad \text{for } x \in \Omega \cup \Omega^{ext}, \tag{3.5}$$

where $\Omega^{ext} = \mathbb{R}^d \setminus \overline{\Omega}$ is the exterior domain.

Lemma 14. *Let $\Omega \subset \mathbb{R}^d$ be a bounded Lipschitz domain, then the single layer potential has the following properties:*

1. *$\tilde{V} : H^{-1/2}(\Gamma) \to H^1(\Omega)$ is bounded and linear with*

$$\left\|\tilde{V}w\right\|_{H^1(\Omega)} \leq c_0^{\tilde{V}} \|w\|_{H^{-1/2}(\Gamma)} \quad \forall w \in H^{-1/2}(\Gamma). \tag{3.6}$$

2. *For $w \in H^{-1/2}(\Gamma)$ the single layer potential is a weak solution of the Laplace equation in $\Omega \cup \Omega^{ext}$:*

$$-\Delta\left(\tilde{V}w\right)(x) = 0 \quad \text{for } x \in \Omega \cup \Omega^{ext}. \tag{3.7}$$

3. *The single layer boundary integral operator $V := \gamma_0^{int}\tilde{V} : H^{-1/2}(\Gamma) \to H^{1/2}(\Gamma)$ is bounded and linear with*

$$\|Vw\|_{H^{1/2}(\Gamma)} \leq c_0^V \|w\|_{H^{-1/2}(\Gamma)} \quad \forall w \in H^{-1/2}(\Gamma). \tag{3.8}$$

4. *For $w \in L_\infty(\Gamma)$ the single layer boundary integral operator V can be represented as*

$$(Vw)(x) = \int_\Gamma U^*(x,y)w(y)\,ds_y \quad \text{for } x \in \Gamma. \tag{3.9}$$

5. *Let $\Omega \subset \mathbb{R}^d$ for $d = 2, 3$. If $d = 2$ an additionally requirement is $\operatorname{diam}(\Omega) < 1$. Then the single layer boundary integral operator V is $H^{-1/2}$-elliptic with*

$$\langle Vw, w\rangle_\Gamma \geq c_1^V \|w\|^2_{H^{-1/2}(\Gamma)} \quad \forall w \in H^{-1/2}(\Gamma). \tag{3.10}$$

6. $\gamma_1^{int}\tilde{V} : H^{-1/2}(\Gamma) \to H^{-1/2}(\Gamma)$ *is bounded and linear with*

$$\left\|\gamma_1^{int}\tilde{V}w\right\|_{H^{-1/2}(\Gamma)} \leq c_0^{\gamma_1^{int}\tilde{V}}\|w\|_{H^{-1/2}(\Gamma)} \quad \forall w \in H^{-1/2}(\Gamma). \tag{3.11}$$

7. *Let $w \in H^{-1/2}(\Gamma)$. Then the conormal trace of the single layer potential can be represented as*

$$\left\langle \gamma_1^{int}\tilde{V}w, v\right\rangle_\Gamma = \langle \sigma w + (K'w), v\rangle_\Gamma \quad \forall v \in H^{1/2}(\Gamma), \tag{3.12}$$

with the adjoint double layer boundary integral operator

$$(K'w)(x) = \lim_{\epsilon\to 0}\int_{y\in\Gamma:\,|y-x|\geq\epsilon} \gamma_{1,x}^{int}U^*(x,y)w(y)\,ds_y \quad \text{for } x \in \Gamma \tag{3.13}$$

and

$$\sigma(x) = \lim_{\varepsilon\to 0}\frac{1}{2(d-1)\pi}\frac{1}{\varepsilon^{d-1}}\int_{y\in\Omega:\,|y-x|=\epsilon} ds_y \quad \text{for } x \in \Gamma. \tag{3.14}$$

8. *The adjoint double layer boundary integral operator $K' : H^{-1/2}(\Gamma) \to H^{-1/2}(\Gamma)$ is bounded and linear:*

$$\|K'w\|_{H^{-1/2}(\Gamma)} \leq c_2^{K'}\|w\|_{H^{-1/2}(\Gamma)} \quad \forall w \in H^{-1/2}(\Gamma).$$

Proof. 1. is given in [6, Theorem 6.11] and [10, Lemma 6.6].
2. is given in [6, p. 202] and [10, Lemma 6.6].
3. is given in [6, Theorem 6.11] and [10, p. 119].
4. is given in [6, p. 202] and [10, Lemma 6.7].
5. is given in [6, Theorem 8.12], [6, Theorem 8.16], [10, Lemma 6.22] and [10, Lemma 6.23].
6. is given in [6, Theorem 6.11] and [10, Lemma 6.8].
7. is given in [6, p. 219] and [10, Lemma 6.8].
8. follows from [6, Theorem 6.11] with $K' = \frac{1}{2}\left(\gamma_1^{int}\tilde{V} + \gamma_1^{ext}\tilde{V}\right)$.

□

Remark 7. *If the boundary Γ is smooth in a neighborhood of $x \in \Gamma$, that means at least differentiable, then it follows that*

$$\sigma(x) = \frac{1}{2} \quad \text{for almost all } x \in \Gamma.$$

3.1.2 Double Layer Potential

Definition 10. *For a bounded domain and a function $v \in H^{1/2}(\Gamma)$ the double layer potential is defined as*

$$(Wv)(x) = \int_\Gamma \left[\gamma_{1,y}^{int} U^*(x,y)\right] v(y)\, ds_y \quad \text{for } x \in \Omega \cup \Omega^{ext}. \tag{3.15}$$

Lemma 15. *Let $\Omega \subset \mathbb{R}^d$ be a bounded Lipschitz domain, then the double layer potential has the following properties:*

1. *$W : H^{1/2}(\Gamma) \to H^1(\Omega)$ is bounded and linear with*

$$\|Wv\|_{H^1(\Omega)} \leq c_0^W \|v\|_{H^{1/2}(\Gamma)} \quad \forall v \in H^{1/2}(\Gamma). \tag{3.16}$$

2. *For $v \in H^{1/2}(\Gamma)$ the double layer potential is a weak solution of the Laplace equation in $\Omega \cup \Omega^{ext}$:*

$$-\Delta (Wv)(x) = 0 \quad \text{for } x \in \Omega \cup \Omega^{ext}. \tag{3.17}$$

3. *Let $v \in H^{1/2}(\Gamma)$. Then the Dirichlet trace of the double layer potential is*

$$\gamma_0^{int} (Wv)(x) = (-1 + \sigma(x))\, v(x) + (Kv)(x) \quad \text{for } x \in \Gamma \tag{3.18}$$

   with the double layer boundary integral operator

$$(Kv)(x) = \lim_{\epsilon \to 0} \int_{y \in \Gamma\, |y-x| \geq \epsilon} \left[\gamma_{1,y}^{int} U^*(x,y)\right] w(y)\, ds_y \tag{3.19}$$

   and σ as in (3.14).

4. *The double layer boundary integral operator $K : H^{1/2}(\Gamma) \to H^{1/2}(\Gamma)$ is bounded and linear:*

$$\|Kv\|_{H^{1/2}(\Gamma)} \leq c_2^K \|v\|_{H^{1/2}(\Gamma)} \quad \forall w \in H^{1/2}(\Gamma).$$

Proof. 1. is given in [6, Theorem 6.11] and [10, Lemma 6.10].
2. is given in [6, p. 202] and [10, Lemma 6.10].
3. is given in [6, p. 219] and [10, Lemma 6.11].
4. follows from [6, Theorem 6.11] with $K = \gamma_1^{int} W + \gamma_1^{ext} W$.

□

3.1.3 Boundary Integral Equation for the Dirichlet Boundary Value Problem

With the single layer potential $\tilde{V}$ and the double layer potential W the solution u of the Dirichlet boundary value problem (3.1) is expressed with the representation formula in Lemma 13. Therefore, the Dirichlet datum $\gamma_0^{int}u$ and Neumann datum $\gamma_1^{int}u$ are needed on the boundary Γ. In the case of the Dirichlet boundary value problem (3.1) the Dirichlet datum $\gamma_0^{int}u$ is given, hence the Neumann datum $\gamma_1^{int}u$ has to be determined. A boundary integral equations for $\gamma_0^{int}u$ and $\gamma_1^{int}u$ is derived from applying the Dirichlet trace to the representation formula in Lemma 13 resulting in

$$\gamma_0^{int}u(x) = (1-\sigma)\,\gamma_0^{int}(x) - \left(K\gamma_0^{int}\right)(x) + \left(V\gamma_1^{int}\right)(x) \tag{3.20}$$

For the Dirichlet boundary value problem (3.1) the unknown Neumann datum $t = \gamma_1^{int}u \in H^{-1/2}(\Gamma)$ can be determined by the boundary integral equation in (3.20) resulting in

$$(Vt)(x) = \sigma(x)g(x) + (Kg)(x) \quad \text{for } x \in \Gamma. \tag{3.21}$$

As stated in Lemma 14 the single layer boundary integral operator
$V : H^{-1/2}(\Gamma) \to H^{1/2}(\Gamma)$ is bounded and $H^{-1/2}$-elliptic when assuming the additional requirement $\operatorname{diam}(\Omega) < 1$ if $\Omega \subset \mathbb{R}^2$. Hence the boundary integral equation (3.21) is uniquely solvable and the solution $t \in H^{-1/2}(\Gamma)$ is bounded with

$$\|t\|_{H^{-1/2}(\Gamma)} \leq \frac{1}{c_1^V}\left\|\left(\frac{1}{2}I + K\right)g\right\|_{H^{1/2}(\Gamma)} \leq \frac{c_1^W}{c_1^V}\|g\|_{H^{1/2}(\Gamma)}, \tag{3.22}$$

see [10, Section 7.1]. The unique solvability is proven using the Lemma of Lax Milgram [6, Lemma 2.32] and [10, Theorem 3.2]. The variational formulation of the boundary integral equation (3.21) for $t \in H^{-1/2}(\Gamma)$ is

$$\langle Vt, \psi\rangle_\Gamma = \left\langle \frac{1}{2}(I+K)g, \psi \right\rangle_\Gamma \quad \forall \psi \in H^{-1/2}(\Gamma). \tag{3.23}$$

In the next section a discrete variational formulation of (3.23) is introduced and the boundary element method.

3.2 Boundary Element Method

For the discrete solution of the boundary integral equation (3.23) finite dimensional trial spaces are introduced. These spaces are based on a parametrization of the boundary $\Gamma = \partial\Omega$. For this it is assumed that the boundary Γ is polygonal or polyhedral. If Γ is not polygonal or polyhedral, Γ is approximated with a polygonal or polyhedral

boundary. For a polygonal or polyhedral boundary Γ an exact mesh on Γ is defined as

$$\Gamma_N = \bigcup_{l=1}^{N} \overline{\tau}_l \tag{3.24}$$

with boundary elements τ_l. For a domain $\Omega \subset \mathbb{R}^2$ the boundary elements τ_l are line segments and for a domain $\Omega \subset \mathbb{R}^3$ the boundary elements τ_l are assumed to be triangles. The set of all nodes of the boundary decomposition Γ_N is given by

$$\{x_k\}_{k=1}^{M}.$$

It is assumed that this mesh is admissible, globally quasi–uniform and shape regular, for more information see [10, Section 10].
For the boundary element discretization the spaces of piecewise constant functions $S_h^0(\Gamma)$ and piecewise linear continuous functions $S_h^1(\Gamma)$ are introduced. The space of piecewise constant functions

$$S_h^0(\Gamma) = \operatorname{span}\{\psi_l^0\}_{l=1}^{N}$$

is defined by the basis functions ψ_l^0 for $l = 1, \ldots, N$:

$$\psi_l^0(x) = \begin{cases} 1 & \text{for } x \in \tau_l, \\ 0 & \text{else.} \end{cases}$$

The space of piecewise constant functions $S_h^0(\Gamma) \subset H^{-1/2}(\Gamma)$ approximates $H^{-1/2}(\Gamma)$:

Lemma 16. *For $u \in H^s(\Gamma)$ with $s \in [-1/2, 1]$ there holds the approximation property of $H^{-1/2}(\Gamma)$ by $S_h^0(\Gamma)$*

$$\inf_{v_h \in S_h^0(\Gamma)} \|u - v_h\|_{H^{-1/2}(\Gamma)} \leq c h^{s+1/2} |u|_{H^s_{PW}(\Gamma)}.$$

Proof. The approximation property for $H^s(\Gamma)$ is proven in [10, Theorem 10.4]. □

Likewise the space of piecewise linear continuous functions

$$S_h^1(\Gamma) = \operatorname{span}\{\psi_k^1\}_{k=1}^{M}$$

is defined by the basis functions ψ_k^1 for $k = 1, \ldots, M$:

$$\psi_k^1(x) = \begin{cases} 1 & \text{for } x = x_k, \\ 0 & \text{for } x = x_l \neq x_k, \\ \text{linear} & \text{else.} \end{cases}$$

Lemma 17. *For $u \in H^s(\Gamma)$ with $s \in [1/2, 2]$ there holds the approximation property of $H^{1/2}(\Gamma)$ by $S_h^1(\Gamma)$*

$$\inf_{v_h \in S_h^1(\Gamma)} \|u - v_h\|_{H^{1/2}(\Gamma)} \leq c h^{s-1/2} |u|_{H^s_{PW}(\Gamma)}.$$

Proof. The approximation property for $H^s(\Gamma)$ is proven in [10, Theorem 10.9]. □

Since the space of piecewise constant functions $S_h^0(\Gamma) \subset H^{-1/2}(\Gamma)$ approximate $H^{-1/2}(\Gamma)$ as stated in Lemma 16 there is a discrete Neumann datum $t_h \in S_h^0(\Gamma)$ which approximates $\gamma_1^{int} u \in H^{-1/2}(\Gamma)$ as

$$t_h(x) = \sum_{l=1}^{N} t_l \psi_l^0(x) \quad \text{for } x \in \Gamma.$$

The discrete Neumann datum $t_h \in X_h = S_h^0(\Gamma)$ is the solution of the discretized variational formulation

$$\langle V t_h, \nu_h \rangle_\Gamma = \left\langle \left(\frac{1}{2} I + K \right) g, \nu_h \right\rangle_\Gamma \quad \forall \nu_h \in X_h, \tag{3.25}$$

which is derived from the continuous variational formulation in $H^{-1/2}(\Gamma)$ given in (3.23). From Céa's Lemma [10, Theorem 8.1] and the boundedness of the double layer boundary operator in Lemma 15 a stability estimate follows

$$\|t_h\|_{H^{-1/2}(\Gamma)} \leq \frac{c_2^W}{c_1^V} \|g\|_{H^{1/2}(\Gamma)},$$

and from Céa's Lemma and the approximation property of $S_h^0(\Gamma)$ in Lemma 16 the error estimate

$$\|t - t_h\|_{H^{-1/2}(\Gamma)} \leq c h^{s+1/2} |t|_{H^s_{PW}(\Gamma)},$$

is concluded for $t \in H^s(\Gamma)$ with $s \in [-1/2, 1]$. For $t \in H^{\tilde{s}}(\Gamma)$ with $\tilde{s} \in [0, 1]$ an L^2-error estimate is given by

$$\|t - t_h\|_{L^2(\Gamma)} \leq c h^{\tilde{s}} |t|_{H^{\tilde{s}}{}_{PW}(\Gamma)},$$

see [10, Lemma 12.2]. The solution of the Dirichlet boundary value problem (3.1) is given by the representation formula in Lemma 13:

$$u(x) = \left(\tilde{V} \gamma_1^{int} u \right)(x) - \left(W \gamma_0^{int} u \right)(x) \quad \text{for } x \in \Omega.$$

With this a discrete solution in the domain Ω can be given by

$$u_h(x) = \left(\tilde{V} t_h \right)(x) - (W g)(x) \quad \text{for } x \in \Omega. \tag{3.26}$$

For the discrete solution u_h the following error estimate is given by [10, Theorem 12.4]:

Theorem 18. *Let $u \in H^1(\Omega)$ be the weak solution of the Dirichlet boundary value problem (3.1), let u_h the discrete solution of (3.1) given by (3.26), let $t \in H^{-1/2}(\Gamma)$ be the solution of (3.23) and let $t_h \in S_h^0(\Gamma)$ be the discrete Neumann datum which is the solution of (3.25). Then there holds the global error estimate*

$$\|u - u_h\|_{H^1(\Omega)} \leq c\|t - t_h\|_{H^{-1/2}(\Gamma)}.$$

If $t \in H^1_{PW}(\Gamma)$ and $u \in H^{5/2}(\Omega)$ there holds the error estimate in $H^1(\Omega)$ is

$$\|u - u_h\|_{H^1(\Omega)} \leq ch^{3/2}|t|_{H^1_{PW}(\Gamma)}.$$

Inserting $t_h(x) = \sum_{i=1}^N t_i \psi_i^0(x)$ into (3.25) and choosing $\nu_h = \psi_l^0$ results in

$$\sum_{i=1}^N t_i \langle V\psi_i^0, \psi_l^0 \rangle_\Gamma = \left\langle \left(\frac{1}{2}I + K\right) g, \psi_l^0 \right\rangle_\Gamma \quad \text{for } l = 1, \ldots, N.$$

This is a equivalent linear system for $\underline{t} = (t_1, \ldots, t_N)^\top$ and can be written as:

$$V_h^{0,0}\underline{t} = \underline{f} \tag{3.27}$$

with

$$\begin{aligned} V_h^{0,0}[l,k] &= \langle V\psi_k^0, \psi_l^0 \rangle_\Gamma, \\ f[l] &= \left\langle \left(\frac{1}{2}I + K\right) g, \psi_l^0 \right\rangle_\Gamma, \end{aligned} \tag{3.28}$$

for $l, l = 1, \ldots, N$. The matrix $V_h^{0,0}$ is symmetric, bounded and positive definite, since V is self-adjiont and $H^{-1/2}$-elliptic and therefore the linear system (3.27) is uniquely solvable.

3.3 Discretization of the Free Boundary Shape Optimization Problem

3.3.1 The Material Solution

For the free boundary problem in (2.1) as introduced in Chapter 2 the material solution is $u \in H^1(\Omega)$ for $\Omega \in M$ which is the weak solution of

$$\begin{aligned} -\Delta u(x) &= 0 \quad \text{for } x \in \Omega, \\ \gamma_0^{int} u(x) &= h(x) \quad \text{for } x \in \Gamma \end{aligned}$$

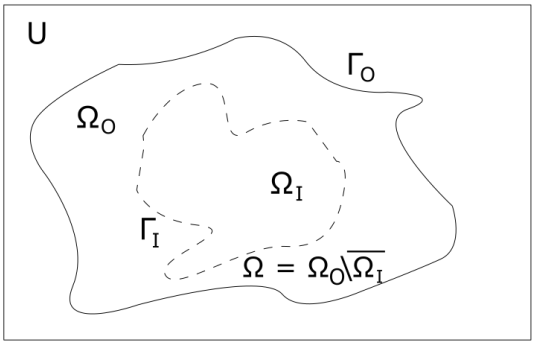

Figure 3.1: A domain Ω of the Bernoulli's free interior boundary problem.

with

$$h(x) = \begin{cases} 1 & \text{for } x \in \Gamma_I, \\ 0 & \text{for } x \in \Gamma_O. \end{cases}$$

This problem is solved in every iteration with a different $\Omega \in M$, see Figure 3.1 for an example domain Ω. The Dirichlet datum

$$h = \sum_{i=1}^{N} h_i \psi_i^0 \in S_h^0(\Gamma) \tag{3.29}$$

is zero if $\tau_i \subset \Gamma_O$ and is 1 if $\tau_i \subset \Gamma_I$. The discrete variational formulation for $t_h \in S_h^0(\Gamma)$, therefore, is

$$\langle V t_h, \nu \rangle_\Gamma = \left\langle \left(\frac{1}{2} I + K \right) h, \nu \right\rangle_\Gamma \quad \forall \nu \in S_h^0(\Gamma). \tag{3.30}$$

This can be rewritten into the equivalent linear system for $\underline{t} = (t_1, \ldots, t_N)^\top$

$$V_h^{0,0} \underline{t} = \left(\frac{1}{2} M_h^{0,0} + K_h \right) \underline{h} \tag{3.31}$$

where $V_h^{0,0}$ is defined as in (3.28), $\underline{h}$ as with (3.29) and

$$M_h^{0,0}[l,k] = \left\langle \psi_k^0, \psi_l^0 \right\rangle_\Gamma,$$
$$K_h^{0,0}[l,k] = \left\langle K \psi_k^0, \psi_l^0 \right\rangle_\Gamma$$

for $l, k = 1, \ldots, N$.

3.3.2 The Speed Vector Field

The speed vector $v = \left(v^1, \ldots, v^d\right)^\top$ with $v^i \in H^{1/2}(\Gamma)$ is the solution of the weak formulation (2.25) in Chapter 2.4 which states

$$\left\langle v^i, \phi \right\rangle_{\Gamma_I} = \left\langle V(gn^i), \phi \right\rangle_{\Gamma_I} \quad \forall \phi \in H^{1/2}(\Gamma). \tag{3.32}$$

In Section 1.6 a generic boundary integral operator A was used, but the single layer boundary integral operator V fulfills the requirement of being $H^{-1/2}$-elliptic.
To solve the equation (3.32) numerically for $i = 1, \ldots, d$ the following problems have to cleared up:

1. The variational formulation (3.32) is only formulated on the inner boundary Γ_I.
2. The Hadamard function $g = \left(\gamma_1^{int} u\right)^2 - \lambda \in H^{-1/2}(\Gamma)$ is discretized in $S_h^0(\Gamma)$.
3. It has to be decided if each component v^i for $i = 1, \ldots, d$ is considered separately and the single layer potential for the Dirichlet problem is used. Or a vector valued single layer operator V is used, to consider all parts v^i at the same time.

Some remarks on these problems and how they have been addressed in this work are summarized in the following:

1. This is solved with a submesh

   $$\Gamma_{N_I} = \bigcup_{l=1}^{N_I} \overline{\tau_l}$$

   of the closed boundary $\Gamma_I \subset \Gamma$. Therefore, the boundary mesh Γ_N can be split into two submeshes

   $$\Gamma_N = \Gamma_{N_I} \cap \Gamma_{N_O},$$

   because the inner boundary Γ_I is separated from the outer boundary Γ_O. Here Γ_{N_I} has all elements $\tau_j \subset \Gamma_I$ with $j = 1, \ldots, N_I$ and Γ_{N_O} has all elements $\tau_k \subset \Gamma_O$ with $k = N_I + 1, \ldots, N_I + N_O$, since the elements are ordered in this way that the first N_I elements are on the inner boundary Γ_I.
   Similarly the nodes can be separated in $\{x_k\}_{k=1}^{M_I}$ on Γ_I and $\{x_k\}_{k=M_I+1}^{M_I+M_O}$ on Γ_O with the number of all nodes $M = M_I + M_O$.
2. This results in an unsymmetrical matrix representation of V, since $\langle Vg, \psi_h \rangle_\Gamma$ is given with $g \in S_h^0(\Gamma)$ and $\psi_h \in S_h^1(\Gamma_I)$.
3. The single layer potential V from the Laplace problem is chosen in this work but a vector valued V is possible as well. An example for this kind of single layer potential is the linear elastostatic single layer potential, see [10, Section 6.7].

Remark 8. *Another interesting possible boundary integral operator for A is the Steklov–Poincaré Operator* $S : H^{1/2}(\Gamma) \to H^{-1/2}(\Gamma)$*, see [10, Section 6.6.3]. Then* $v_S = \left(v_S^1, \ldots, v_S^d\right)^\top$ *is the solution of the boundary integral equation*

$$Sv_S^i = gn^i \quad on\ \Gamma_I.$$

This is equivalent to a Fredholm integral equation of the second kind

$$(\sigma I + K)\left(v_S^i\right)(x) = V\left(gn^i\right)(x) \quad for\ x \in \Gamma_I,$$

which is equivalent to a mixed boundary value problem where the speed vector is $v_S^i = \gamma_1^{int} w^i$ *and the funcion* $w^i \in H^1(\Omega)$ *is the solution of*

$$\begin{aligned} -\Delta w^i(x) &= 0 \quad for\ x \in \Omega, \\ \gamma_1^{int} w^i(x) &= g(x) n^i(x) \quad for\ x \in \Gamma_I, \\ \gamma_0^{int} w^i(x) &= 0 \quad for\ x \in \Gamma_O \end{aligned}$$

for $i = 1, \ldots, d$.

This work takes $A = V$ and then the discrete variational formulation for the speed vector field $v_h^i = \sum_{n=1}^{M_I} v_n^i \psi_n^1 \in S_h^1(\Gamma_I)$ is

$$\begin{aligned} \left\langle v_h^i, \psi_h \right\rangle_{\Gamma_I} &= \langle V(gn_i), \psi_h \rangle_{\Gamma_I} \\ &= \sum_{j=1}^{N_I} \left\langle V\left(\left((t_j)^2 - \lambda\right) n_j^i \psi_j^0\right), \psi_h \right\rangle_{\Gamma_I} \quad \forall \psi_h \in S_h^1(\Gamma_N) \end{aligned} \tag{3.33}$$

for $i = 1, \ldots, d$, where $t_h = \sum_{j=1}^{N} t_j \psi_j^0 \in S_h^0(\Gamma)$ is the solution of (3.31) and $n^i = \sum_{j=1}^{N_I} n_j^i \psi_j^0$ is the normal vector on Γ_I. Thus, the equivalent linear system of (3.33) for $\underline{v}^i = \left(v_1^i, \ldots, v_{M_I}^i\right)$ for $i = 1, \ldots, d$ is

$$M_{h,I}^{1,1} \underline{v}^i = V_{h,I}^{0,1} \underline{g^i} \tag{3.34}$$

with

$$\begin{aligned} M_{h,I}^{1,1}[\tilde{l}, \tilde{k}] &= \left\langle \psi_{\tilde{k}}^1, \psi_{\tilde{l}}^1 \right\rangle_{\Gamma_I}, \\ V_{h,I}^{0,1}[\tilde{l}, k] &= \left\langle V\psi_k^0, \psi_{\tilde{l}}^1 \right\rangle_{\Gamma_I}, \\ g^i[k] &= \left((t_k)^2 - \lambda\right) n_k^i \end{aligned}$$

for $i = 1, \ldots, d$, $\tilde{l}, \tilde{k} = 1, \ldots, M_I$ and $k = 1, \ldots, N_I$. This linear system is uniquely solvable since $M_{h,I}^{1,1}$ is symmetric and positive definite. Then the deformation for Γ_I is

$$\varphi_h(s, x) = x + s v_h(x) \quad \text{for } x \in \Gamma$$

and s suitable small. The boundaries are $\Gamma_I^s = \{\varphi_h(s,x) \text{ for } x \in \Gamma_I\}$ and $\Omega^s = \Omega_O \setminus \overline{\Omega_I^s}$ where Ω_I^s is chosen such that $\partial\Omega_I^s = \Gamma_I^s$.
The step size s is chosen such that $J(\Omega^s) \leq J(\Omega)$, see Section 1.6. A possible step size s can be found with the Arminjo rule:

$$J(\Omega^s) \leq J(\Omega) + \mu s dJ(\Omega; v_h) \quad \text{for } 0 < \mu < 1.$$

The resulting procedure to find a domain Ω^s such that

$$J(\Omega^s) \leq J(\Omega)$$

from a domain Ω is:

1. Calculating an approximation $t_h = \sum_{i=1}^{N} t_i \psi_i^0$ of $\frac{\partial u}{\partial n}$ by

$$V_h^{0,0} \underline{t} = \left(\frac{1}{2} M_h^{0,0} + K_h \right) \underline{h}.$$

2. Calculating the speed vector $v_h^i = \sum_{n=1}^{M_I} v_n^i \psi_n^1$ by

$$\begin{aligned} M_{h,I}^{1,1} \underline{v^j} &= V_{h,I}^{0,1} \underline{g^j}, \\ g^j[k] &= \left(t_k^2 - \lambda\right) n_k^j \quad \text{for } j = 1, \ldots, d \end{aligned}$$

   for $k = 1, \ldots, N_I$.

3. Calculating the deformed inner boundary Γ_I^s by

$$\Gamma_I^s = \{x + s v_h \mid x \in \Gamma_I\}$$

   and $\Omega^s = \Omega_O \setminus \overline{\Omega_I^s}$ where $\partial\Omega_I^s = \Gamma_I^s$. The parameter s fulfills

$$J(\Omega^s) \leq J(\Omega) + \mu s dJ(\Omega; v_h)$$

   for a $\mu \in (0,1)$.

In Chapter 4 this procedure is used to solve the Bernoulli free boundary problem. In that chapter domains are considered with different outer boundaries Γ_O and different initial domains Ω_{init}. Furthermore, it is examined how different choices of v_h affect the convergence of domains.

4 Examples

In this chapter some numerical examples of the interior free boundary shape optimization problem are investigated. This shape optimization problem is the model problem of this work which is introduced and discussed in detail in Chapter 2. The boundary element method is used to solve these examples numerically, see Chapter 3. All example domains $\Omega \subset \mathbb{R}^2$ are bounded Lipschitz domains.

Domains in the Examples

The numerical examples in Sections 4.2 - 4.4 consider a simple domains Ω_O which is a disk with radius 1 around the center $(0, 0)$. For this outer domain Ω_O the minimizer domain $\Omega^{opt} = \Omega_O \setminus \overline{\Omega_I^{opt}}$ is calculated analytically in Section 4.1. The focus in Sections 4.2 - 4.4 is on the different initial inner domains Ω_I^0 and the effect they have on the convergence towards Ω^{opt}, especially if the initial domain Ω_I^0 is not a C^1 domain and the optimal domain Ω^{opt} is. The initial inner domains Ω_I^0 considered are:

- A square with side length 0.4 around the center $(0, 0)$, see Figure 4.1.
- A square with side length 0.4 around the center $(0.2, 0)$, see Figure 4.2.
- A L-shape with an inner angles 90°, see Figure 4.3.
- A L-shape with an inner angles 120°, see Figure 4.4.

Initial domains investigated in this work.

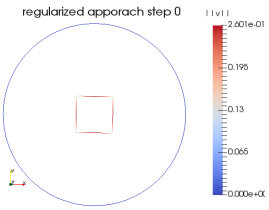

Figure 4.1: Initial domain in Section 4.2.

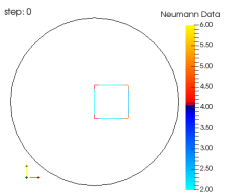

Figure 4.2: Initial domain in Section 4.3.

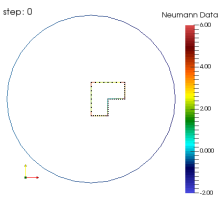

Figure 4.3: Initial domain in Section 4.4.

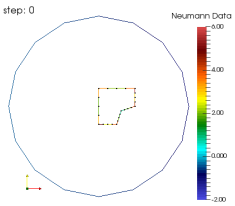

Figure 4.4: Initial domain in Section 4.4.

Additionally, in the examples in Sections 4.2 and 4.3 the difference in the shape optimization process for different choices of the speed vector field v are demonstrated for polygonal domains.

In Section 4.5 a L-shape as a outer domain Ω_O is examined. This shape is more complicated and the focus is on the optimal domain Ω^{opt} and the deformation towards Ω^{opt}. The initial inner domains Ω_I^0 are:

- A square with side length 0.2 around the center $(0.1, 0.1)$, see Figure 4.5.
- A square with side length 0.4 around the center $(-0.5, 0.5)$, see Figure 4.6.

Initial domains investigated in this work.

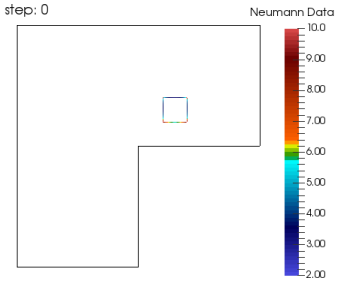

Figure 4.5: Initial domain in Section 4.5.

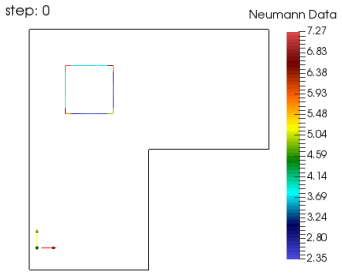

Figure 4.6: Initial domain in Section 4.5.

Additionally, in these examples the smallest possible $\lambda > 0$ is calculated such that the shape optimization problem (2.3) is solvable. As stated in Chapter 2 this λ can be interpreted as the stress on the inner boundary Γ_I.

4.1 Analytical Solution

Before the above mentioned examples are solved numerically, the analytical solution for a disk as outer domain Ω_O is calculated, because in Sections 4.2 - 4.4 the solutions of the iterative speed method are validated using this analytical optimal solution. The analytical optimal domain is called Ω^{opt}.
The shape optimization problem introduced in Chapter 2 consists of the cost functional

$$J(\Omega) = \int_\Omega |\nabla u|^2 \, dx + \lambda^2 \int_\Omega dx \tag{4.1}$$

subject to the constraint

$$\begin{aligned} -\Delta u &= 0 \quad \text{in } \Omega, \\ u &= 1 \quad \text{on } \Gamma_I, \\ u &= 0 \quad \text{on } \Gamma_O. \end{aligned} \tag{4.2}$$

The analytical solution of the optimal domain Ω^{opt} is calculated for Ω_O being a disk with radius 1 and Ω_I is assumed to be a disk with radius $0 < r_I < 1$. Therefore, the admissible domains $\Omega = \Omega_O \setminus \overline{\Omega}_I \in M$ are of the form

$$\Omega = \Omega_{r_I} = \{(r\cos(\phi), r\sin(\phi)) \mid r_I < r < 1,\ \phi \in [0, 2\pi)\}. \tag{4.3}$$

4.1.1 Calculation of the Anayltical Solution

First, the boundary value problem for the Laplace equation in (4.2) is solved using a transformation in polar coordinates. This results in the solution of (4.2):

$$u(r, \phi) = u(r) = \frac{\ln(r)}{\ln(r_I)} \quad \text{for } r \in (r_I, 1),\ \phi \in [0, 2\pi).$$

This solution $u(r, \phi)$ is inserted in the cost functional (4.1), which is expressed as a function of the interior radius r_I by

$$\begin{aligned} J(\Omega_{r_I}) = J(r_I) &= \int_\Omega |\nabla u|^2 \, dx + \lambda^2 \int_\Omega dx \\ &= \int_{r=r_I}^{1} \int_{\phi=0}^{2\pi} \frac{1}{r^2 \ln(r_I)^2} r \, dr \, d\phi + \lambda^2 \pi (1 - r_I^2) \\ &= -\frac{2\pi}{\ln(r_I)} + \lambda^2 \pi (1 - r_I^2). \end{aligned} \tag{4.4}$$

Remark 9. *Let $\lambda = 0$. Then it holds $J(r_I) \geq 0$ and $\lim_{r_I \to 0} J(r_I) = 0$. Consequently, the shape optimization problem with the cost functional*

$$\tilde{J}(\Omega) = \int_\Omega |\nabla u|^2 \, dx$$

does not have a solution domain in M, which minimizes $\tilde{J}$. Therefore, the shape optimization problem (4.1) *does not have a solution for every $\lambda \geq 0$.*

To find the radius $r_I \in (0, 1)$ such that the cost functional (4.4) is minimal the derivative of (4.4) with respect to r_I is calculated as

$$\frac{dJ(\Omega_{r_I})}{dr_I} = 2\pi \left(\frac{1}{\ln(r_I)^2 r_I} - \lambda^2 r_I \right), \tag{4.5}$$

$$\frac{d^2 J(\Omega_{r_I})}{dr_I^2} = -2\pi \left(\frac{2\ln(r_I) + \ln(r_I)^2}{(\ln(r_I)^2 r_I)^2} + \lambda^2 \right). \tag{4.6}$$

Then the radius $r_I^{opt} \in (0, 1)$, which defines the extrema domain $\Omega_{r_I^{opt}}$ of J by (4.3), is calculated by

$$0 = \left. \frac{dJ(\Omega_{r_I})}{dr_I} \right|_{r_I = r_I^{opt}} = 2\pi \left(\frac{1}{\ln(r_I^{opt})^2 r_I^{opt}} - \lambda^2 r_I^{opt} \right),$$

depending on the chosen $\lambda > 0$. This reduces to

$$\ln(r_I^{opt}) r_I^{opt} = -\frac{1}{\lambda}, \tag{4.7}$$

because $\ln(r_I^{opt}) < 0$ for $r_I^{opt} \in (0,1)$. Substituting $r_I^{opt} = e^x$ in (4.7) gives

$$xe^x = -\frac{1}{\lambda}. \tag{4.8}$$

The solution of equation (4.8) is calculated with Lambert's W-Funktion, see [3]. The Lambert's W-Funktion is defined as inverse function of

$$f(x) := xe^x,$$

see Figure 4.7, and fulfills

$$z = W(z)e^{W(z)},\ z \in \mathbb{C}.$$

The Lambert's W-function is a multi-valued function in $[-\frac{1}{e}, 0)$ and it is not defined

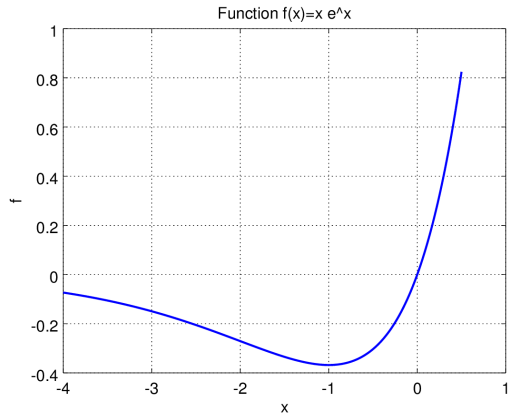

Figure 4.7: Plot of function $f(x) = xe^x$ in $[-4, 1]$.

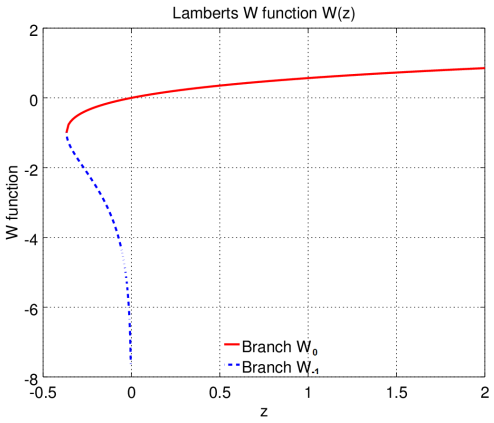

Figure 4.8: Plot of the two branches of Lambert's W-function.

for $x < -\frac{1}{e}$ and there are two real-valued branches W_0 and W_{-1}, see Figure 4.8. Therefore, the value $W(-\frac{1}{\lambda}) \in \mathbb{R}$ exists only for $\lambda \geq e^2$. Thus, for all $\lambda \geq e$ there exists at least one solution r_I^{opt}, which is explicitly given by

$$r_I^{opt} = e^{W(-\frac{1}{\lambda})}. \tag{4.9}$$

Since W is a multi-valued function in $[-\frac{1}{e}, 0)$ and $-\frac{1}{\lambda} < 0$ for $e \leq \lambda \in \mathbb{R}$ there exist two possible r_I^{opt} as in (4.9) for $\lambda > e$ and one solution for $\lambda = e$. But if the second derivative of $J(r_I)$ in (4.6) is considered it is seen that the minimizer of J is

$$\Omega^{opt} = \Omega_{r_0}$$

with

$$r_0 = e^{W_0(-\frac{1}{\lambda})}.$$

But for both domains $\Omega_{r_I^{opt}}$ with r_I^{opt} as in (4.9) the value of the conormal derivative of u in (4.2) on the interior boundary $\Gamma_I^{r_I^{opt}} = \partial\Omega_{r_I^{opt}}$

$$\left.\frac{\partial u(x)}{\partial n}\right|_{x\in\Gamma_I} = -\frac{1}{r_I^{opt}\ln(r_I^{opt})} = \lambda. \tag{4.10}$$

This shows that both domains $\Omega_{r_I^{opt}}$ are solution of the Bernoulli Free Boundary Problem.

4.1.2 Comparison between Solutions of the Bernoulli Free Boundary Problem and the Shape Optimization Problem

The shape optimization problem in (4.1) and (4.2) is derived from the Bernoulli free boundary problem (2.1), where a domain $\Omega \in M$ is found, such that $\hat{u}$ fulfills the boundary value problem

$$\begin{aligned} -\Delta\hat{u} &= 0 \quad \text{in } \Omega, \\ \hat{u} &= 1 \quad \text{on } \Gamma_I, \\ \hat{u} &= 0 \quad \text{on } \Gamma_O, \\ \frac{\partial\hat{u}}{\partial n} &= \lambda \quad \text{on } \Gamma_I. \end{aligned} \tag{4.11}$$

Generally the problem (4.11) does not have a unique solution. This is illustrated in Figure 4.9, where $\frac{\partial\hat{u}}{\partial n}$ on Γ_I is plotted for Ω as in (4.3) with the inner radius $r_I \in (0.05, 0.95)$. This shows that

- for $\lambda > e$ the problem (4.11) has two solutions,
- for $\lambda = e$ the problem (4.11) has one solution,
- for $\lambda < e$ the problem (4.11) has no solution.

This behavior corresponds to the solutions $\Omega_{r_I^{opt}}$ of $\frac{dJ(\Omega_{r_I})}{dr_I} = 0$ given by (4.9), where the number of solutions is the same as above, and these solution are the branches of the Lambert's W-function. For $\lambda = 4$ and Ω_O being a disk with radius 1 the extrema $\Omega_{r_I^{opt}}$ are given by (4.9). The two $r_I^{opt} \in \mathbb{R}$ which fulfill (4.9) are

$$\begin{aligned} r_0 &= e^{W_0(-1/4)} = 0.69949, \\ r_1 &= e^{W_{-1}(-1/4)} = 0.11610. \end{aligned}$$

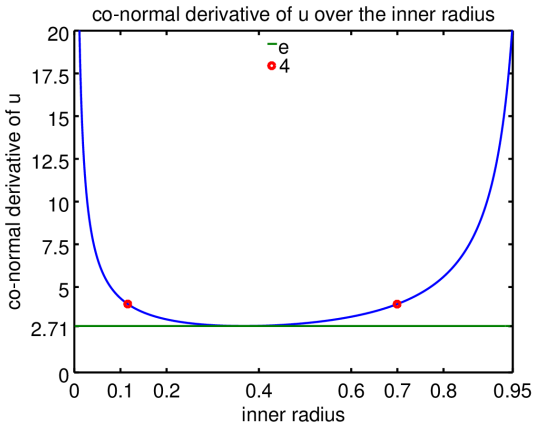

Figure 4.9: Conormal derivative $\frac{\partial u(x)}{\partial n}$ described in (4.10). The marker $\circ$ represents the radii where $\frac{\partial u(x)}{\partial n} = 4$ for $x \in \Gamma_I$.

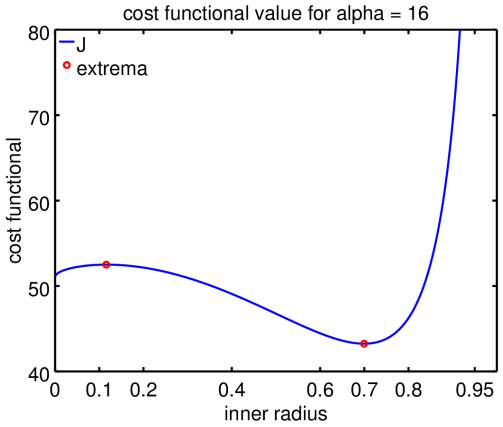

Figure 4.10: Cost functional $J(\Omega)$ described in (4.4) for $\lambda = 4$.

Therefor there are two solutions to the Bernoulli free boundary problem (4.11) with $\lambda = 4$, see Figure 4.9, which are the inner disk with radius $r_I = r_0$ and $r_I = r_1$. But Figure 4.10 shows that this domains are not both minimizer of the cost functional J. This illustrates, that all solutions of the shape optimization problem are solutions of the Bernoulli free boundary problem. On the other hand there are solutions of the Bernoulli free boundary problem which are not solutions of the shape optimization problem (4.1). This is not a general property of all shape optimization problems. Other cost functionals, which model the problem (4.11) differently, have both Ω_{r_0} and Ω_{r_1} as solutions.
Additionally, Figure 4.10 shows that for any initial domain with inner radius $r_I < r_1$ the speed method tends to a local infimum of M which is not in M this is the set where $\Omega_I = \emptyset$.
To summarize:

- An optimal domain does not exist for every $\lambda \in \mathbb{R}_+$.
- Not every domain which fulfills the Bernoulli free boundary problem (4.11) is a solution of the shape optimization problem. But every solution of the shape optimization problem fulfills (4.11).

Overview of the next few Sections

In the following sections some variations of the shape optimization problem are examined:

- Sections 4.2 - 4.4 uses $\lambda = 4$, that means the optimal radius is

$$r_I^{opt} \approx 0.6995$$

and the cost functional has the value

$$J(\Omega^{opt}) \approx 43.2106.$$

But the circle is discretized with a polygonal domain, therefore, the optimal value of the cost functional $J(\Omega)$ is slightly different.

- In Section 4.2 the outer domain is a disk with radius 1 but the initial inner domain Ω_I is a square. Thus, the shape optimization algorithm has to deform a domain with corners into a domain without corners, because the optimal domain is the annulus domain in (4.3) with $r_I = r_I^{opt} \approx 0.6995$.
- In Section 4.5 the outer domain Ω_O is a L-shape, which is a non-convex piecewise C^1-domain. Therefore, the domain Ω^{opt}, which minimizes $J(\Omega)$, is not the same as in Subsection 4.1.1. Additionally, in that section the minimal $\lambda > 0$ such that there exists a domain $\Omega^{opt} \in M$, which minimizes $J(\Omega)$, is calculated.

In the examples in Section 4.2 - 4.3 the normal approach with the speed vector v_G and the regularized approach with the speed vector v_A are compared to each other. Both are introduced in Section 2.4 and they only differ in the choice of the speed vector field v.

1. In the normal approach the speed vector field is

$$v(0,x) = v_G(x) := -g(x)n(x) \quad \text{for } x \in \Gamma_I. \tag{4.12}$$

The speed vector v_G is needed for each node x_l with $l = 1, \dots, N$ but g and n are only given for each element τ_k for $k = 1, \dots, N$. In the following it is assumed that there are two element τ_{l_1} and τ_{l_2} which are neighbors of the node x_l. Then the v_G is approximated by

$$\begin{aligned} v(x_l) = v_G(x_l) = -g(u)n(x_l) &= \left(16 - \left(\frac{\partial u(x_l)}{\partial n}\right)^2\right) n(x_l) \\ &\approx \frac{1}{2}\left(16 - \left(\frac{\partial u(\tau_{l_1})}{\partial n}\right)^2\right) n(\tau_{l_1}) + \frac{1}{2}\left(16 - \left(\frac{\partial u(\tau_{l_2})}{\partial n}\right)^2\right) n(\tau_{l_2}). \end{aligned}$$

2. In the regularized approach the speed vector field is

$$\begin{aligned} v(0,\cdot) = v_A(x) &= \left(v_A^1, \cdot, \dots, v_A^d\right)^\top, \\ v_A^i(x) &:= -V\left(gn^i\right)(x) \quad \text{for } x \in \Gamma_I \quad i = 1, \dots, d. \end{aligned} \tag{4.13}$$

For the regularized approach no additional approximation is needed since v_A is naturally given on each node x_l for $l = 1, \dots, M$.

The analysis of these two approaches is provided in Section 2.4. Most of these examples two aspects are examined:

1. **Validation**: The approximated optimal domains are compared to the theoretical optimal domain (4.3):
   a) Is the optimal domain a disk?
   b) Is the radius of the optimal domain $r_I^{opt} \approx 0.6995$?
   c) Is the cost functional $J(\Omega^{opt}) \approx 43.2106$ for the optimal domain Ω^{opt}?

   This is only possible if the outer domain Ω_O is a disk with radius 1. This is the case in Sections 4.2 - 4.4.
2. **Comparison**: The two different speed vectors (4.12) and (4.13) are compared to each other and the effect they have on the convergence of the domains:
   a) The constraint to the step size ϵ. In other words, the largest ϵ has to be found such that the speed method converges with $s < \epsilon$.
   b) Rate of convergence: Namely, how many steps does it take until the optimal domain is reached?

   The comparison of the two speed vectors is only done in Sections 4.2 - 4.3, because in the other sections no parameters were found such that the domains converge with v_G.

4.2 Box in a Circle

4.2.1 Overview

- The outer domain is $\Omega_O = \{x \in \mathbb{R}^2 \mid x_1^2 + x_2^2 < 1\}$.
- The initial inner domain is $\Omega_I^0 = \{x \in \mathbb{R}^2 \mid -0.2 < x_1, x_2 < 0.2\}$.
- The boundary Γ^0 of $\Omega^0 = \Omega_O \setminus \overline{\Omega_I^0}$ is discretized with $N = 64$ number of elements.
- The regularization parameter is $\lambda = 4$.
- The constraint ϵ to the step size s is:
  - $\epsilon = 0.5$ for the regularized approach,
  - $\epsilon \in \{0.5, 0.005\}$ for the normal approach, where it converges for $\epsilon = 0.005$ and diverges for $\epsilon = 0.5$.
- The boundary element method (BEM) is used resulting in linear systems, see (3.27) and (3.34).

As in Section 4.1 the outer domain Ω_O is a disk with radius 1 and $\lambda = 4$. But the initial domain Ω_I^0 is not a disk as seen in Figure 4.11. The optimal inner domain Ω_I^{opt} is still, as outlined in Section 4.1, a disk with radius

$$r_I^{opt} \approx 0.6995.$$

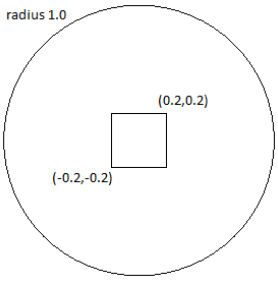

Figure 4.11: Starting domain Ω_0

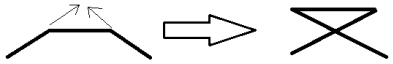

Figure 4.12: An irregular domain.

And the value of the cost functional for the optimal domain $\Omega^{opt} = \Omega_O \setminus \overline{\Omega_I^{opt}}$ is

$$J(\Omega^{opt}) \approx 43.2106.$$

The regularized approach with

$$v(x) = v_A(x) = -V(gn)(x) \quad \text{for } x \in \Gamma_I$$

manages the transition of a non-smooth initial domain to a smooth optimal domain Ω^{opt} very well, see Subsection 4.2.3. But the normal approach with

$$v(x) = v_G(x) = -g(x)n(x) \quad \text{for } x \in \Gamma_I$$

does not manage the transition as well, see Subsection 4.2.2. This means the normal approach with the speed vector v_G results in a less stable convergence from the initial domain to the optimal domain Ω^{opt}. This is seen in the needed constraint ϵ on the step size s:

- For the normal approach with v_G the domains Ω_n^i converge if the step size s is constraint by
$$s < \epsilon = 0.005,$$
where Ω_n^i is the deformation in step i, see Section 4.2.2.
- For the regularized approach with v_A the domains Ω_r^i converge if the step size is constraint by
$$s < \epsilon = 0.5,$$
where Ω_r^i is the deformation in step i, see Section 4.2.3.

Therefore, the regularized approach with v_A is much more stable than the normal with v_G if applied to domains with corners, because it deals differently with inward corners, see Remark 10.

But both algorithms do not work if the domain becomes irregular, i.e. if the domain is deformed in a way that a point is moved to far towards another element, see

Figure 4.12. If that happens then the deformation $\Omega_s \notin M$ and hence $J(\Omega_s)$ and $dJ(\Omega_s; v)$ do not make any sense any more. That means $J(\Omega_s)$ can have values smaller than the minimal value and $dJ(\Omega_s; v)$ is negative for random directions v. This could be fixed if a control for irregular domains is implemented. In the current algorithm this can only be achieved with a restriction ϵ to the step size s.

4.2.2 Normal Approach with v_G

Domains for the Normal Approach for $\epsilon = 0.5$, Steps 1, 2 and 3

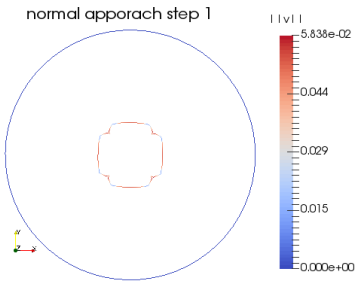

Figure 4.13: Domain after step 1 and $J(\Omega_n^1) = 51.3872$

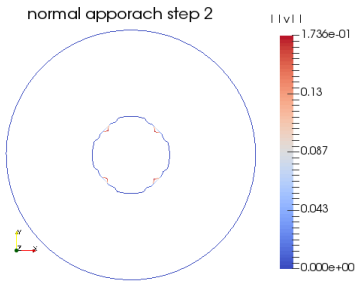

Figure 4.14: Domain after step 2 and $J(\Omega_n^2) = 51.1645$

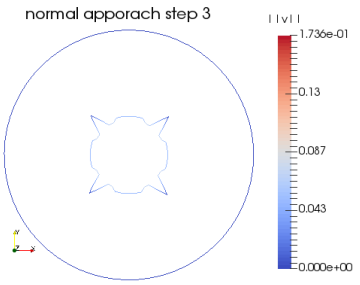

Figure 4.15: Domain after step 3 and $J(\Omega_n^3) = 51.1217$

Domains for the Normal Approach for $\epsilon = 0.5$ Steps 4, 5 and 6

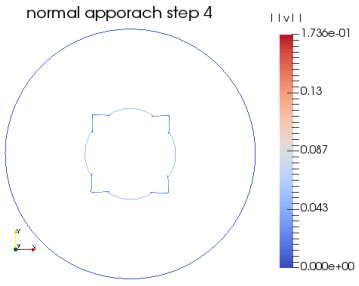

Figure 4.16: Domain after step 4 and $J(\Omega_n^4) = 49.7556$

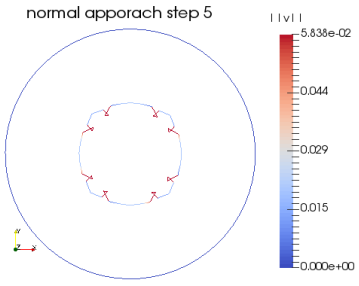

Figure 4.17: Domain after step 5 and $J(\Omega_n^5) = 48.8473$

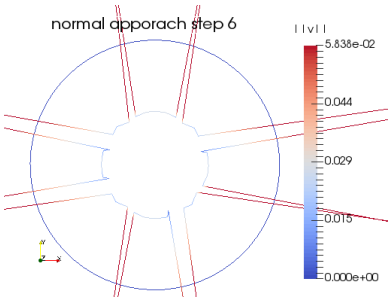

Figure 4.18: Domain after step 6 and $J(\Omega_n^6) = 33.1433$

The Figures 4.13 - 4.18 show the domains Ω_n^i calculated with the normal approach (4.12). When the parameter is $\epsilon = 0.5$ the domains Ω_n^i do not converge, because in the corners the domains oscillate and eventually get irregular. But as seen later if ϵ is small enough the first deformation from the initial domain transforms Ω_I in a disk. Then the normal approach produces domains that converge to the optimal domain

$\Omega^{opt} = \Omega_0 \setminus \overline{\Omega_I^{opt}}$.

The normal approach has deformed Ω_I into an irregular domain after the second step, see Figure 4.14. The algorithm could stop here, because $\Omega_n^2 \notin M$. When the irregular Ω_I is deformed again with the normal approach it transforms back into a regular domain for some steps, see Figures 4.15 - 4.16. This is already unforeseen, because in the irregular elements the normal vector n points in the wrong direction. The problem with the normal approach is seen in the steps 3-6:

- Figure 4.14 shows that the initial outward corners of Ω_I are transformed into inward corners.
- But in contrast to the regularized approach, the normal approach transforms inward corners into outward corners again and the domains start to oscillate and become irregular, see Figure 4.15 - 4.18.

As seen in Subsection 4.2.3, the regularized approach does not directly transform inward corners into outward corners, but makes these corners smaller until they disappear when the domain oscillates around the optimal domain. But if a restriction $s < \epsilon$

Domains for the Normal Approach for $\epsilon = 0.005$

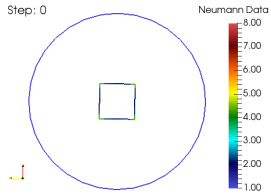

Figure 4.19: Domain before step 1.

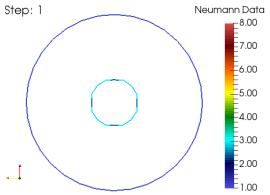

Figure 4.20: Domain after step 1.

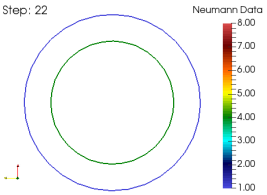

Figure 4.21: Domain after step 22.

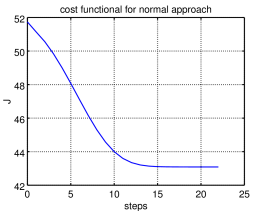

Figure 4.22: $J(\Omega)$ for the normal approach with $v = gn$

with ϵ small enough is placed on s the normal approach deforms the initial domain Ω^0 in a smooth domain. And from there on it works perfectly. For instance if

$$s < \epsilon = 0.005$$

is chosen, the normal approach does converge. But only because the first deformation transforms Ω_I into a disk. This shows that the normal approach only works if smooth domains are transformed. Therefore, it has to deform the domain Ω^0 in the first step to a smooth domain to deform the domain further.
To improve the speed of convergence, this condition could be weakened in later steps, when the shape is more regular, but this is not implemented at the moment.

Figures 4.19 - 4.21 show the domains with the normal approach for $s < 0.005$. The first step transforms Ω_I into disk, see Figure 4.20, and after that only the radius r_I grows until it reaches the optimal inner radius

$$r_I = 0.6995$$

which results in the optimal domain seen in Figure 4.21. Hence, the domains converge to the correct optimal domain, but only if the step size is kept very small and if the domain is transformed in a smooth domain in the first step.
The cost functional $J(\Omega)$ for the normal approach for $s \leq 0.005$ is seen in Figure 4.22. The figure shows that the algorithm converges and that it takes 22 steps to converge and the cost functional descends uniformly.

4.2.3 Regularized Approach with v_A

Domains for the Regularized Approach for $\epsilon = 0.5$, Steps 0, 1 and 2

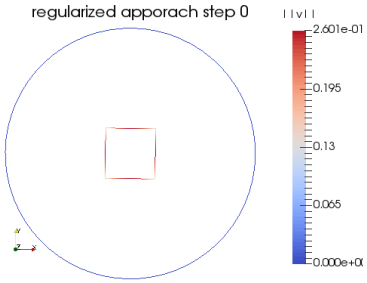

Figure 4.23: Domain before step 1 and $J(\Omega_r^0) = 51.9769$

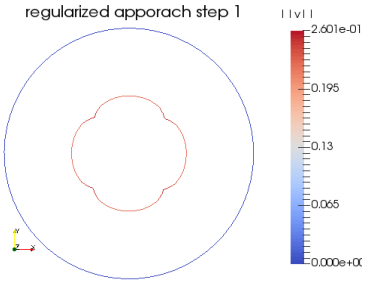

Figure 4.24: Domain after step 1 and $J(\Omega_r^1) = 48.0404$

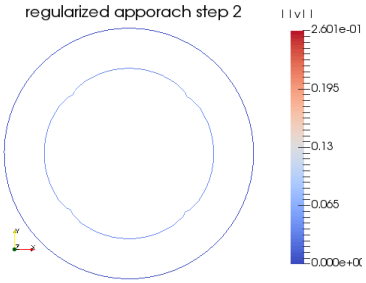

Figure 4.25: Domain after step 2 and $J(\Omega_r^2) = 43.3318$

The Figures 4.23 - 4.27 show the same initial domain deformed with the regularized approach in (4.13) with v_A. The restriction $\epsilon = 0.5$ is used again and the regularized approach produces domains Ω_r^i which converge to Ω^{opt}.
In Figures 4.24 - 4.25 it is seen that the speed vector v is larger in the corners compared to the smoother parts of the boundary, because the corners get smaller. But v is not so large as in Section 4.2.2, because the inward corner do not transform into outward corners. In step 3 onward the smooth parts are close to the optimal circle and the speed vector v on these parts is very small, see Figure 4.25. In those steps the inward corners of Ω_I get smaller (Figure 4.26) until they disappear (Figure 4.27). In the last 8 steps the domain oscillates around the optimal domain until the error is

$$|J(\Omega_r^{i-1}) - J(\Omega_r^i)| < 10^{-7},$$

then it stops. The value of the cost functional J is shown in Figure 4.28. The regularized approach with v_A shows a different behavior to the normal approach in Figure

Domains for the Regularized Approach for $\epsilon = 0.5$ Steps 3, 4 and the Cost Functional Value

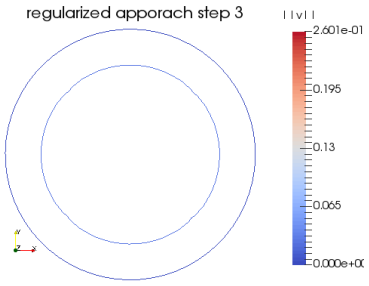

Figure 4.26: Domain after step 3 $J(\Omega_r^3) = 43.2515$

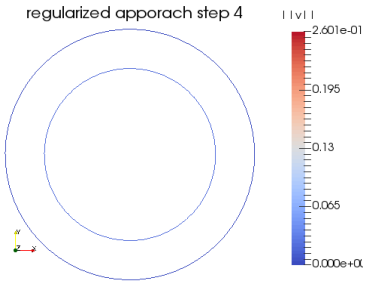

Figure 4.27: Domain after step 4. $J(\Omega_r^4) = 43.2368$

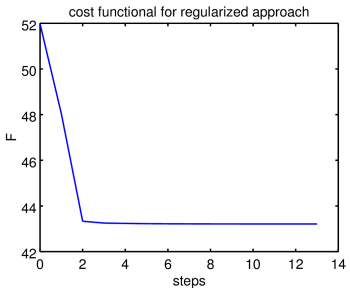

Figure 4.28: $J(\Omega)$ for the regularized approach with $v = -V(gn)$

Cost Functional Value for $\epsilon = 0.005$

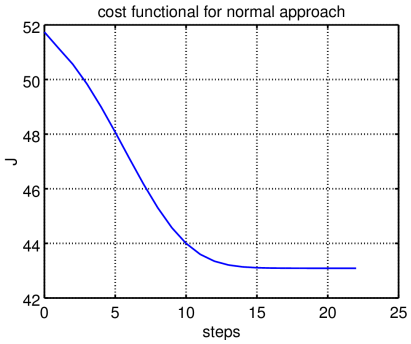

Figure 4.29: $J(\Omega)$ for the normal approach with $v = -gn$

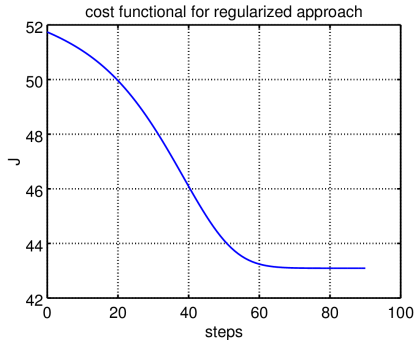

Figure 4.30: $J(\Omega)$ for the regularized approach with $v = -V(gn)$

4.22. The cost functional value decreases rapidly in the first 2 steps and then the gradient is

$$\frac{dJ(\Omega_r^i)}{di} \approx 0$$

as the domain oscillates around the optimal inner domain $\Omega_{r_I^{opt}}$ with radius $r_I^{opt} = 0.6995$. Some of this behavior could also come from the different restriction ϵ, especially the above mentioned cost functional behavior.

4.2.4 Comparison

Figures 4.29 - 4.30 show the cost functional value for both approaches. But in this simulation the restriction is $\epsilon = 0.005$ for both approaches, so that the speed of

the convergence can be compared. The regularized approach with v_A (Figure 4.30) converges more slowly than the normal approach with v_G (Figure 4.29). This and the above mentioned results suggest that the stability for general Lipschitz domains is improved with a regularized speed vector like

$$v_A = -V(gn),$$

but the speed of the convergence is reduced.

Remark 10. *As seen in Sections 4.2.2 and 4.2.3 the different choices of the speed vector field v in the two approaches has a large effect on the behavior in the inward corners. For the normal approach the speed vector is*

$$v(x) = -g(x)n(x)$$

with

$$g(x) = \left(\left(\frac{\partial u}{\partial n}(x) \right)^2 - 16 \right).$$

The normal derivative before the first step on the initial inner boundary Γ_I^0 is

$$\frac{\partial u(x)}{\partial n} \approx \begin{cases} 4.3 & \text{on the corners,} \\ 2 & \text{everywhere else.} \end{cases}$$

That means $g(x)$ is much smaller in the corners. It follows that v is smaller in the corners which get deformed less. That means the initial outward corners get deformed into inward corners.
Nearly the same happens if the regularized approach with the speed vector

$$v_i(x) = -V(gn_i)(x) \quad \text{for } i = 1, 2$$

is applied, except that the inward corners have a larger angle. That means the difference of v in the corners to v in the rest of Γ_I^0 is smaller.

When the normal approach is applied to the domain Ω_n^1 after step 1, the normal derivative for $x \in \Gamma_I$ is

$$\frac{\partial u}{\partial n}(x) \approx \begin{cases} 0 & \text{in the inward corners,} \\ 5 & \text{in the straight,} \\ 2 & \text{in between.} \end{cases}$$

That means the inward corners get deformed more than the straights, and because of the $90°$ angle of the inward corner it deforms into an irregular domain.

For the regularized approach the normal derivative for $x \in \Gamma_I$ is

$$\frac{\partial u}{\partial n}(x) \approx \begin{cases} 2 & \text{in the inward corners,} \\ 3.7 & \text{else.} \end{cases}$$

That would mean the inward corners have to be transformed more than the straights. This does happen but the regularization with V has the effect that the inward corners stay inward corners. Additionally, the angles get bigger and the corners get smaller. This behavior for inward corners makes it a lot stabler for domains with corners, because the oscillation between inward and outward corner does not happen.

4.3 Off-Center Box in a Circle

4.3.1 Overview

- The outer domain is $\Omega_O = \{x \in \mathbb{R}^2 \mid x_1^2 + x_2^2 < 1\}$.
- The initial inner domain is

$$\Omega_I^0 = \{x \in \mathbb{R}^2 \mid 0 < x_1 < 0.4;\ -0.2 < x_2 < 0.2\}.$$

- The boundary Γ^0 of $\Omega^0 = \Omega_O \setminus \overline{\Omega_I^0}$ is discretized with $N = 64$ elements.
- The regularization parameter is $\lambda = 4$.
- The constraint ϵ to the step size s is:
  - $\epsilon = 0.4$ for the regularized approach.
  - $\epsilon \in \{0.005, 0.001\}$ for the normal approach where the normal approach only converges for $\epsilon = 0.001$.
- The boundary element method (BEM) is used resulting in linear systems, see (3.27) and (3.34).

In this example Ω_O is again a disk with radius 1 as before, but the initial domain Ω_I^0 is not rotational symmetric. Thus, the deformation is not the same in all directions. The regularized approach with v_A given in (4.13) is compared to the normal approach with v_G given in (4.12), which is a regularly used approach in shape optimization.

The following issues are especially relevant in this section:

1. The maximal constraint ϵ_{max} needed for the domains to converge to the optimal domain for the different approaches is vastly different:
   - For the regularized approach $\epsilon = 0.4$ is needed for convergence,
   - For the normal approach $\epsilon = 0.001$ is needed for convergence of the domains.

2. The inner boundary converges differently towards the optimal domain, since the domain is not rotational symmetric. Consequently, the $-x_1$ side and the $+x_1$ behave differently. There are two possible ways the points of the inner domain deform:
   a) Every point deforms towards the $-x_1$ direction, which means in the optimal domain the point distribution is equal on the $-x_1$ and $+x_1$ side. This is called **moving the center**.
   b) Only the points on the $-x_1$ sides are deformed, which means in the optimal domain there are less points on the $-x_1$ side. This is called **stretching in the $-x_1$ direction**.

   The point distribution on the x_1 axis illustrates this and in the figures of the domain
   $$\Omega^i = \Omega_O \setminus \overline{\Omega_I^i} \quad \text{in steps } i$$
   the nodes are plotted as black dots.
3. The change of the normal derivative on the inner boundary during the convergence of the domains shows that the regularized approach generally oscillates more around the optimum value of 4.

4.3.2 Normal Approach with v_G

Domains for the Normal Approach for $\epsilon = 0.005$ steps 0, 1 and 2

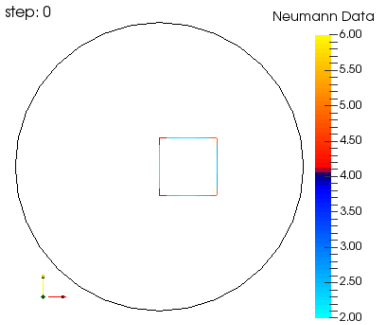

Figure 4.31:
$J(\Omega_n^0) = 52.2321$

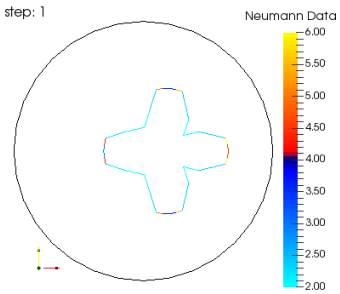

Figure 4.32:
$J(\Omega_n^1) = 50.4851$

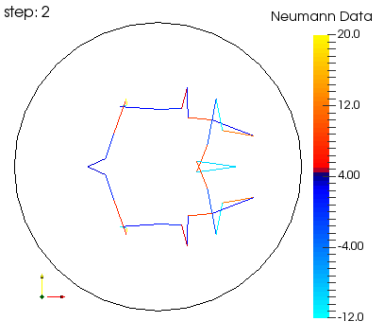

Figure 4.33:
irregular domain

First, the normal approach is applied with the speed vector v_G, as in Section 4.2.2. Figures 4.31 - 4.33 show the domains Ω_n^i in step i when the normal approach is used with the restriction $\epsilon = 0.005$. The domains do not converge although ϵ is already very small. The corners oscillate between inward and outward corners and the domain deforms into an irregular domain. The behavior of the normal and regularized approach in the corners is described in more detail in Remark 10.

Domains for the Normal Approach for $\epsilon = 0.001$

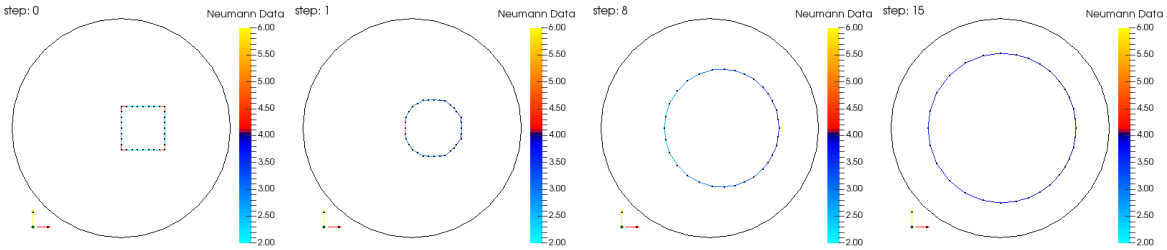

Figure 4.34: $J(\Omega_n^0) = 51.8746$

Figure 4.35: $J(\Omega_n^1) = 50.8148$

Figure 4.36: $J(\Omega_n^8) = 46.0547$

Figure 4.37: $J(\Omega_n^{15}) = 43.1742$

Cost Functional Values, Neumann Data and Point Distribution for the Normal Approach

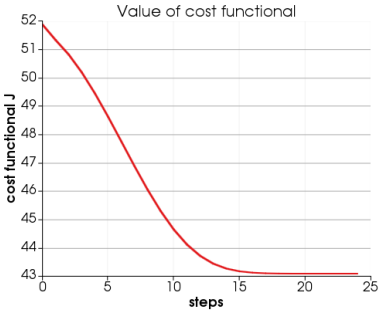

Figure 4.38: Cost functional $J(\Omega)$.

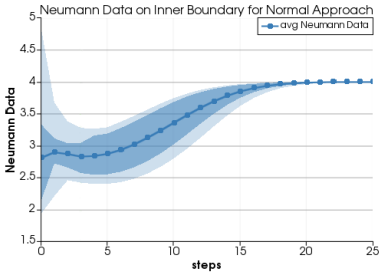

Figure 4.39: Neumann Data on the inner boundary Γ_I^i.

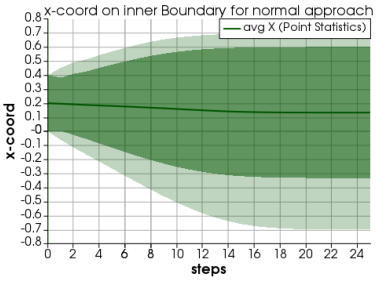

Figure 4.40: Distribution of x_1-coord of the Points on Γ_I^i.

This behavior only appears because the corners get deformed so differently then the C^1-parts between the corners. If the restriction ϵ is small enough the domain with corners gets deformed into a circle. And with this smooth domain the normal approach works very well. Figures 4.34 - 4.37 show the domains

$$\Omega_n^i = \Omega_O \setminus \overline{\Omega_I^i} \quad \text{in step } i$$

for the normal approach with the restriction $\epsilon = 0.001$.

1. The domains converge in 25 steps, see the value of the cost functional $J(\Omega_n^i)$ in the Figure 4.38 over step i.
2. Figure 4.39 shows that the Neumann data on $\Gamma_I^i = \partial\Omega_I^i$ is almost constant after step 2, because the step size is so small that Γ_I^0 deforms into a circle in step 1 and stays a circle after that.
3. Figure 4.40 shows that the distribution of the points on Γ_I^i over the x_1 coordinate are centered around $x_1 = 0.1$ and not around 0.0 which is the center of the circle. So, the inner boundary Γ_I is only stretched in the $-x_1$ direction to achieve the

correct center. But most points have a positive x_1 coordinate. This is also visible in Figure 4.37 which shows that the half circle on the $+x_1$ side is modeled by more points as the one on the $-x_1$ side. In Figure 4.37 the black dots are the nodes on Γ_I^{15}.

To summarize, the domains converge with the normal approach but the restriction $\epsilon_{max} = 0.001$ is very small. This and the results from Section 4.2 suggests that the normal approach is unstable for domains with corners, **because it only converges when the inner boundary Γ_I is transformed into a circle at the beginning and stays a circle.**

4.3.3 Regularized Approach with v_A

Domains for the Regularized Approach for $s < 0.4$ Steps 0,1 and 2

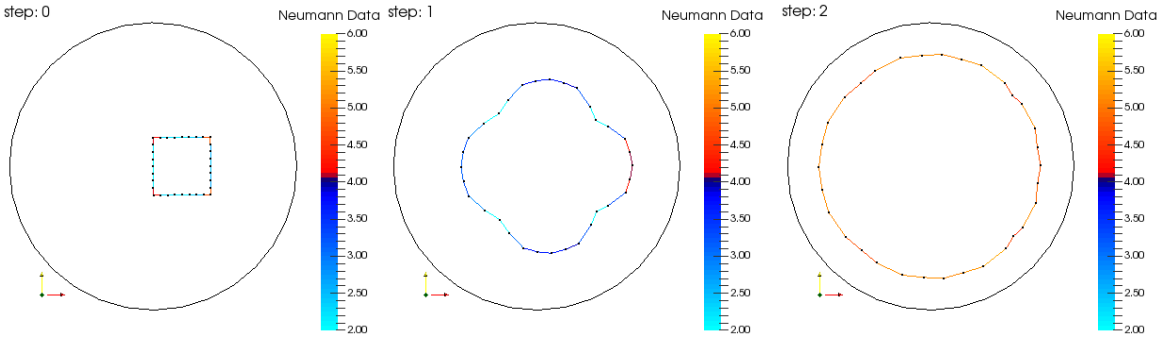

Figure 4.41: $J(\Omega_r^0) = 51.8746$

Figure 4.42: $J(\Omega_r^1) = 45.5652$

Figure 4.43: $J(\Omega_r^2) = 44.5571$

This subsection uses the regularized approach, where the speed vector is

$$v(x) = -V\left(gn\right)(x),$$

which regularizes the piecewise constant vector gn, which depends on u, with an elliptic boundary operator. This results in a continuous piecewise linear vector v. Therefore, the speed vector v in a node x_l does not have to be approximated as in Subsection 4.3.2.

The regularized approach (4.13) is applied to the given geometry with the restriction $\epsilon = 0.4$ on the step size s. Figure 4.47 shows the value of the cost functional depending on the steps and shows that the domains converge in 9 steps.
The regularized approach seems to be much more stable than the normal approach for domains with corners, because the maximum $\epsilon_{max} = 0.4$ is much larger.

The domains Ω_r^i, produced with the regularized approach, behave generally in a

Domains for the Regularized Approach for $s < 0.4$ Steps 3,4 and 5

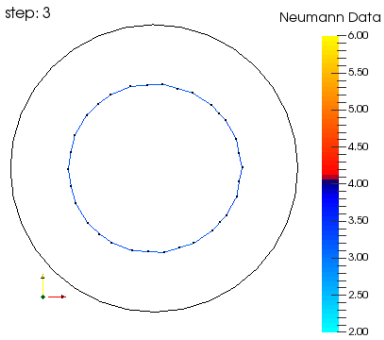

Figure 4.44:
$J(\Omega_r^3) = 44.4006$

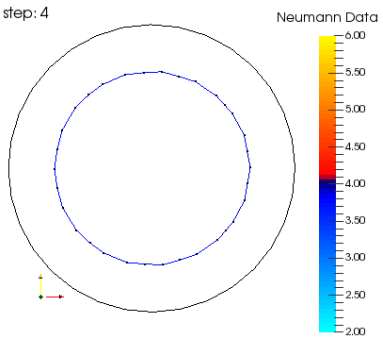

Figure 4.45:
$J(\Omega_r^4) = 43.1743$

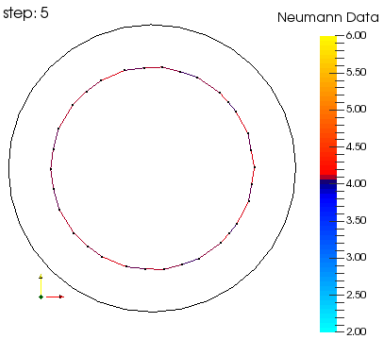

Figure 4.46:
$J(\Omega_r^5) = 43.1022$

Cost Functional Values, Neumann Data and Point Distribution for the Regularized Approach

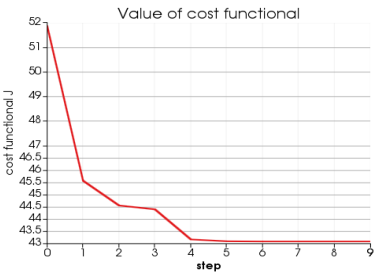

Figure 4.47: Cost functional $J(\Omega^i)$.

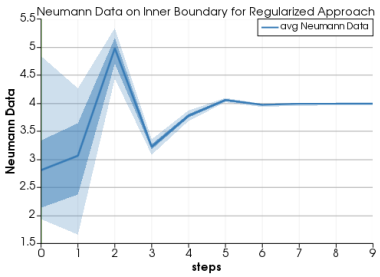

Figure 4.48: Neumann data on the inner boundary Γ_I^i.

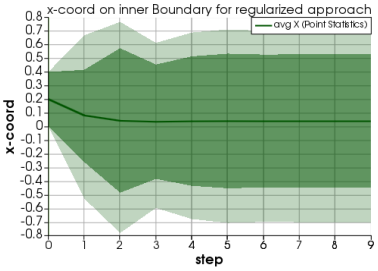

Figure 4.49: Distribution of x_1 coordinates of Points on Γ_I^i.

similar way as the normal approach as seen in Figures 4.31 - 4.32. That means if the difference

$$\left| \lambda^2 - \left(\frac{\partial u}{\partial n}(x) \right)^2 \right|$$

is large, the deformation of the domain is large at the point x, see Remark 10. Figure 4.42 shows the domain after the first step. This shape has inward corners as in the normal approach in Section 4.3.2. But the angle is not so small in the regularized approach, this is important for the convergence as explained in Section 4.3.

Figures 4.44 - 4.46 show that the corners are smoothed out when the shape becomes close to the optimal domain. This is a big difference to normal approach where the shape has to be smooth first and then it is scaled up to the optimal radius. Next, some effects are discussed which only occur if the step size is large enough:

1.) **Oscilation around the optimum**: Figure 4.48 shows that the Neumann data in step 2 is nearly constant on Γ_I and has the value 5. This is the case because the domain in step 2 is larger than the optimal domain. After that the radius of Γ_I and the average Neumann data on Γ_I oscillates around the optimum. After step 5 the oscillation becomes very small but is still there.

2.) **Moving of the center**: Figure 4.49 shows the distribution of points on the x_1-axis for the regularized approach. In step 2 the center of Γ_I is moved close to 0, that means all points are moved in contrast to Subsection 4.3.2 where only the points on the $-x_1$ side are moved.

These effects do **not** occur if the step size s is forced to be small enough. For example if $\epsilon = 0.001$ then 1) and 2) do not happen. Most likely this is the reason that they do not occur in the deformation with the normal approach in Subsection 4.3.2.

4.3.4 Conclusion

The regularized approach with v_A seems to be more stable than the normal approach for domains with corners, since the domains converge for a much larger value of ϵ. This was expected as the speed vector field v belongs to $H^{1/2}(\Gamma_I)$ if Ω is a Lipschitz domain and v_G belongs to $H^{-1/2}(\Gamma_I)$, see Section 1.6. Moreover, all points of the geometry propagate in a uniform way. But the two approaches have another significant difference:

- The normal approach first transforms the domain Ω_I in a disk and then expands and moves Ω_I.
- The regularized approach first expands and moves Ω_I and then transforms Ω_I into a disk.

The reason for this is that for general Lipschitz domains Ω_I the speed vector $v_G = (v_G^1, v_G^2)^\top$ fulfills

$$v_G^i = -gn^i \in H^{-1/2}(\Gamma_I) \quad \text{for } i = 1, 2,$$

and the speed vector $v_A = (v_A^1, v_A^2)^\top$ fulfills

$$v_A^i = -V(gn^i) \in H^{1/2}(\Gamma_I) \quad \text{for } i = 1, 2.$$

Therefore, the shape derivative is $u'(\cdot; v_A) \in H^{1/2}(\Omega)$, but for $v = v_G$ this regularity is not achieved and maybe $u'(\cdot; v_G)$ does not even exists, see Section 2.2. On the other hand the shape derivative $u'(\cdot; v) \in H^{1/2}(\Omega)$ is needed for the shape optimization problem to be solvable, see Section 2.3. But if Ω_I is a C^1-domain then $v_G^i \in H^{1/2}(\Gamma_I)$, $u'(\cdot; v_A), u'(\cdot; v_G) \in H^{1/2}(\Omega)$. Consequently, the normal approach does converge if the inner domain Ω_I is a disk.

4.4 L-Shape in a Circle

4.4.1 Overview

- The outer domain is a circle $\Omega_O = \{x \in \mathbb{R}^2 \mid x_1^2 + x_2^2 < 1\}$.
- The two initial inner domains are domains with inward corners:

$$\begin{aligned}\Omega_{I_1}^0 =&\{x \in \mathbb{R}^2 \mid 0 < x_1 < 0.4; \quad -0.2 < x_2 < 0.2\}\\ &\setminus \{x \in \mathbb{R}^2 \mid 0.2 \leq x_1 \leq 0.4; \quad -0.2 \leq x_2 \leq 0\},\\ \Omega_{I_2}^0 =&\{x \in \mathbb{R}^2 \mid 0 < x_1 < 0.4; \quad -0.2 < x_2 < 0.2\}\\ &\setminus \{x \in \mathbb{R}^2 \mid 0.2 \leq x_1 \leq 0.4; \quad -0.2 \leq x_2 \leq 3x_1 - 0.8; \quad x_2 \leq \frac{1}{3}x_1 - \frac{2}{15}\}.\end{aligned}$$

- The boundary Γ_1 of $\Omega_1^0 = \Omega_O \setminus \overline{\Omega_{I_1}^0}$ is discretized with $N = 96$ elements, 32 elements make up Γ_O and 64 make up Γ_{I_1}.
- The boundary Γ_2 of $\Omega_2^0 = \Omega_O \setminus \overline{\Omega_{I_2}^0}$ is discretized with $N = 36$ elements, 16 elements make up Γ_O and 20 make up Γ_{I_2}.
- The regularization parameter is $\lambda = 4$.
- The constraint ϵ to the step size s is 0.2 if Ω_1^0 is used and 0.1 if Ω_2^0 is used.
- Only the regularized approach (4.13) is used to deform Ω_1^0 and Ω_2^0.
- The boundary element method (BEM) is used resulting in linear systems, see (3.27) and (3.34).

This section uses only the regularized approach (4.13) with

$$v_A = -V(gn),$$

because no parameters were found where the domains calculated with normal the direction approach (4.12) with

$$v_G = -gn,$$

converges, because the initial inner domains have a inward corner. **The normal approach only works if the domain deforms into a smooth domain at the start**, see Sections 4.2 and 4.3. In Sections 4.2 - 4.3 this was possible but here $\Omega_{I_1}^0$ or $\Omega_{I_2}^0$ are used as initial inner domains and it is not possible, because of the inward corner.

4.4.2 Regularized Direction applied to $\Omega_{I_1}^0$

The regularized approach also has problems with inner domains Ω_I with inward corner with an angle $\omega < 120°$, as is seen in the following figures. But the domains still converge and the resulting optimal domain has the correct radius r_I^{opt} almost everywhere,

Domains in Steps 0, 4 and 8 for initial Domain Ω_1^0.

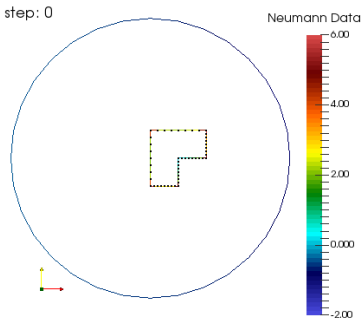

Figure 4.50:
$J(\Omega^0) = 52.2321$

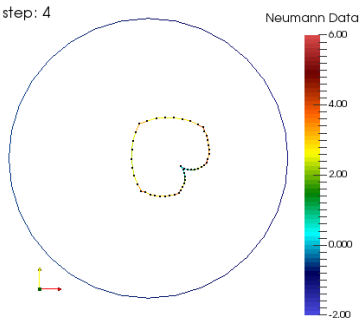

Figure 4.51:
$J(\Omega^4) = 51.1652$

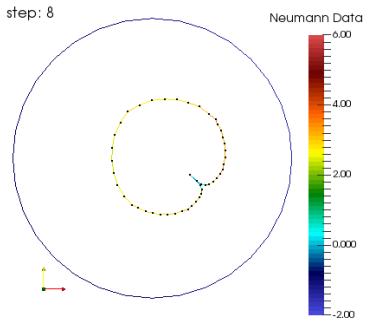

Figure 4.52:
$J(\Omega^8) = 48.7558$

Domains in Steps 12, 19 for initial Domain Ω_1^0 and Cost Function Value over all Steps.

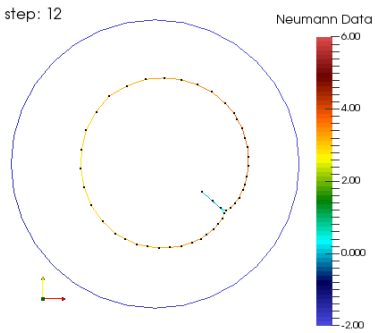

Figure 4.53:
$J(\Omega^{12}) = 44.6899$

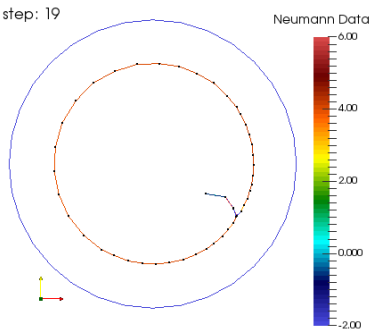

Figure 4.54:
$J(\Omega^{19}) = 43.1025$

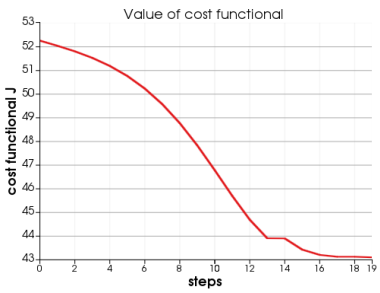

Figure 4.55: $J(\Omega^i)$ for $i \in [0, 19]$

see Figure 4.54.

Figures 4.50 - 4.53 show that the smooth parts of the inner boundary Γ_I are transformed more than the corners, this is the same behavior as in the previous examples. But because the initial angle is 90° the inner domain gets sliced. This behavior was not a problem in the previous examples, where the inward corners had larger angles and got smoothed when the domains oscillated around the optimum domain, because two conditions where met:

1. During the convergence towards the optimal domain the angle of the corner did not get smaller.
2. The number of elements in the corner has to be two, before it smooths out.

Both of this conditions are not met in this example. The angle gets smaller during

the convergence until the two sides of the corner are parallel in step 12, see Figure 4.53. And the number of elements is 16 before step 1 and 6 elements in step 12, where 4 elements are parallel to each other. And when the elements are parallel they are only transformed toward each other, because v_A is still a regularization of gn, i.e it deforms the element in the normal direction. Nevertheless, the regularized approach does still converge to a shape resembling a circle with the optimal radius, see Figure 4.54. The shape even gets temporally irregular in step 13, as shown in Figure 4.56. And the absolute value of the Neumann data explodes to 150 on the irregular part of the inner boundary Γ_I. But this does not affect the average Neumann data much as is seen in Figure 4.57 and the shape still converges.

Irregularity of the Domain in Step 13 for initial L-shape with 90° Angle.

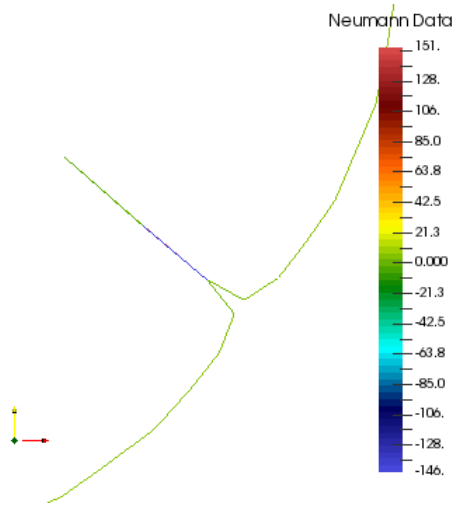

Figure 4.56: Zoom in on the slit in step 13.

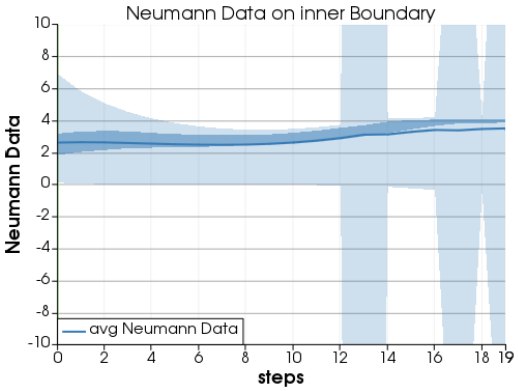

Figure 4.57: Statistical distribution of Neumann data on Γ_I^i.

Inward Corners: Next, the inward corners and their transformation are examined. Figures 4.58 and 4.59 show the corner $P1$ and four surrounding points $P2$, $P3$, $P4$, $P5$ and the speed vector v_A is represented as a vector.
The Figures 4.58 - 4.59 show that the $\|v_A\|_2$ is almost the same in all five points and that the points are deformed towards each other. The speed vector is split into a normal direction n and a tangential direction t as

$$v_A = an + bt,$$

and since $a \neq 0$ the sides of the corner gets transformed towards each other. Because the speed vector $v_A = -V(gn)$ is a regularization of $-gn$, the transformation in the tangential direction bt is not large enough in comparison to the transformation in the

Speed Vector v in the Corner for Step 1 and 4 for initial Domain 90° L-shape.

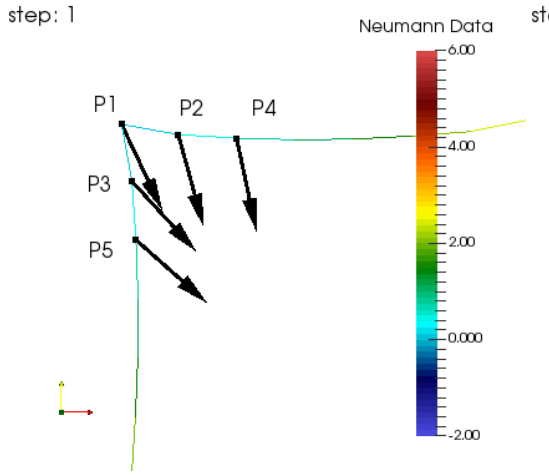

Figure 4.58: v^1 after step 1

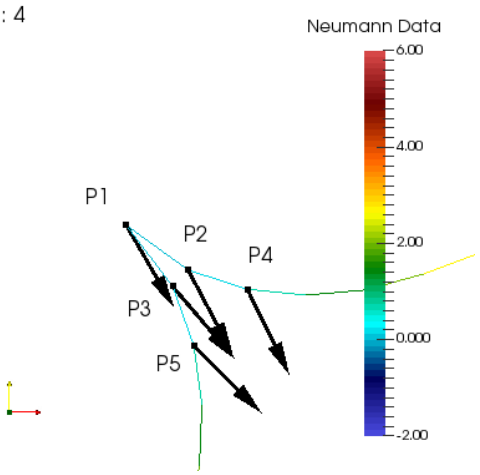

Figure 4.59: v^4 after step 4

normal direction an. And so, the corner does not get smoothed out.

To fix this a speed vector v with a larger tangential component could be considered. This means a term could be added to the original speed vector v_A:

$$v(0,x) = v_A(x) + \beta t(x). \tag{4.14}$$

A term βt can always be added because the Fréchet derivative of the cost functional $J(\Omega)$ is always zero for βt:

$$dJ(\Omega; v) = \int_{\Gamma_I} g(v_a(x) + \beta t(x), n(x))\, ds_x = \int_{\Gamma_I} g(v_a(x), n(x))\, ds_x.$$

But this is only theoretical and has not be proven to work yet. But Section 4.4.5 contains an example where the forming of the split is prevented using different meshes.

4.4.3 Regularized Direction applied to $\Omega^0_{I_2}$

The in Section 4.4.2 described problems only occur if the initial inward angle is too small. For the instance if the same algorithm is applied to the initial domain Ω^0_2, where $\Omega^0_{I_2}$ has an inward angle $w \geq 120°$, the domains do converge to a domain without slit, see Figures 4.60 - 4.64. The vector in the figures represents the speed vector v as in Figure 4.58 and 4.59.
For this example the inward corner is transformed in the same manner as the outward corners in Section 4.2. That means the angle of the Ω^i_I does not get smaller during the convergence and the number of elements in the corner reduces from 8 elements before

Domains in Steps 0, 1 and 3 for an initial Domain Ω_2^0

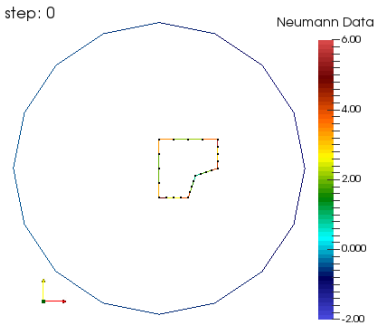

Figure 4.60: $J(\Omega^0) = 51.1540$

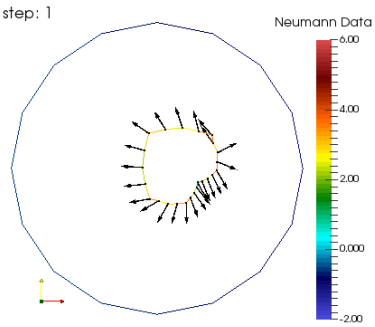

Figure 4.61: $J(\Omega^1) = 50.4477$

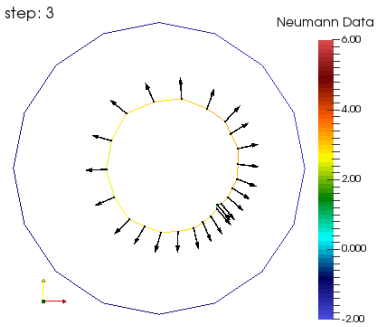

Figure 4.62: Starting domain $J(\Omega^3) = 46.8986$

Domains in Steps 5, 6 and the Neumann Data for an initial Domain Ω_2^0

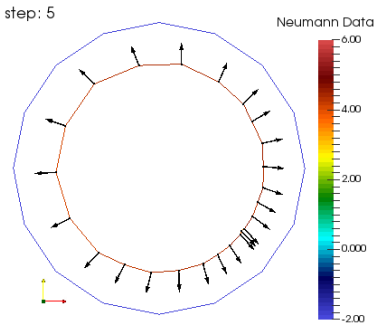

Figure 4.63: Starting domain $J(\Omega^5) = 42.7579$

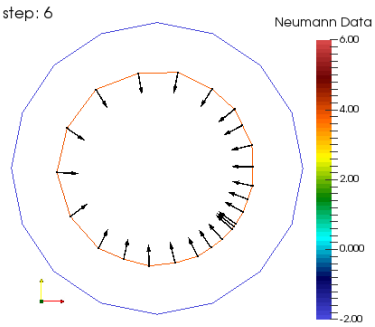

Figure 4.64: Domain after step 1 $J(\Omega^6) = 42.7027$

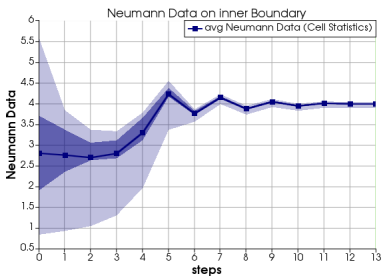

Figure 4.65: Statistical distribution of Neumann data on Γ_I^i.

step 1 (Figure 4.60) to 2 elements in step 3 (Figure 4.62).
This happens because the normal vectors in the corner are not pointed toward each other and thus the domain does not get sliced.

This underlines the importance of the angle of the inward corners which come up often, because both the regularized approach and the normal approach transforms outward corners into inward corners, see Remark 10. But the regularized approach transforms outward corners into inward corners with angle larger than 120°, see Section 4.2, and these corners are stable as seen in Section 4.4.

4.4.4 Multiresolution method

A multisresolution method is a method where more than one mesh is considered at the same time or after each other. As seen in this section, a part of the problem is the

The Regularized Approach applied on the Shape Ω_{I_1}, discretized with 16 Elements.

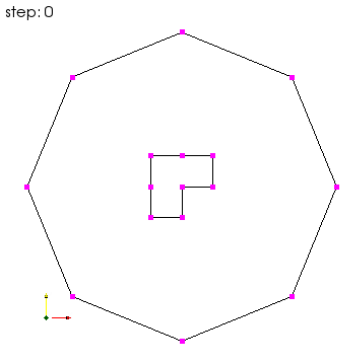

Figure 4.66: Shape and points before step 1.

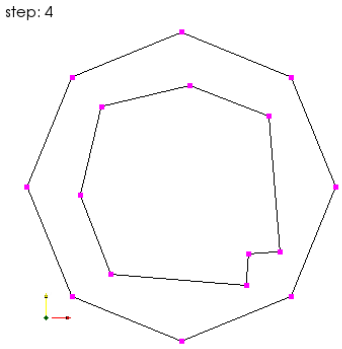

Figure 4.67: Shape and points after the last step.

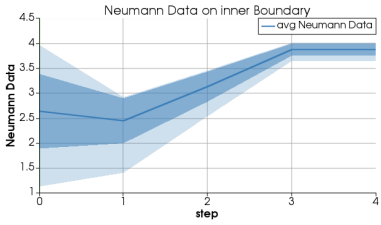

Figure 4.68: Statistical distribution of Neumann data on Γ_I^i.

number of elements in the corner and a method with different meshes is used to stop the developing of a slit.
In this subsection the regularized approach is applied to $\Omega_{I_1}^0$. But a coarser mesh is used, where there are only 2 elements in the corner, see Figure 4.66. The resulting shape from this optimization is called Ω_{I_3}, see Figure 4.67. When the regularized approach is applied to Ω_{I_1} with a coarser mesh no parallel elements develop. But the shape is transformed into a regular shape closer to the optimized shape, as seen in Figure 4.67.

The Regularized Approach applied on the Shape Ω_{I_3}, discretized with 64 Elements.

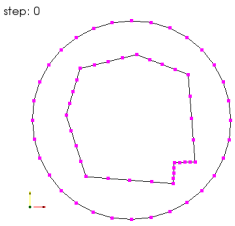

Figure 4.69: Shape and points before step 1.

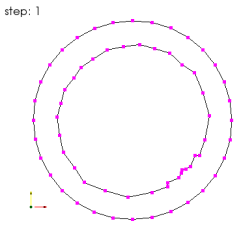

Figure 4.70: Shape and points after step 1.

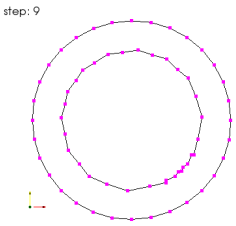

Figure 4.71: Shape and points after the last step.

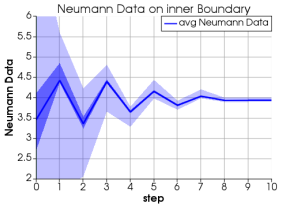

Figure 4.72: Statistical distribution of Neumann data on Γ_I^i.

When the shape Ω_{I_3} is remeshed with 64 elements and the regularized approach is applied to this shape, the optimal shape is neither sliced nor has any corners, see Figure 4.69 - 4.71.
Figure 4.68 shows that, iff the coarser mesh is used, the Neumann data converges

towards 4 from the bottom and does not oscillate around the optimum 4. But Figure 4.72 shows that the Neumann Data does oscillate around the optimum 4 if the finer mesh is used. This means that the corner is not changed when the coarser mesh is used. But when the finer mesh is used on Ω_{I_3} the corner is smoothed out because the shape is already closer to the optimal shape.

In conclusion it has been shown that the regularized approach has problems with corners with small angles but a solution to this problem has been shown by using different meshes with different coarseness, so that the shape converges to the optimal shape.

4.4.5 Conclusion

In conclusion, this approach and probably every approach which is based on the transformation in the normal direction n has problems with inner corners with small angles. This approach has problems with angles $w < 120°$. But it does still converge to a domain with the correct optimal radius nearly everywhere which is sliced as seen in Figure 4.54. This shows that the regularized approach also works on Lipschitz domains like the sliced domain in Figure 4.52.
Solutions for domains which small corners are:

- Remeshing and smoothing out any elements, which are parallel to each other and are very close to each other. After that the shape optimization could be restarted with the smoothed domain and the domains converge.
- A multiresolution method with different meshes and different element size h could be applied, see Subsection 4.4.4.
- A different speed vector field $v(0, x) = v_1(x) + \beta t(x)$ could be used, see (4.14).

4.5 L-Shape

4.5.1 Overview

- The outer domain is a L-shape

$$\Omega_O = \{x \in \mathbb{R}^2 \mid -1 < x_1; x_2 < 1\} \setminus \{x \in \mathbb{R}^2 \mid 0 \leq x_1 \leq 1, -1 \leq x_2 \leq 0\}.$$

- The initial inner domains are
  - An off-center domain

$$\Omega^0_{I_1} = \{x \in \mathbb{R}^2 \mid -0.1 < x_1, x_2 < 0.3\}.$$

  - A more centered domain

$$\Omega^0_{I_2} = \{x \in \mathbb{R}^2 \mid -0.7 < x_1 < -0.3; 0.3 < x_2 < 0.7\}.$$

– An larger of center domain

$$\Omega_{I_3}^0 = \{x \in \mathbb{R}^2 \mid 0.2 < x_1 < 0.5;\ 0.3 < x_2 < 0.6\}.$$

- The boundary Γ_1 of $\Omega_1^0 = \Omega_O \setminus \overline{\Omega_{I_1}^0}$ is discretized with $N = 320$ elements, 192 elements make up Γ_O and 128 make up Γ_{I_1}.
- The boundary Γ_2 of $\Omega_2^0 = \Omega_O \setminus \overline{\Omega_{I_2}^0}$ is discretized with $N = 80$ elements, 48 elements make up Γ_O and 32 make up Γ_{I_2}.
- The boundary Γ_3 of $\Omega_3^0 = \Omega_O \setminus \overline{\Omega_{I_3}^0}$ is discretized with $N = 80$ elements, 48 elements make up Γ_O and 32 make up Γ_{I_3}.
- The regularization parameters used are $\lambda \in \{\sqrt{14},\ \sqrt{15},\ \sqrt{17.5},\ \sqrt{20},\ 5,\ \sqrt{28.5},\ 6\}$.
- The constraint ϵ to the step size s is 0.01.
- Only the regularized approach (4.13) is used to deform Ω_1^0, Ω_2^0 and Ω_3^0.
- The boundary element method (BEM) is used resulting in linear systems, see (3.27) and (3.34).

In this example a different outer domain is examined, than in the previous examples. This outer domain Ω_O is a so called L-shape. The change of the outer domain changes the problem significantly:

- The optimal domain $\Omega^{opt} = \Omega_O \setminus \overline{\Omega_I^{opt}}$ for each given λ changes,
- the minimum λ changes,
- the deformation algorithm has to deal with a corner in the outer domain, which it has to deform the inner domain around.

This section examines two different aspects:

- How does the regularized approach deal with a corner in the outer domain Ω_O, see Subsection 4.5.2.
  In Subsection 4.5.2 an initial inner domain is used which is far from the optimal domain and $\lambda = 6$ to investigate the deformation process. This initial inner domain $\Omega_{I_1}^0$ is a very small square in the right-hand side corner of the L-shape Ω_O. This means during the shape optimization process the inner domain has to deform around the inward corner of Ω_O. The focus is on how this initial inner domain is deformed and how the stages of deformation are different. Only the regularized approach is used, because as in Section 4.4 no parameter was found such that the normal direction approach converges.
- In Subsection 4.5.3 the minimal $\lambda > 0$ is calculated such that the shape algorithm converges.
  In Subsection 4.5.3 different initial domains $\Omega_{I_2}^0$ and $\Omega_{I_3}^0$ are considered, which are closer to the optimal domain. The domain $\Omega_{I_2}^0$ is centered and does not have

to deform around the inward corner of Ω_O. The domains $\Omega^0_{I_3}$ is similar to $\Omega^0_{I_1}$ but the hole is larger. The domains $\Omega^0_{I_2}$ and $\Omega^0_{I_3}$ are used because if the initial domain Ω_I is to small it tends towards $\emptyset$. A reason for this convergence toward $\emptyset$ is that the cost functional rises monotonically for a domain with a very small radius, which means the derivative of the cost functional $dJ(\Omega; v)$ is always negative for an inward direction $v = -n$, see Figure 4.10 for an example of this behavior. This affect the minimum $\lambda > 0$ such that the regularized approach produces domains Ω^i which converge towards Ω^{opt}.

4.5.2 Optimal Domain for $\Omega^0_{I_1}$ and $\lambda = 6$

First, the deformation of the inner domain Ω_{I_1} with the regularized approach is examined. The focus is on how the regularized approach with the speed vector

$$v(0, x) = v_A(x) = -V(gn)(x) \quad \text{for } x \in \Gamma_I$$

deals with more complicated shapes. In total there are 64 steps until the domain $\Omega^{opt} = \Omega_O \setminus \overline{\Omega_I^{opt}}$ is reached which minimizes $J(\Omega)$ in M. In this section the regularization parameter is $\lambda = 6$. The Figures 4.73 - 4.84 show critical steps.

Domains for the Regularized Approach Steps 0, 1 and 4 applied on initial domain Ω^0_1

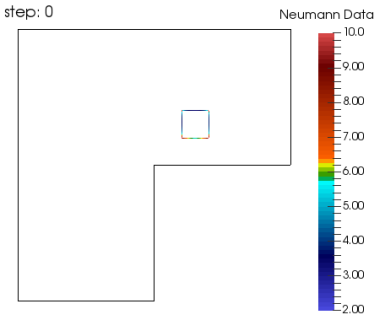

Figure 4.73:
$J(\Omega^0) = 110.89$

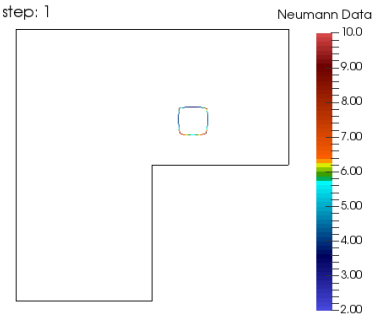

Figure 4.74:
$J(\Omega^1) = 110.64$

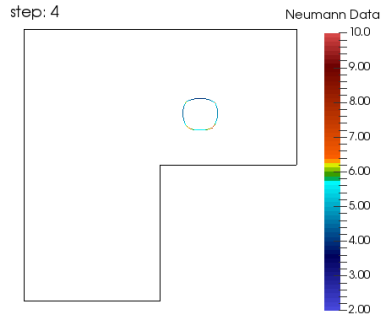

Figure 4.75:
$J(\Omega^4) = 110.32$

Visual Behavior: First, the visual behavior of the domains

$$\Omega^i = \Omega_O \setminus \overline{\Omega_I^i} \quad \text{in step } i$$

is examined. Five different visual stages can be recognized where the deformation of Ω^i is different in each stage. In the beginning the inner domain Ω^i_I is a square which is off center and situated in the right hand side corner of Ω_O.

Domains for the Regularized Approach Steps 6, 12 and 20 applied on initial domain Ω_1^0

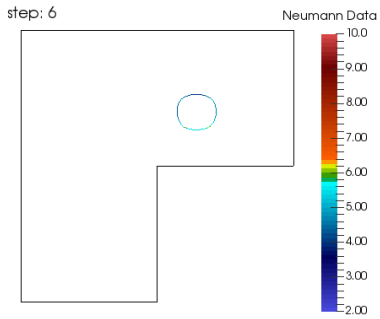

Figure 4.76:
$J(\Omega^6) = 110.11$

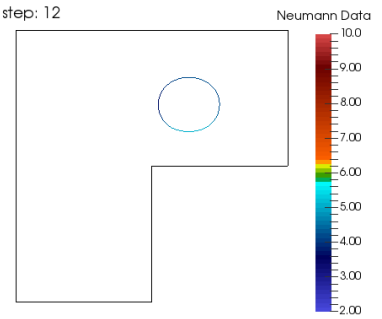

Figure 4.77:
$J(\Omega^{12}) = 108.67$

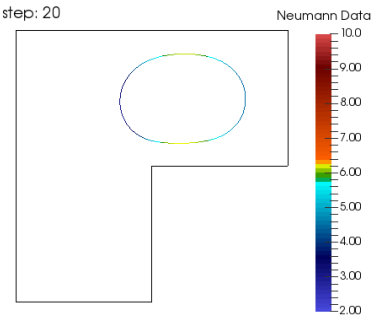

Figure 4.78:
$J(\Omega^{20}) = 102.49$

Domains for the Regularized Approach Steps 24, 28 and 32 applied on initial domain Ω_1^0

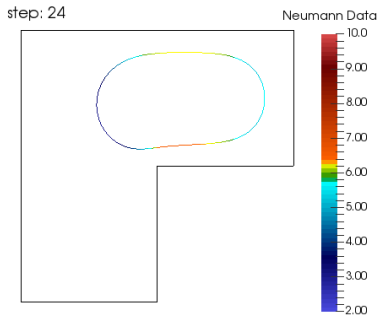

Figure 4.79:
$J(\Omega^{24}) = 98.36$

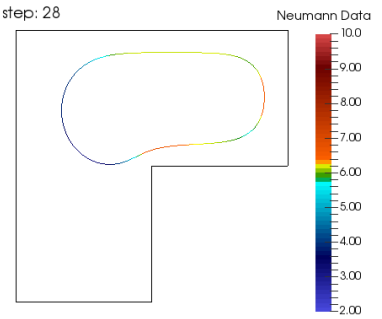

Figure 4.80:
$J(\Omega^{28}) = 93.77$

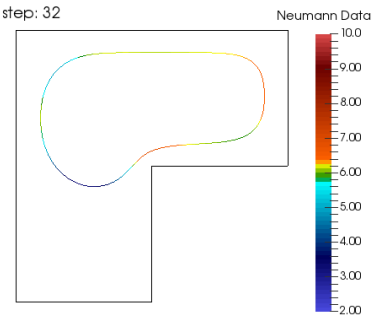

Figure 4.81:
$J(\Omega^{32}) = 89.80$

1. Steps $i = 1, \ldots, 4$: The square moves upwards (Figure 4.74) to make the distance between Ω_I^i and the outer boundary Γ_O larger. The domain Ω_I^i also becomes rounder as it moves upwards (Figure 4.75).

2. Steps $i = 5, \ldots, 20$: The square Ω_I^i deforms into a circle and increases the radius until it fills nearly the whole right-hand side (Figures 4.76 - 4.78). Here the circle Ω_I^i is deformed into an ellipse with similar distance of $\tilde{x} \in \Gamma_I^i$ to Γ_O on three sides. The domain Ω_I^i expands towards the open part in the center. In this stage it can already be seen that the optimal inner domain Ω_I^{opt} has the same distance from Γ_O everywhere.

3. Steps $i = 21, \ldots, 32$: The ellipse Γ_I^i slowly deforms around the inner corner of the L-shape (Figures 4.79 - 4.81). Additionally, the right-hand side deforms such that it holds for the Neumann data $\frac{\partial u(x)}{\partial n} = 6$, since the distance between Γ_I^i and

Domains for the Regularized Approach Steps 36, 50 and 64 applied on initial domain Ω_1^0

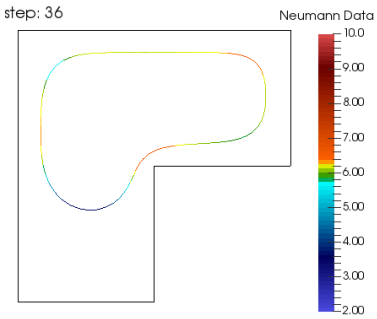

Figure 4.82: $J(\Omega^{36}) = 87.48$

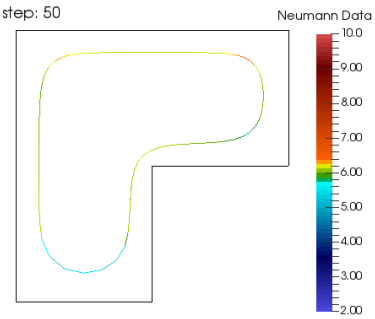

Figure 4.83: $J(\Omega^{50}) = 82.80$

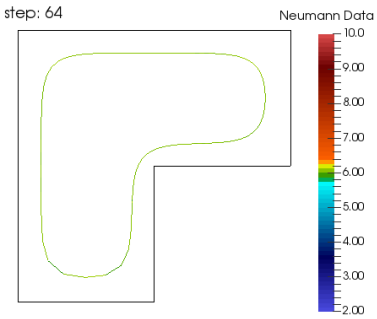

Figure 4.84: $J(\Omega^{64}) = 82.68$

Γ_O determines the value of the Neumann data on Γ_I^i.

4. Steps $i = 33, \ldots, 50$: The inner domain Ω_I^i grows into the bottom corner of Ω_O to achieve the correct distance to Γ_O there as well. At the same time the rest of the boundary Γ_I^i smooths out and is adjusted such that it holds for the normal derivative $\frac{\partial u}{\partial n}\lambda = 6$, see Figures 4.82 - 4.83.
5. Steps $i = 51, \ldots, 64$: The inner boundary Γ_I^i is smoothed and adjusted so that $\frac{\partial u}{\partial n} = \lambda = 6$, as seen in Figure 4.84.

Nodes at step 64, the cost functional and the Neumann data on Γ_I

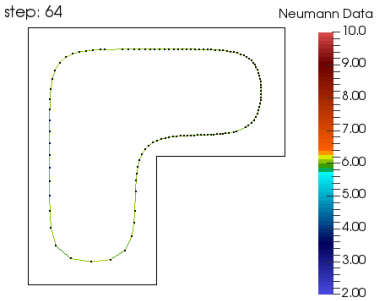

Figure 4.85: Nodes $J(\Omega^{64})$

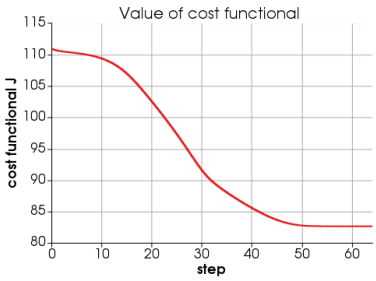

Figure 4.86: $J(\Omega^i)$ over steps i

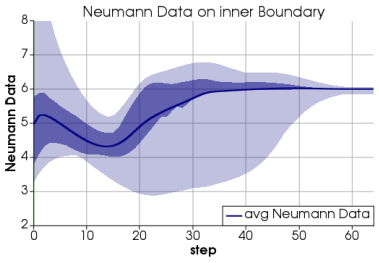

Figure 4.87: Statistical distribution of Neumann data on Γ_I^i.

Cost Functional Behavior: Figure 4.86 shows the value of the cost functional J depending on the steps. The value of the cost functional $J(\Omega)$ for the initial domain is 100.89, and the minimum value of $J(\Omega)$ is 82.68. But the cost functional decreases not as fast as in previous examples. There are at least two reasons for this:

- The first is that for the restriction to the steps size s is $\epsilon = 0.01$,

- The second reason is that the inner domain has to deform around the inward corner of Ω_O before the cost functional decreases significantly, which happens in the step 20 in Figure 4.78.

From the cost functional value only 4 different stages can be recognized:

1. A very slow decrease between steps 1-15.
2. In steps 15-35 is the fastest decrease.
3. In steps 35-50 the decrease slows down.
4. In steps 50-64 the decrease is the smallest, i.e. almost 0.

In stage 1 the initial domain grows in the right-hand corner. In stage 2 the cost functional J decreases the fastest, and in this stage Ω_I deforms around the corner. In stage 3 the cost functional decreases slower again. In stage 4 the cost functional does not change much anymore.
The visual stages 1-2 are a single cost functional stage 1. But the other visual stages 3-5 are the same as in the stages shown in the cost functional value 2-4.

Neumann Data Behavior: The last perspective is the Neumann data which is examined in the statistical distribution of the Neumann data, see Figure 4.87. This results in three stages:

I. In steps 1-15 the mean Neumann data decreases from 5 to 4.35. This happens even so the optimal Neumann data is 6, because at the same time the maximum and minimum tend toward each other.

II. In steps 15-35 the mean increases towards the optimum 6, but the minimum gets smaller again.

III. In steps 35-64 the mean is 6 and the minimum and maximum also converge towards 6.

The Stage 3 and Stage 4 are lumped together into Stage III. Figure 4.88 shows how the different stages overlap. The stages shown by the statistical distribution of the

Visual Stages	$J(\Omega)$ Stages	Neumann Stages	Steps
1.	1.	I.	1-4
2.	1.	I.	5-15
3.	2.	II.	16-35
4.	3.	III.	36-50
5.	4.	III.	51-64

Figure 4.88: Table showing how the different stages overlap.

Neumann data show a different process happening:

- In Stage I. the inner domain tries to find the optimal domain only in the right hand side corner of the L-shape.
- In Stage II. the inner domain deforms around the inner corner of the L-shape.
- In Stage III. the inner domain deforms into the optimal domain in the bottom corner of the L-shape.

The transition from Stage I to Stage III only happens, because there is no other local minimal domain which is only in the right-hand side. Since the speed method only finds the nearest local minimal domain. But this cost functional J only has two local minimal domains: $\emptyset \notin M$ and the $\Omega^{opt} \in M$, where M is the set of all admissible domains, i.e.

$$M = \{\Omega = \Omega_O \setminus \overline{\Omega_I} \subset \mathbb{R}^d \mid \emptyset \neq \Omega_I \,, \overline{\Omega_I} \subset \Omega_O\},$$

where Ω_I is a bounded Lipschitz domain. The optimal domain

$$\Omega^{opt} = \Omega_O \setminus \overline{\Omega_I^{opt}}$$

for the L-shape Ω_O is seen in Figure 4.84.
The statistical distribution of the Neumann data in Γ_I in Figure 4.87, shows that generally the Neumann data is smaller than the optimum 6, because the initial domain Ω_1^0 is much smaller than the optimal domain Ω^{opt}, excepting for the Neumann data on parts of the inner boundary of the domains $\Omega^{20} - \Omega^{35}$ where Γ_I oscillates around Γ_I^{opt} in the right-hand side corner.

Next, the node distribution on the inner boundary Γ_I in step 64 is considered, see Figure 4.85. Most points stay in the right-hand side corner, where the initial inner domain $\Omega_{I_1}^0$ is located. In the beginning the center of the square is moved upwards, but later the left side is only stretched around the corner, not moved.

Conclusion: When the regularized approach is used the domains converge to the optimal domain, even though it has to deform in many stages and around the corner. But the center does not move the shape only gets stretched.

4.5.3 Optimal Domain for Different Relaxation Parameter λ.

In the previous subsection it is shown how the initial domain $\Omega_{I_1}^0$ converges to the optimal domain for the relaxation parameter $\lambda = 6$. But the question remains: **For which minimum $\lambda \geq 0$ can a optimal domain be found and how does it look like?**

Experiments show that if the initial domain Ω_1^0 is used and $\lambda \leq \sqrt{28.5}$ is chosen the domain tend towards $\emptyset$ and becomes irregular eventually. Therefore, different initial domains $\Omega_{I_2}^0$, $\Omega_{I_3}^0$ are examined to investigate $\lambda \leq \sqrt{28.5}$. Additionally, the

domains $\Omega^0_{I_2}$, $\Omega^0_{I_3}$ are used to show that the domain Ω^{opt} which minimize the cost functional

$$J(\Omega) = \int_\Omega |\nabla u|^2 \, dx + \lambda^2 \int_\Omega dx$$

for $\lambda > 0$ depends on the initial domain.

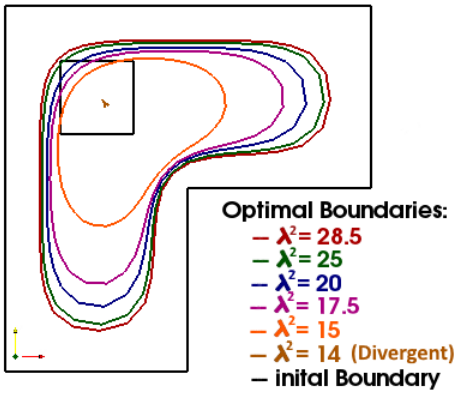

Figure 4.89: Optimal domains with initial domain Ω_{I_2} for $\lambda^2 \in \{15, 17.5, 20, 25, 28.5\}$ and divergent domain for $\lambda = \sqrt{14}$.

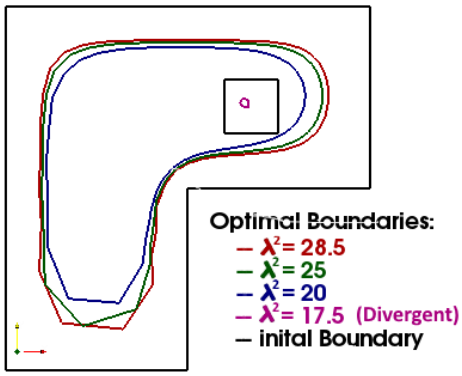

Figure 4.90: Optimal domains with initial domain Ω_{I_3} for $\lambda^2 \in \{20, 25, 28.5\}$ and divergent domain for $\lambda = \sqrt{17.5}$.

Figures 4.89 - 4.90 show the different optimal domains for the different regularization parameters $\lambda > 0$ and different initial domain. If the domains calculates with the regularized approach tend toward $\emptyset$ the last regular domain is shown.

Observations:

1. For each the relaxation parameter λ the optimal domain are the same independent of the initial domain, if they converge. This is seen for $\lambda = \sqrt{28.5}\,, 5, \sqrt{20}\,$.
2. For the initial domain Ω_{I_2} the domains converge for $\lambda \geq \sqrt{15}$ and for Ω_{I_3} the domains converge only for $\lambda \geq \sqrt{20}\,$.
3. With decreasing λ the distance of Γ_I^{opt} to Γ_O gets larger.
4. The points on Γ_I are not equally distributed if the initial domain $\Omega^0_{I_3}$ is used. This is especially true in the two corners, because there are a lot less points in the bottom corner.
5. For the optimal domain it holds

$$\frac{\partial u(x)}{\partial n} = \lambda \quad \text{for } x \in \Gamma_I,$$

this is not shown in the Figures 4.89 - 4.90 but is true nonetheless. This agrees with the results shown in Section 2.3.

The Observation 2 shows us that the possible relaxation parameter λ for which a optimal domain can be calculated with regularized approach dependents on the initial domain. But Observation 1 also says that if the domains converge the optimal domain is independent on the initial domain. Even so the mesh of the optimal domains is not the same for different initial domains. When the initial domain is $\Omega_{I_3}^0$ the mesh stretches around the corner of Γ_O, as in Subsection 4.5.2, that means that the mesh is coarser in the bottom corner if the initial domain is "further away".
Figure 4.89 show that the last regular domain for $\lambda = \sqrt{14}$ is a very small circle. This happens because the inner domain Ω_I tends towards $\emptyset$. This is the same for Figure 4.90 and $\lambda = \sqrt{17.5}$. The divergence of small domains in M and for small λ is a property of the cost functional

$$J(\Omega) = \int_\Omega |\nabla u|^2 \, dx + \lambda^2 \int_\Omega dx.$$

The same happens when Ω_O is disk with radius 1 the cost functional $J(\Omega)$ has two extrema $\tilde{\Omega}_1$ and Ω^{opt}, see Section 4.1. The domain $\tilde{\Omega}_1$ is the local maximizer of $J(\Omega)$. Therefore, if the inner domain $\Omega_I \subset \tilde{\Omega}_1$ is smaller than the local maximizer domain then $dJ(\Omega; v) < 0$ for $v = -n$, that means the inner domain Ω_I tends towards $\emptyset$. The same seems to be true if Ω_O is a L-shape.

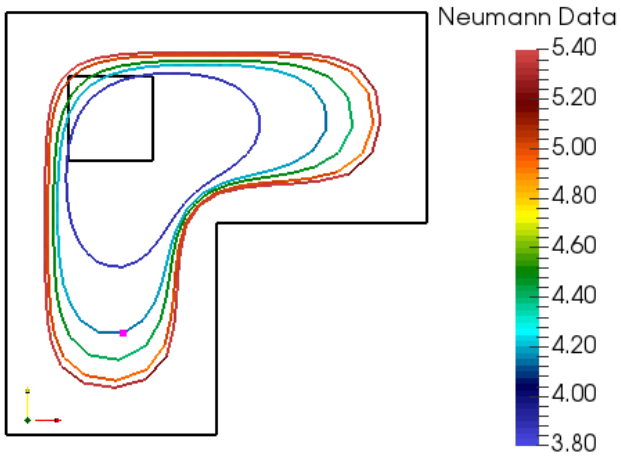

Figure 4.91: Neumann data on optimal boundary Γ_I, for different optimal domains.

Conclusion: The minimal $\lambda > 0$ for which the shape optimization with the cost functional $J(\Omega)$ converges is

$$\lambda = \sqrt{15} \ = 3.87.$$

On the inner boundary Γ_I^{opt} of the minimizer domain Ω^{opt} of J the Neumann data is

$$\frac{\partial u(x)}{\partial n} = \lambda = 3.87 \quad \text{for } x \in \Gamma_I^{opt}.$$

The domain Ω^{opt}, which is calculated with the regularized approach, is seen in Figure 4.89 in orange. But Ω^{opt} can not be calculated from any initial domain. This again emphasizes that the speed method only finds the closest local minima and for $\Omega_I = \emptyset$ the cost functional has an infimum but $\Omega_0 \setminus \emptyset \notin M$. This is true for the regularized direction approach with v_A as for the normal direction approach with v_G.

5 Conclusions

In this work the Bernoulli free boundary problem (5.1) is examined and it is reformulated as a shape optimization problem (5.2). This shape optimization problem is used as an example to introduce a variation of the speed method (5.6), which is more stable for deformations of Lipschitz domains into Lipschitz domains.
The domain $\Omega = \Omega_O \setminus \overline{\Omega_I}$ is a solution to the Bernoulli free boundary problem if the state function $\hat{u}$ satisfies

$$\begin{aligned} -\Delta\hat{u} &= 0 \quad \text{in } \Omega = \Omega_O \setminus \overline{\Omega}_I, \\ \hat{u} &= 1 \quad \text{on } \Gamma_I = \partial\Omega_I, \\ \hat{u} &= 0 \quad \text{on } \Gamma_O = \partial\Omega_O, \\ \frac{\partial\hat{u}}{\partial n} &= \lambda \quad \text{on } \Gamma_I \end{aligned} \tag{5.1}$$

for a given $\lambda \geq 0$ and a given outer Lipschitz domain $\Omega_O \subset \mathbb{R}^d$. The inner domain $\overline{\Omega_I} \subset \Omega_O$ with $\emptyset \neq \Omega_I$ is a free parameter.
In Chapter 2 a possible reformulation of the Bernoulli free boundary problem (5.1) as a shape optimization problem is introduced. A solution to this shape optimization problem is a domain

$$\Omega \in M = \{\text{Lipschitz domain } \tilde{\Omega} = \Omega_O \setminus \overline{\Omega_I} \mid \overline{\Omega_I} \subset \Omega_O,\, \Omega_I \neq \emptyset\}$$

for a given bounded Lipschitz domain Ω_O. A domain $\Omega \in M$ is a solution of the shape optimization problem for a given $\lambda \geq 0$ if Ω minimizes the cost functional

$$J(\Omega) = \int_\Omega |\nabla u|^2 \, dx + \lambda^2 \int_\Omega dx \tag{5.2}$$

subject to the constraint

$$\begin{aligned} -\Delta u &= 0 \quad \text{in } \Omega, \\ u &= 1 \quad \text{on } \Gamma_I, \\ u &= 0 \quad \text{on } \Gamma_O. \end{aligned}$$

For the shape optimization problem (5.2) it has been shown that the derivative of J at Ω is the Fréchet derivative

$$dJ(\Omega; v) = \int_\Gamma g(x)(v(0,x), n(x)) \, ds_x$$

with

$$g(x) = \left(\lambda^2 - \left(\frac{\partial u(x)}{\partial n}\right)^2\right) \quad \text{for } x \in \Gamma_I.$$

Additionally, this work shows that a deformation

$$\Omega^s = \{\varphi(s, x) \mid x \in \Omega\},$$

of Ω is found such that

$$J(\Omega^s) \leq J(\Omega), \tag{5.3}$$

if s is small enough. The domain Ω^s fulfills (5.3) if the descent vector $v(0, x) = \frac{d}{ds}\left[\varphi(s, x)\right]_{s=0}$ fulfills

$$dJ(\Omega; v(0, \cdot)) \leq 0. \tag{5.4}$$

In Chapter 3 a numerical formulation of the shape optimization (5.2) is introduced with the boundary element method.

In Chapter 4 the numerical formulation is used to find a approximation of the domain which minimizes $J(\Omega)$ in M. In that Chapter the initial domain seen in Figures 5.1 - 5.4 are examined.

Initial Domains investigated in this Work.

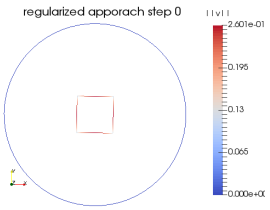

Figure 5.1: Initial domains in Section 4.2.

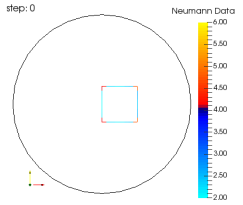

Figure 5.2: Initial domains in Section 4.3.

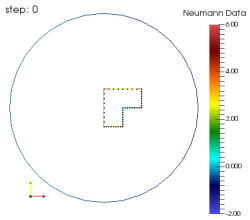

Figure 5.3: Initial domains in Section 4.4.

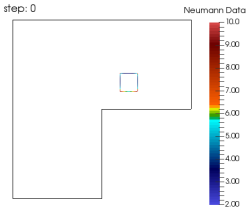

Figure 5.4: Initial domains in Section 4.5.

The main focus of this work is to introduce a different descent direction $v_A = \left(v_A^1, \ldots, v_A^d\right)^\top$ to the normally used descent direction $v_G = \left(v_G^1, \ldots, v_G^d\right)^\top$, which are defined as

$$v_G^i(x) = -g(x)n^i(x) \quad \text{for } x \in \Gamma_I, i = 1, \ldots, d, \tag{5.5}$$

$$v_A^i(x) = -V(gn^i)(x) \quad \text{for } x \in \Gamma_I, i = 1, \ldots, d, \tag{5.6}$$

where V is the single layer boundary integral operator. This work contrasted the two descent direction v_A and v_G to each other by comparing the two deformed domains

$$\Omega_G^s = \{x + sv_G(x) \mid x \in \Omega\},$$
$$\Omega_A^s = \{x + sv_A(x) \mid x \in \Omega\}.$$

An important difference between the two descent direction is the regularity of the speed vector:

- Let $gn^i \in H^r(\Gamma)$ with $r \in [-1, 0]$,
- then $v_G^i \in H^r(\Gamma)$,
- and $v_A^i \in H^{r+1}(\Gamma)$

for $i = 1, \ldots, d$. This has an impact on the solvability of the shape optimization problem (5.2), see Section 1.6. An example for this is if $gn^i \in H^r(\Gamma)$ with $r < 0$ then the integral in $dJ(\Omega; v_G(0, \cdot)$ is not necessarily defined.

Likewise the numerical examples in Chapter 4 of the shape optimization problem (5.2) show that:

- The deformation with v_G (5.5) is faster for C^1-domains.
- The deformation with v_A (5.6) is more stable for domains with polygonal boundaries.

In this work these two descent directions are compared, but other descent direction

$$v^i(x) = A\left(gn^i\right)(x) \quad \text{for } x \in \Gamma_I \text{ and } i = 1, \ldots, d$$

with a $H^{-1/2}$-elliptic boundary integral operator A, are possible. The Steklov-Poincaré Operator

$$S = V^{-1}(\sigma I + K) \; : \; H^{1/2}(\Gamma) \to H^{-1/2}(\Gamma)$$

is a interesting example for A^{-1}. This would result in the speed vector $v_S = \left(v_S^1, \ldots, v_S^d\right)^\top$ as the solution of the boundary integral equation

$$\begin{aligned} S v_s^i &= -gn^i \quad \text{on } \Gamma_I, \\ \Leftrightarrow (\sigma I + K)\, v_s^i &= -V\left(gn^i\right) \quad \text{on } \Gamma_I, \end{aligned} \tag{5.7}$$

for $i = 1, \ldots, d$. If S is $H^{1/2}(\Gamma_I)$-elliptic and bounded, (5.7) is uniquely solvable and v_S is a valid descent direction, since

$$dJ(\Omega; v_S) = -\int_{\Gamma_I} (v_S, S(v_S)) ds_x \leq -\sum_{i=1}^{d} c_1^S \left\| v_S^i \right\|_{H^{1/2}(\Gamma_I)}^2 \leq 0.$$

The boundary integral equations (5.7) are equivalent to the mixed boundary value problem, where $w^i \in H^1(\Omega)$ is the weak solution of

$$\begin{aligned} -\Delta w^i &= 0 \quad \text{in } \Omega, \\ w^i &= gn^i \quad \text{on } \Gamma_I, \\ w^i &= 0 \quad \text{on } \Gamma_O, \end{aligned} \tag{5.8}$$

for $i = 1, \dots, d$. This results in the descent direction $v_S^i = \gamma_0^{int} w^i \in H^{1/2}(\Gamma)$. The solution w^i is a H^1-extension of the descent direction v_S^i, if $gn^i \in H^{-1/2}(\Gamma_I)$ for $i = 1, \dots, d$. To our knowledge this is not yet examined, and would be an interesting deformation to investigate. Especially since the mixed boundary value problem (5.8) can be solved in various different ways for example with the finite element method (FEM). Therefore, the speed vector with $v^i = \gamma_0^{int} w^i$ for $i = 1, \dots, d$ can be used without using the BEM at all.

In Section 4.4 it is considered how inward corners affect the approach with speed vector v_A. In that section it is demonstrated that the approach has problems with domains Ω_I which have inward corners with small angels.

The question of **"What is the minimal $\lambda > 0$ for a given outer domain Ω_O so that the shape optimization problem (5.2) is solvable?"** is discussed in Section 4.5. A domain is found which is a local minimizer of $J(\Omega)$ in M for the initial domain in Figure 5.4 and the minimal parameter is $\lambda = 3.7417$. That means it holds

$$\min_{\Omega \in M} \left[\frac{\partial \hat{u}}{\partial n} \right]_{\Gamma_I} \leq 3.7417,$$

where $\hat{u}$ is the solution of (5.1).

Additionally, to the investigation of different speed vectors like v_S, there are some matters which could be examined in the future:

- This work only applies the shape optimization to example domains $\Omega \subset \mathbb{R}^2$, this approach would be interesting for example domains $\Omega \subset \mathbb{R}^3$.
- Here the shape optimization process is only applied to problems where the optimal domain is a C^1-domain. How does this approach behave if the optimal domain has corners?
- For Lipschitz domains $\Omega \subset \mathbb{R}^3$ the Theorem 11 shows that $v \in H^{\frac{3}{2}+\epsilon}(\Gamma)$ is needed for the existence of the shape derivative $u'(\cdot; v) \in H^{1/2}(\Omega)$. How can the speed method be used if $v \in H^t(\Gamma)$ with $t < \frac{3}{2}$?
- Can a speed vector v be chosen with lower regularity than $H^{1/2}(\Gamma)$ and can the existence of $u'(\cdot; v) \in L^2(\Omega)$ be still proven?
- The speed vector is chosen as $v = -V(gn)$, what other boundary integral operator like S can be used? Or can a completely different v be used?

6 Appendix

Notations

$\mathbb{N}$ – the set of all positve integers,
$\mathbb{Z}$ – the set of all integers,
$\mathbb{Z}_+$ – the set of all non-negative integers,
$\mathbb{R}$ – the set of real numbers,
$\mathbb{R}^d$ – $\mathbb{R} \times \ldots \mathbb{R}$ d factors,
$\{x \in X \mid P(x)\}$ – the subset of X containing all elements that have property P(x),
$E \subset X$ – E subset of metric space X,
$\overline{E}$ – the closure of E in X,
∂E – boundary of E,
X' – dual space of X.

For vectors $v, w \in \mathbb{R}^d$ the scalar product is $(v, w) = \sum_{i=1}^{d} v_i w_i$.

Function Spaces

Here $\Omega \subset \mathbb{R}^d$ is a bounded domain, which is a open and connected subset of $\mathbb{R}^d$ for $d \in \mathbb{N}$.

For $k \geq 0$ the space $C^k(\Omega)$ is the space of all functions defined in Ω, which are k times continuously differentiable:

$$C^k(\Omega) := \{u \in C(\Omega) \mid D^\alpha u \in C(\Omega) \text{ for } |\alpha| \leq k\}, \tag{6.1}$$

$$D^\alpha u(x) := \frac{\partial^{|\alpha|} u(x)}{\partial_{x_1}^{\alpha_1} \partial_{x_2}^{\alpha_2} \cdots \partial_{x_d}^{\alpha_d}} \tag{6.2}$$

with $\alpha = (\alpha_1, \ldots, \alpha_d)$, $|\alpha| = \alpha_1 + \ldots + \alpha_d$ and $C(\Omega) = C^0(\Omega)$ is the space of continuous function defined in Ω.

The set $C_0^k(\Omega)$ is the set of functions u, which are k times continuously differentiable and the support of u is compact and contained in Ω:

$$C_0^k(\Omega) := \{f \in C^k(\Omega) \mid \operatorname{supp} u \subset \Omega\}.$$

The set of test functions $C_0^\infty(\Omega)$ is

$$C_0^\infty(\Omega) := \bigcap_{k=0}^{\infty} C_0^k(\Omega),$$

and the set of infinitely often differentiable function in in $\overline{\Omega}$ is

$$C^\infty(\overline{\Omega}) := \{u|_{\overline{\Omega}} \mid u \in C^\infty(\mathbb{R}^d)\}$$

where $C^\infty(\mathbb{R}^d) = \bigcap_0^\infty C^k(\mathbb{R}^d)$, for more information see [6, page 61].

The set of Lipschitz continuous functions is denote by $C^{0,1}(\Omega)$, i.e. a function $u \in C^{0,1}(\Omega)$ fulfills

$$|u(x) - u(y)| \leq C\|x - y\| \quad \text{for all } x, y \in \Omega.$$

Here only functions $u : \Omega \to \mathbb{R}$ are considered, if a function is $v : \Omega \to \mathbb{R}^d$ then

$$v \in C^k(\Omega; \mathbb{R}^d) \text{ if } v_i \in C^k(\Omega) \text{ for } i = 1, \ldots, d. \tag{6.3}$$

The same is considered for the function spaces $C^{0,1}(\Omega; \mathbb{R}^d)$, $C_0^\infty(\Omega; \mathbb{R}^d)$ and $C^\infty(\Omega; \mathbb{R}^d)$.

Domains

The definition of Lipschitz domains and C^k-domains is based on [6, Definition 3.28].

Definition 11 (Hypograph)**.** *If there exists a function $\zeta : \mathbb{R}^{d-1} \to \mathbb{R}$ such that*

$$\Omega = \{x = (x_1, \ldots, x_d) \in \mathbb{R}^d : x_d < \zeta(x') \text{ and } x' = (x_1, \ldots, x_{d-1}) \in \mathbb{R}^{d-1}\},$$

and $\zeta \in C^{0,1}(\mathbb{R}^{d-1})$, then Ω is a Lipschitz hypograph. If $\zeta \in C^k(\mathbb{R}^{d-1})$ then Ω is a C^k hypograph.

Definition 12 (Lipschitz Domains)**.** *The open and connected set $\Omega \subset \mathbb{R}^d$ is a Lipschitz domain if its boundary $\Gamma = \partial\Omega$ is compact and if there exists finite families $\{W_j\}$ and $\{\Omega_j\}$ having the following properties:*

1. *The family $\{W_j\}$ is an open cover of Γ, i.e. each W_j is an open subset of $\mathbb{R}^d$ and $\Gamma \subset \cup_j W_j$.*
2. *Each Ω_j can be transformed to a Lipschitz hypograph by a rigid motion, i.e. by a rotation and a translation.*

3. *The set Ω satisfies $W_j \cap \Omega = W_j \cap \Omega_j$ for each j.*

Definition 13 (C^k-Domains)**.** *The open and connected set $\Omega \subset \mathbb{R}^d$ is a C^k-domain for $k \geq 0$ if its boundary $\Gamma = \partial\Omega$ is compact and if there exists finite families $\{W_j\}$ and $\{\Omega_j\}$ having the following properties:*

1. *The family $\{W_j\}$ is an open cover of Γ, i.e. each W_j is an open subset of $\mathbb{R}^d$ and $\Gamma \subset \cup_j W_j$.*
2. *Each Ω_j can be transformed to a C^k hypograph by a rigid motion, i.e. by a rotation and a translation.*
3. *The set Ω satisfies $W_j \cap \Omega = W_j \cap \Omega_j$ for each j.*

For a Lipschitz hypograph Ω the function ζ is Fréchet-differentiable with

$$\|\operatorname{grad}\zeta\|_{L^\infty(\mathbb{R}^{d-1})} \leq M,$$

where M is a Lipschitz constant for ζ, see [11, Theorem 11A]. Then the normal vector is

$$n(x) = \frac{1}{\sqrt{1 + |\operatorname{grad}\zeta(x')|^2}} \left(-\operatorname{grad}\zeta(x'), 1\right)^\top \quad \text{for } x = (x', x_d) \in \Gamma \tag{6.4}$$

and the surface measure is

$$ds_x = \sqrt{1 + |\operatorname{grad}\zeta(x')|^2}\; dx' \quad \text{for } x = (x', x_d) \in \Gamma,$$

see [6, p. 97].

Theorem 19 ([6, Theorem 3.34])**.** *Let Ω be a Lipschitz domain and let $F : \mathbb{R}^d \to \mathbb{R}^d$ be a C^1 vector field with compact support. Then*

$$\int_\Omega \operatorname{div} F(x)\, dx = \int_\Gamma (F(x), n(x)) ds_x.$$

Sobolev Spaces

Let $\Omega \subset \mathbb{R}^d$ be a Lipschitz domain.

Definition 14 ([6, page 58])**.** *The Banach spaces $L^p(\Omega)$ are defined with the norm*

$$\|u\|_{L^p(\Omega)} := \left(\int_\Omega |u(x)|^p\, dx\right)^{1/p} \quad \text{for } 1 \leq p < \infty,$$

and $L^\infty(\Omega)$ is defined with the essential supremum and the norm

$$\|u\|_{L^\infty(\Omega)} := \operatorname{esssup}_{x\in\Omega} |u(x)|.$$

The scalar product is defined by

$$\langle u, v\rangle_\Omega := \int_\Omega u(x)v(x)\,dx \tag{6.5}$$

whenever $uv \in L^1(\Omega)$.
The space $L^2(\Omega)$ is a Hilbert space with the scalar product in (6.5).
The space $L^2(\Gamma)$ is also a Hilbert space with the scalar product

$$\langle u, v\rangle_\Gamma := \int_\Gamma u(x)v(x)\,ds_x.$$

Theorem 20. *Let $\Omega \subset \mathbb{R}^d$ be a Lipschitz domain and $v, w \in C^1(\overline{\Omega})$. Then the Green formula*

$$\int_\Omega \frac{\partial w(x)}{\partial x_i} v(x)\,dx = -\int_\Omega w(x)\frac{\partial v(x)}{\partial x_i}\,dx + \int_\Gamma w(x)v(x)n^i(x)\,ds_x$$

holds, where n^i is the i-th component of the unit vector of the outward normal n to $\Gamma = \partial\Omega$.

From Theorem 20 follows the first Green identity for $W \in C^2(\overline{\Omega}), v \in C^1(\overline{\Omega})$:

$$\int_\Omega (\nabla v(x), \nabla w(x))\,dx = \int_\Gamma w(x)\frac{\partial w(x)}{\partial n}\,ds_x - \int_\Omega v(x)\Delta w(x)\,dx$$

with the normal derivative

$$\gamma_1^{int} w(x) = \frac{\partial w(x)}{\partial n} := \lim_{\Omega \ni \tilde{x} \to x \in \Gamma} (\nabla w(\tilde{x}), n(x)),$$

where for Lipschitz domains the normal vector n is defined by (6.4). The weak partial derivative of $u \in L^2(\Omega)$ is $\partial^\alpha u = f$, if there exists a function $f \in L^2(\Omega)$ such that

$$\langle u, D^\alpha \phi\rangle_\Omega = (-1)^\alpha \langle f, \phi\rangle_\Omega \quad \forall \phi \in C_0^\infty(\Omega).$$

For $k \geq 0$ the Sobolev space $H^k(\Omega)$ is

$$H^k(\Omega) = \{u \in L^2(\Omega) \,:\, \partial^\alpha u \in L^2(\Omega) \text{ for } |\alpha| \leq k\}, \tag{6.6}$$

with the Sobolev norm

$$\|u\|_{H^k(\Omega)} = \left(\sum_{|\alpha|\leq k} \int_\Omega |\partial^\alpha u(x)^2\,dx\right)^{1/2}.$$

For $0 < \mu < 1$ the Slobodeckij semi norm is

$$|u|_{\mu,\Omega} = \left(\int_\Omega \int_\Omega \frac{|u(x) - u(y)|^2}{|x-y|^{d+2\mu}} \, dx \, dy \right)^{1/2}$$

and with this norm the Sobelv space for $s = k + \mu \geq 0$ is

$$H^s(\Omega) = \{u \in H^k(\Omega) \, : \, |\partial^\alpha u|_{\mu,\Omega} < \infty \text{ for } |\alpha| = k\}$$

with the norm

$$\|u\|_{H^s(\Omega)} = \left(\|u\|^2_{H^k(\Omega)} + \sum_{\alpha=k} |\partial^\alpha u|^2_{\mu,\Omega} \right)^{1/2}.$$

Function Spaces on the Boundary

Let Ω be a bounded domain and let there exist a overlapping decomposition

$$\Gamma = \bigcup_{i=1}^{p} \Gamma_i, \quad \text{with } \Gamma_i = \{x \in \mathbb{R}^d \mid x = \chi_i(x'), \, x' \in \tau_i \subset \mathbb{R}^{d-1}\}. \tag{6.7}$$

Furthermore, there exists a partition of unity $(\phi_i)_{i=1}^p$ in terms of the decomposition (6.7) with non-negative cut-off functions $\phi_i \in C_0^\infty(\mathbb{R}^d)$ with

$$1 = \sum_{i=1}^{p} \phi_i(x) \quad \text{for } x \in \Gamma, \quad \phi_i(x) = 0 \quad \text{for } x \in \Gamma \setminus \Gamma_i. \tag{6.8}$$

Then

$$v(x) = \sum_{i=1}^{p} \phi_i(x) v(x) \quad \text{for } x \in \Gamma.$$

For $i = 1, \ldots, p$ let

$$\tilde{v}_i(x') := \phi_i(\chi_i(x')) v(\chi_i(x')) \quad \text{for } x' \in \tau_i \subset \mathbb{R}^{d-1}$$

with the local parametrization χ_i in (6.7). Let $k \geq 1$ and let Ω be a C^k-domain. Then there exists a decomposition (6.7) and partition of unity (6.8) with $\chi_i \in C^k(\tau_i)$ for $i = 1, \ldots, p$. The function v fulfills $v \in C^l(\Gamma)$ for $0 \leq l \leq k$ if

$$\sum_{i=1}^{p} \tilde{v}_i \in C^l(\mathbb{R}^{d-1}).$$

Let Ω be a Lipschitz domain. Then there exists a decomposition (6.7) and partition of unity (6.8) with $\chi_i \in C^{0,1}(\tau_i)$ for $i = 1, \ldots, p$, see [6, p. 97- 98]. The function v fulfills $v \in H^s(\Gamma)$ for $0 \leq s < 1$ if

$$\tilde{v}_i \in H^s(\tau_i) \quad \text{for } i = 1, \ldots, p$$

with the norm

$$\|v\|_{H^s_\chi(\Gamma)} := \left[\sum_{i=1}^{p} \|\tilde{v}_i\|^2_{H^s(\tau_i)}\right]^{1/2}.$$

The L^2 norm

$$\|v\|_{L^2(\Gamma)} := \left[\int_\Gamma |v(x)|^2 \, ds_x\right]^{1/2}$$

is a equivalent norm to $\|\cdot\|_{H^0_\chi(\Gamma)}$, see [10, Lemma 2.19]. For $s \in (0, 1)$ the Sobolev-Slobodeckij norm

$$\|v\|_{H^s(\Gamma)} = \left[\|v\|^2_{L^2(\Gamma)} + \int_\Gamma \int_\Gamma \frac{|v(x) - v(y)|^2}{|x - y|^{d-1+2s}} \, ds_x ds_y\right]^{1/2}$$

is a equivalent norm to $\|\cdot\|_{H^s_\chi(\Gamma)}$. And for $-1 < s < 0$ the Sobolev space is the dualspace

$$H^s(\Gamma) := \left[H^{-s}(\Gamma)\right]'$$

with the norm

$$\|w\|_{H^s(\Gamma)} := \sup_{0 \neq v \in H^{-s}(\Gamma)} \frac{|\langle w, v\rangle_\Gamma|}{\|v\|_{H^{-s}(\Gamma)}},$$

see [6, p. 98]. For a closed boundary Γ which is piecewise smooth, i.e

$$\Gamma = \bigcup_{i=1}^{p} \overline{\Gamma_i}, \quad \Gamma_i \cap \Gamma_j \text{ for } i \neq j,$$

with Γ_i being C^1 hypograph. For $s > 0$ the set of piecewise smooth function is defined by

$$H^s_{PW}(\Gamma) := \{v \in L^2(\Gamma) \mid v|_{\Gamma_i} \in H^s(\Gamma_i) \text{ for } i = 1, \ldots, p\}, \tag{6.9}$$

with the norm

$$\|v\|_{H^s_{PW}(\Gamma)} := \{\sum_{j=1}^{p} \left\| v|_{\Gamma_j} \right\|^2_{H^s(\Gamma_j)}\}^{1/2},$$

see [10, p. 37]. For $s < 0$ set of piecewise of piecewise function is defined by

$$H^s_{PW}(\Gamma) := \prod_{j=1}^{p} \tilde{H}^s(\Gamma_j)$$

with the norm

$$\|v\|_{H^s_{PW}(\Gamma)} := \sum_{j=1}^{p} \sup_{0\neq w_j\in H^{-s}(\Gamma_j)} \frac{\left\langle v|_{\Gamma_j}, w_j \right\rangle_{\Gamma_j}}{\|w_j\|_{H^{-s}(\Gamma_j)}},$$

see [10, p. 37].

Properties of Sobolev Spaces

Let Ω be a Lipschitz domain and $s \geq 0$, than $H^s(\Omega)$ is the closure of the space $C^\infty(\overline{\Omega})$ with the norm $\|\cdot\|_{H^s(\Omega)}$:

$$H^s(\Omega) = \overline{C^\infty(\overline{\Omega})}^{\|\cdot\|_{H^s(\Omega)}}.$$

The trace on $\Gamma = \partial\Omega$ for $f \in C(\overline{\Omega})$ is defined as

$$\gamma_0^{int} f(x) := \lim_{\Omega\ni\tilde{x}\to x\in\Gamma} f(\tilde{x}) \quad \text{for } x \in \Gamma. \tag{6.10}$$

Theorem 21 ([10, Theorem 2.21])**.** *Let $\Omega \subset \mathbb{R}^d$ be a Lipschitz domain. For $s \in (1/2, 1]$ the trace on $\Gamma = \partial\Omega$ is*

$$\gamma_0^{int} \ : \ H^s(\Omega) \to H^{s-1/2}(\Gamma)$$

a bounded linear operator, i.e.

$$\left\|\gamma_0^{int} v\right\|_{H^{s-1/2}(\Gamma)} \leq c_T \|v\|_{H^s(\Omega)} \quad \textit{for } v \in H^s(\Omega),$$

as extension of $v|_\Gamma = \gamma_0^{int} u$ for $u \in C(\overline{\Omega})$.

The space $H_0^s(\Omega)$ is the space of Sobolev function in $H^s(\Omega)$, which vanish on the boundary $\Gamma = \partial\Omega$:

$$H_0^s(\Omega) = \{u \in H^s(\Omega) \mid \gamma_0^{int} u(x) = 0 \text{ for } x \in \Gamma\}. \tag{6.11}$$

For Lipschitz domains $\Omega \subset \mathbb{R}^d$ and $s \geq 0$ the space $H_0^s(\Omega)$ is the closure of the space of test functions with the norm $\|\cdot\|_{H^s(\Omega)}$:

$$H_0^s(\Omega) = \overline{C_0^\infty(\Omega)}^{\|\cdot\|_{H^s(\Omega)}},$$

and there also is

$$\tilde{H}^s(\Omega) = \overline{C_0^\infty(\Omega)}^{\|\cdot\|_{H^s(\mathbb{R}^d)}}.$$

For $s < 0$ the Sobolev space $H^s(\Omega)$ is the dual space

$$H^s(\Omega) = \left(\tilde{H}^{-s}(\Omega)\right)'$$

with the norm

$$\|v\|_{H^s(\Omega)} = \sup_{0\neq w\in H^{-s}(\Omega)} \frac{|\langle v, w\rangle_\Omega|}{\|w\|_{H^{-s}(\Omega)}}.$$

Theorem 22 ([10, Theorem 2.5])**.** *Let $\Omega \subset \mathbb{R}^d$ be a bounded Lipschitz domain and $\frac{d}{2} < s$. Then for $u \in H^s(\Omega)$ the function $u \in C(\Omega)$ satisfies*

$$\|u\|_{L_\infty(\Omega)} \leq c\|u\|_{H^s(\Omega)} \quad \forall u \in H^s(\Omega).$$

Bibliography

[1] Bacani, J. B. *Methods of Shape Optimization in Free Boundary Problems.* PhD thesis, Karl-Franzen Universität, 2013.

[2] Bandara, K., Cirak, F., Of, G., Steinbach, O., Zapletal, J. Boundary element based multiresolutional shape optimisation in electrostatics. *Computational Physics*, 297(1):584–598, 2015.

[3] Corless, R. M., Gonnet, G. H., Hare, D. E., Jeffrey, D. J., Knuth, D. E. On the Lambert W Function. *Advances in Computational Mathematics*, 5:329–359, 1996.

[4] Grivard, P. *Elliptic Problem in Nonsmooth Domains.* Pitman, London, 1985.

[5] Haslinger J., Neittaanmäki, P. *Finite Element Approximation for Optimal Shape Design.* Wiley, Chichester, 1988.

[6] McLean, W. *Strongly Elliptic Systems and Boundary Integral Equations.* Cambridge Univ. Press, Cambridge, 2000.

[7] Nečas, J. *Direct methods in the theory of elliptic equations.* Springer, Berlin, 2012.

[8] Rudin, W. *Principles of Mathematical Analysis.* McGraw-Hill, New York, 1976.

[9] Sokolowski, J., Zolesio, J. *Introduction to Shape Optimization.* Springer, Berlin, 1992.

[10] Steinbach, O. *Numerical Approximation Methods for Elliptic Boundary Value Problems.* Springer, New York, 2008.

[11] Whitney, H. *Geometric Integration Theory.* Cambridge Univ. Press, 1966.

Eidesstattliche Erklärung

Ich erkläre an Eides statt, dass ich die vorliegende Arbeit selbständig verfasst, andere als die angegebenen Quellen/Hilfsmittel nicht benutzt, und die den benutzten Quellen wörtlich und inhaltlich entnommenen Stellen als solche kenntlich gemacht habe. Das in TUGRAZonline hochgeladene Textdokument ist mit der vorliegenden Masterarbeit identisch.

Datum	Unterschrift